RADC-TR-78-182
In-House Report
August 1978

LONG-TERM STATISTICS OF ATMOSPHERIC TURBULENCE NEAR THE GROUND

James L. Spencer, 1st Lt, USAF

Sponsored by
Defense Advanced Research Projects Agency (DoD)
ARPA Order No. 2646

Approved for public release; distribution unlimited.

The views and conclusions contained in this document are those of the authors and should not be interpreted as necessarily representing the official policies, either expressed or implied, of the Defense Advanced Research Projects Agency or the U. S. Government.

ROME AIR DEVELOPMENT CENTER
Air Force Systems Command
Griffiss Air Force Base, New York 13441

This report has been reviewed by the RADC Information Office (OI) and is releasable to the National Technical Information Service (NTIS). At NTIS it will be releasable to the general public, including foreign nations.

RADC-TR-78-182 has been reviewed and is approved for publication.

APPROVED: Vincent J. Coyne

VINCENT J. COYNE, Assistant Chief
Strategic Surveillance Branch
Surveillance Division

APPROVED: Joseph L. Ryerson

JOSEPH L. RYERSON
Technical Director
Surveillance Division

FOR THE COMMANDER: John P. Hess

JOHN P. HESS
Acting Chief, Plans Office

If your address has changed or if you wish to be removed from the RADC mailing list, or if the addressee is no longer employed by your organization, please notify RADC (OCSE) Griffiss AFB NY 13441. This will assist us in maintaining a current mailing list.

Do not return this copy. Retain or destroy.

UNCLASSIFIED

SECURITY CLASSIFICATION OF THIS PAGE (When Data Entered)

REPORT DOCUMENTATION PAGE

READ INSTRUCTIONS BEFORE COMPLETING FORM

1. REPORT NUMBER: RADC-TR-78-182	2. GOVT ACCESSION NO.
3. RECIPIENT'S CATALOG NUMBER	
4. TITLE (and Subtitle): LONG-TERM STATISTICS OF ATMOSPHERIC TURBULENCE NEAR THE GROUND	5. TYPE OF REPORT & PERIOD COVERED: In-House Report, 1 Jan 75 — 1 Jan 78
6. PERFORMING ORG. REPORT NUMBER: N/A	
7. AUTHOR(s): James L. Spencer, 1st Lt, USAF	8. CONTRACT OR GRANT NUMBER(s): N/A
9. PERFORMING ORGANIZATION NAME AND ADDRESS: Rome Air Development Center (OCSE), Griffiss AFB NY 13441	10. PROGRAM ELEMENT, PROJECT, TASK AREA & WORK UNIT NUMBERS: 62301E, 26460107
11. CONTROLLING OFFICE NAME AND ADDRESS: Defense Advanced Research Projects Agency, 1400 Wilson Blvd, Arlington VA 22209	12. REPORT DATE: August 1978
	13. NUMBER OF PAGES: 128
14. MONITORING AGENCY NAME & ADDRESS (if different from Controlling Office): Rome Air Development Center (OCSE), Griffiss AFB NY 13441	15. SECURITY CLASS (of this report): UNCLASSIFIED
	15a. DECLASSIFICATION DOWNGRADING SCHEDULE: N/A

16. DISTRIBUTION STATEMENT (of this Report)

Approved for public release; distribution unlimited.

17. DISTRIBUTION STATEMENT (of the abstract entered in Block 20, if different from Report)

Same

18. SUPPLEMENTARY NOTES

Program Code Number: 8E20

19. KEY WORDS (Continue on reverse side if necessary and identify by block number)

Turbulence
Propagation
Microtemperature probes
Diurnal Cycle
Probability distribution

20. ABSTRACT (Continue on reverse side if necessary and identify by block number)

A long-term experiment has measured ground-level atmospheric turbulence during all types of weather. From four months of accumulated data, long-term averages have been calculated. Probability distributions and other pertinent statistics have also been evaluated.

The daily cycle of turbulence expressed in terms of the temperature structure constant, C_t^2, usually displayed one of three basic forms. The form of the daily cycle depended on sky condition. Data analysis concentrated on

DD FORM 1 JAN 73 1473 EDITION OF 1 NOV 65 IS OBSOLETE

UNCLASSIFIED

SECURITY CLASSIFICATION OF THIS PAGE (When Data Entered)

turbulence which exhibited a well-behaved diurnal cycle and which was usually associated with clear or only partly cloudy skies.

Definite conclusions cannot be drawn about the probability distributions of C_t^2. The discrepancy between the calculated probabilities and the anticipated lognormal distribution is discussed.

PREFACE

The turbulence data presented in this paper were collected using sensors known as "fat-wire microtemperature probes." These sensors were a relatively new version of the more widely used "fine-wire" probes. The validity of fat-wire probe data has been questioned and discussed since a presentation of the data at an OSA conference on turbulence in August, 1977. The concern centered on probability distribution functions calculated from the data, which did not exhibit the expected lognormal behavior. Discussions on the performance of fat-wire probes have since taken place among RADC, NOAA and AFWL. The general conclusion was that fat-wire probe data are valid if a correction is made for the probe's limited frequency response. In this report, the author offers three possible explanations for the discrepancy between the theoretical and experimental probability distributions.

The report is primarily concerned with the presentation of data and certain analytical work. Remarks on the physical meaning of the data are occasionally made, but final interpretation is left for the reader to make.

The assistance provided by Major John Bradham of the Staff Meteorology Office at RADC is appreciated. Special appreciation is expressed to David Youmans for his efforts which kept the sensors in operation through a cold winter.

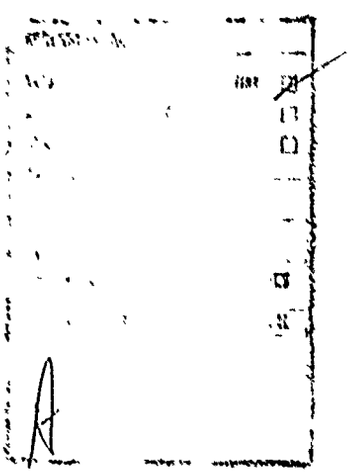

TABLE OF CONTENTS

		Page
I.	INTRODUCTION	1
II.	EXPERIMENTAL APPROACH	3
	A. Location and Instrumentation	3
	B. Data Acquisition and Processing	4
III.	EXPERIMENTAL FINDINGS	5
	A. Early Results and Problems	5
	B. Monthly Results	9
IV.	STATISTICAL ANALYSIS	13
	A. Probability	13
	B. Power Spectra	17
V.	SUMMARY	19
	FIGURES 1-45	21-65
	TABLES 1-10	66-76
	REFERENCES	77
	APPENDIX A - AVERAGING TIMES	78
	APPENDIX B - SENSOR NORMALIZATION ERRORS	89
	APPENDIX C - PROBABILITY DISTRIBUTIONS	92

I. INTRODUCTION

Atmospheric degradation of an optical wavefront is an important consideration to researchers concerned with the optical transmission or reception of information. The surveillance and high energy laser communities are now developing systems aimed at minimizing the distortions produced by atmospheric turbulence. Turbulence and beam degradation data have helped formulate and refine the atmospheric models used as a basis for the competent design of these systems. In fact, the collection of turbulence data during optical experiments has become an almost vital requirement at test ranges.

Although the collection of turbulence data during optical experiments is an improvement in procedure over previous years, several problems remain. To schedule the testing of an instrument under specified turbulence conditions, the researcher has had to guess when such conditions would occur. His guess would probably be based on personal experience and the published results of a few short-term experiments. A need has therefore existed for several years for an experiment which would establish a data base that related turbulence strength to local conditions, such as time and weather. This experiment would also demonstrate an ability to describe "characteristic" behavior (or behaviors) of atmospheric turbulence near the ground, in spite of the atmosphere's inhomogeneous nature and statistical nonstationarity.

A long-term experiment measuring atmospheric turbulence was therefore conducted at the Rome Air Development Center (RADC). It was quickly established that the "typical" diurnal turbulence cycle observed by others[1]

actually depended on the local weather, in particular on sky conditions. The experiment had to be terminated after four months, but much had already been learned. Monthly averages of the diurnal cycle, probability distributions and other statistics have been evaluated and are discussed in this report.

II. EXPERIMENTAL APPROACH

A. LOCATION AND INSTRUMENTATION

The data were collected at the Advanced Optical Test Facility (AOTF) of RADC in Verona, New York. Data were collected for the months of February through May, 1975. The physical layout of the site is shown in Figure 1. The flat terrain is covered mostly by grassy fields which range in height from 0.1 m in the winter to 1.5 m in the summer. Snow reached its greatest depth at 0.6 m in February, but traces of snow were recorded into April. Cloudy skies dominated the winter months, which was typical for the region (see Table 1 for climatic probabilities of cloud cover [2]). Actual weather conditions recorded at the Griffiss AFB weather station (approximately 25 km east of the AOTF) during the months of the experiment are found in Tables 2-6 later in the report.

The instrumentation for the experiment consisted of microtemperature probes, wind speed and wind direction sensors, and an ambient temperature system. The microtemperature probes were fat-wire versions of the fine-wire probe described in detail by Greenwood and Youmans [3,4]. The temperature-sensing element of the fat-wire probe was a platinum wire 12.7 μm in diameter, as compared to the 2.5 μm diameter wire of the fine-wire probe. Although the system response of the two versions were different, Greenwood and Spencer[5] found a relation which corrected the fat-wire probe values to give an accurate measurement of C_t^2, the temperature structure constant. The wind speed and direction systems were standard products of the Climet Instruments Company. The wind speed sensor had a 0-5 volt analog output, corresponding to 0-25 m/s velocities. The wind direction

sensor was a 0-5 volt, 360 degree system. The ambient temperature system was EG&G's Model 110S-M Temperature and Dew Point Measuring Set.

Three microtemperature probes were mounted in a triangular configuration on a small tower approximately 120 meters SSE of the AOTF building (Fig. 2). The probes were mounted in a "standing" position, with the wire element 3 m above ground level (see Figure 3). Wind speed and direction sensors were placed on the same tower at a height of 2.6 m. The ambient temperature sensor was located 2 m above the ground on another tower 26 meters SSE of the AOTF building.

B. DATA ACQUISITION AND PROCESSING

Data from the six instruments on the towers were sequentially sampled, digitized and recorded by a "datalogger" at a nominal rate of one cycle (six data channels) per second. The datalogger was a 12-bit system made by Analog-Digital Data Systems, Inc. Six to eight days of continuously sampled data were stored on a standard ten inch magnetic tape at 556 bits per inch. A new file was marked on the tape daily (except weekends) at 1200 EST. All magnetic tapes were processed at RADC on a Honeywell 635/645 computer. A modified version of a FORTRAN program written by Pattern Analysis and Recognition Corporation[6] was used to reduce the raw data to 30-minute averages. These averages included the mean and standard deviation for wind speed, wind direction and ambient temperature, as well as C_t^2 for each of the three possible probe pairings. The averages formed the basis for almost all subsequent analysis. Appendix A examines the "smoothing" effect of using 30-minute periods as compared to shorter 5-minute periods.

III. EXPERIMENTAL FINDINGS

A. EARLY RESULTS AND PROBLEMS

The temperature structure constant is calculated from two microtemperature probes from the relation[3]

$$C_t^2 = [\sigma_i^2 + \sigma_j^2 - 2C_{ij}]\, r_{ij}^{-2/3} \quad , \quad \ell_o << r_{ij} << L_o \qquad (1)$$

where σ_i^2 and σ_j^2 are the variances of the probes with separation r_{ij}, C_{ij} is the probes' covariance, ℓ_o is the "inner scale" of Kolmogorov's inertial subrange (of the temperature temporal power spectrum) and L_o is the "outer scale." The inner scale is typically a few millimeters in size, while the outer scale is on the order of height above ground. An analysis shows that even if the two probes are not accurately calibrated, the calculated value of C_t^2 is not affected significantly (see Appendix B).

Equation (1) applies to fine-wire probes - it does not include the frequency response correction for fat-wire probes. Multiplying the results of equation (1) by

$$1.2\,(v/r_{ij})^{0.182} \quad , \quad v/r_{ij} < 20 \qquad (2)$$

where v is the wind speed, yields the "corrected" value for C_t^2 from fat-wire probes. The correction factor given by (2) underestimates the needed correction for values of v/r>20. At v/r=20, the error in (2) is 2.7%. The error increases to 9% at v/r=40. Since the values of v/r which occurred during the experiment were rarely greater than 40, the correction given by (2) is considered adequate.

Analysis of initial data showed that the smoothest, most regular diurnal profiles of C_t^2 were obtained by selecting the C_t^2 values from the probe pairings whose line of separation was most perpendicular to the

wind direction. This apparent dependence on wind/probe orientation has been a topic of discussion for many years, but no experimental studies have been reported. The probes were mounted in a triangular configuration in this experiment specifically to avoid any problems with wind/probe-pair orientation. For each 30-minute average, the computer program which reduced the raw data automatically picked the "best" pair of probes according to wind direction.

The triangular configuration did not resolve other problems, however. Spurious effects were observed when the wind was not "good" for any of the three probe pairings - specifically, problems occurred when the wind direction was within 15° of the angle bisector of either acute angle of our (obtuse) triangle configuration. Similar effects occurred when the winds were light and variable. This condition was identified by a standard deviation for wind direction greater than 30 degrees. To avoid the apparent wake effect problems of these two conditions, C_t^2 was calculated from the single, windward probe using the relation[7]

$$C_t^2 = 1.91\sigma_i^2 L_o^{-2/3} \qquad (3)$$

Approximately 10-30% of the 48 averages of each day were calculated using equation (3). Since the outer scale, L_o, is not a static quantity, the use of equation (3) undoubtedly introduced an error in the calculated value of C_t^2. Ideally, L_o would have been derived from data immediately preceding the period when equation (3) was needed. This proved to be impossible for such a long-term experiment. Average values of L_o were calculated instead by substituting 60 known values of C_t^2 from various times of day into equation (3). The mean values obtained in this manner were

L_o = 5.42 m (night)

L_o = 1.26 m (day)

which only apply to fat-wire probes. Comparison of known C_t^2 values with values calculated from equation (3) showed that the error was usually less than a factor of 2. Also, each daily turbulence profile was examined to insure that the single-probe calculations remained reasonable.

Another early observation was the dependence of the daily turbulence profile on sky conditions. The turbulence profile for each 24 hours of data was eventually classified as belonging to three categories. Type I turbulence, as defined here, exhibits a clear diurnal cycle. Figure 4, a typical example, shows the turbulence levels for the 24-hour period beginning at noon (local standard time) on 1 February 1975 (note that all similar references to specific dates also imply noon as the start of the period).

For Type I turbulence, the profile peaks at midday, but it rapidly falls off just prior to sunset. After this dip, it usually regains much of its strength, but subsequently decreases during the night. A few nights show a moderate peak later similar to the daytime peak. Type I turbulence is usually associated with clear skies, scattered clouds or perhaps a light overcast. Type II turbulence is a degraded form of Type I turbulence. Type II turbulence profiles are not as smooth, with more spikes and dips. The profile for 29 April 1975 (Figure 5) is an example. Strong midday turbulence still occurs, and the "sunset" dip can still be identified. This type of turbulence is generally associated with sky conditions ranging from partly cloudy to moderate overcast.

Type III turbulence profiles are even further degraded. As seen in Figure 6, the characteristic profile is difficult to identify. This type of turbulence is usually associated with total cloud cover and possibly some precipitation. The occurrence of precipitation makes the interpretation of Type III turbulence a difficult proposition, if the values have any meaning at all.

Examination of Figures 4, 5 and 6 reveal the characteristic features of the different turbulence categories. Strong daytime turbulence dominates the profiles for both 1 Feb 75 and 29 Apr 75. Pronounced "sunset" and "sunrise" dips are also evident in both. The sunset dips are 30 to 60 minutes before actual sunset (note that the data points are plotted against the beginning time of each 30-minute averaging period). The sunrise dips occur near or after the actual time of sunrise. Whereas the sunset dip is universal to all Type I and Type II turbulence profiles, the sunrise dip is not as common. This will be evident in the monthly averages discussed later. The profile of 29 Apr 75 has been classified as Type II because of its jumpy behavior between 1200 and 2000 EST, not because of the strong nighttime turbulence. Such nighttime turbulence was part of a trend which will be discussed with the monthly averages. Note that about 0600, the profile is observed transitioning to Type I again. The profile from 20 Feb 75 demonstrates the irregular behavior of Type III turbulence, although sunset and sunrise dips might still be identified.

Certain aspects of the experiment should be clarified before proceding further. The classification of the turbulence "type" resulted from a series of subjective decisions made over an extended period time.

No single criterion was used to distinguish between types. The decision to use three turbulence categories was based on the desire to obtain better statistics than those which could be obtained from a simpler good/bad classification. Periods of low wind speeds (below 1 m/s) were not omitted, in contrast with short-term experiments by others. Light precipitation sometimes occurred even in connection with Type I turbulence profiles. The actual weather conditions recorded at Griffiss AFB Weather Station are summarized in Tables 2-6, according to month, day, relative time, and turbulence classification.

B. MONTHLY RESULTS

The monthly results were computed two different ways. In both cases, the turbulence values from the 30-minute blocks of raw data were combined into 60-minute blocks corresponding to the hours of the day. The initial approach was to calculate the arithmetic mean and the standard deviation for each period. The second approach was to obtain a median value for each 60-minute period. The median was obtained from a discrete cumulative probability distribution which was calculated for each period. The number used here as the "median" is the discrete value below which lies 50 percent of the distribution.

The monthly averages of the daily turbulence profiles were calculated and plotted in terms of the temperature structure constant, C_t^2. The refractive index structure constant, C_n^2, can be found from these values using a simple relation (see Greenwood and Youmans, p. 55). Wind speed and ambient temperature associated with periods of Type I turbulence were also averaged.

Several important findings are evident in the monthly averages of Type

I turbulence (see Figures 7-14). The strength of the turbulence during the daylight hours is, of course, the outstanding characteristic of the profiles. As the hours of sunshine increased from February to May, the strong daytime turbulence also lengthened. The strongest values always occurred between 1100 and 1300 EST. The peak values of the four monthly profiles are almost constant even though ambient temperatures change dramatically. The midday peaks of C_t^2 vary only between 0.48 $°C^2m^{-2/3}$ for March and 0.37 $°C^2m^{-2/3}$ for February. Figures 11-14 show that the average temperatures were over 20°C warmer in May than they were in February.

Other characteristics and trends can be found in the plots of Type I turbulence. Nighttime turbulence drops to its lowest strengths for February and March, but it is stronger for the warmer months (see Figure 15). February has the lowest nighttime value of C_t^2 with 0.004 $°C^2m^{-2/3}$, while May's lowest value at night (excluding the "sunset dip") is only down to 0.023 $°C^2m^{-2/3}$. If this trend continues into the summer months, it would support the common belief that the best nights for "seeing" are cold winter nights. The sunset dip seen in the profiles occurs at later times as local sunset gets later. The value of this dip is fairly constant from month to month, varying only between 0.0085 and 0.017 $°C^2m^{-2/3}$. There is no "sunrise dip" which can be clearly identified in all the monthly profiles, although it does occur occasionally on certain days (see Figures 4 and 5). The strongest sunrise dip in a monthly average occurred in April for the 0600-0700 time period (see Figure 9), which is roughly 30 minutes after the median time of sunrise for that data.

Upon examining the averages of Type II turbulence (Figures 16-19), slightly "rougher" profiles are seen. February's profile is omitted from the following discussion and is addressed in the next paragraph. As compared to the Type I profile, the Type II profile for March is different by a later build-up and an earlier falloff in the daytime turbulence. The April and May Type II profiles differ from Type I by irregular jumps in the turbulence values during daylight hours. All three months show stronger turbulence at night for Type II profiles than for Type I profiles, while maintaining the trend toward stronger nighttime turbulence in the warmer months (see Figure 20).

The February profile which has been plotted as Type II turbulence (Figure 16) obviously does not fit the usual definition. Only three unusual days in February were classified as Type II, so statistics are extremely poor. Figure 16 has been included only for completeness. It is strongly recommended that no conclusions should be drawn from any reference to the February Type II turbulence data.

When all the turbulence types are combined for an "all weather" average, an obvious effect takes place. The diurnal cycle of the Type I turbulence profile is still exhibited, but the midday peak is weaker and the nighttime turbulence is stronger (see Figures 21 and 24). This suggests that turbulence during cloudy weather changes less from night to day. April's "all weather" profile shows the least change from the Type I profile because there were no Type III turbulence data available for that month. That lack was probably due to the heavy rain showers in April, which would have broken the microtemperature probes' sensing elements more readily than would February's and March's snows. The drastic degradation in

February's profile is due mostly to Type III turbulence (snow?) and only slightly to the Type II turbulence profile.

The standard deviations of the monthly averages of turbulence are plotted as short dashes in many of the figures. The standard deviations are often as high as the average, which is to be expected from the non-stationarity of the atmosphere. For Type I turbulence profiles, the standard deviations tend to be the smallest (relative to the mean) during the day. Almost all their values at night are on the same order as the means. The situation almost reverses for Type II turbulence, with the smallest standard deviations occurring late at night. All the standard deviations of the "all weather" profiles are high. In the plots, the smaller standard deviations indicate that similar values of turbulence were observed from day to day, in spite of the nonstationarity of the atmosphere. The large standard deviations introduce an uncertainty to the average values which must not be ignored. This does not alter the general interpretation of the monthly averages, but rather it reinforces the appreciation for the statistical nature of this type of data.

Because of the large standard deviations associated with the monthly averages, the median values were also examined. The monthly median values of Type I turbulence are plotted in Figures 25 - 28. They show that the medians for 4-6 hours around midday were almost the same as the arithmetic means, but the nighttime median values were roughly 2-5 times lower than the corresponding mean values. This was expected from the behavior of the standard deviations. For the other types of turbulence, the use of median values instead of average values caused more noticeable changes in the shapes of the profiles.

IV. STATISTICAL ANALYSIS

A. PROBABILITY

The statistical distribution of C_t^2 values has been debated for several years. Most of these discussions have been based on a few days of data, whereas four months of data were collected for this experiment. It was hoped that the question of C_t^2 distributions could finally be answered. An initial look at the data was made for each of the three types of turbulence for day versus night. The distributions were not well-defined, so it was suggested[8] that data collected around dawn and dusk be excluded.

The final analysis calculated the discrete probability distribution function and the cumulative probability function from all the 30-minute C_t^2 values according to turbulence type and time period. The day was divided into the following four time periods:

night - 1900 to 0400 EST

day - 0800 to 1530 EST

dusk - 1530 to 1900 EST

dawn - 0400 to 0800 EST

The long times allowed for "dusk" and "dawn" were specified to prevent contamination of the day and night periods by the sunset and sunrise dips. The plots of the probability functions for Type I turbulence, Type II turbulence and "all weather" conditions are included in Appendix C.

After examining some of the calculated functions, it is evident that there is no distinct lognormal distribution (since log C_t^2 is plotted, a Gaussian distribution is the actual focus of the search). The daytime category has a probability distribution which appears to be characteristic for most months. The distribution is usually strongly skewed to the left,

and it sometimes has a Gaussian-like peak. An extreme example of this is the daytime distribution for Type I turbulence in May (see Figure 29). The distribution for the nighttime category are less consistent, except that they have a much milder skew than the daytime distribution. For all types of turbulence, most dusk and dawn categories have wide, flat distributions.

The quantitative statistics associated with the distributions are summarized in Tables 7-9. A true Gaussian distribution would have a skewness of 0 and a kurtosis of 3. Very few of the distributions are quantitatively close to a Gaussian form. The daytime distributions for Type I turbulence are particularly aberrant. This was not expected. From the tables, the distributions of log C_t^2 values which come closest to Gaussian statistics are February's daytime Type II turbulence (described earlier as atypical and not usable) and March's nighttime "all weather" turbulence. The March data is plotted on a probability scale in Figure 30. A Gaussian distribution plotted on this scale would give a straight line. For a different perspective, the March data is plotted conventionally with a Gaussian fit (Figure 31). This example is not bad by itself, but unfortunately it is the curve closest to Gaussian form from all types of turbulence.

Skimming through all the distributions plotted in Appendix C and not consulting the statistics tables, the reader might want to pick the distribution for May Type II turbulence at night as closest to a Gaussian distribution. A plot of it in Figure 32 confirms that this distribution was worse than the one picked from the tables.

To examine the difference between the observed distributions and a

true Gaussian distribution, mean squared errors were calculated for the coefficients of skewness and kurtosis. Table 10 summarizes the results. The figures in Table 10 suggest that, for overall values, the "all weather" distributions are the closest to Gaussian form, while the Type I turbulence distributions are the least Gaussian. After breaking the results down according to time, however, the apparent differences fade. The dusk and dawn values will continue to be ignored, since their characteristic dips contaminate the distributions. Type I turbulence for daylight hours is definitely the least Gaussian-like of the daytime data. The mean squared difference in skewness is 1.50, which is due to consistently strong skews to the left. The high error in kurtosis is almost entirely due to strongly peaked distributions for February and May. For the daytime periods, Type II turbulence distributions have the lowest skewness, while "all weather" conditions have the lowest error in kurtosis. At night, Type I turbulence distributions are the least skewed but the worst in kurtosis. The least error in kurtosis at night is found for the "all weather" conditions.

By now it is clearly obvious that the predicted laynormal behavior is not confirmed by this experiment. The most Gaussian-like distributions were expected from the daytime values for Type I turbulence, but these distributions are strongly skewed. Since they show an unexpected, abrupt cutoff of high values, the problem appears to be related to the data rather than theory. There are at least three possible explanations for such behavior. The first possibility is that 30-minute averaging periods are too long and the data is smoothed too much to observe the true distribution. The implication is that periods of high turbulence are short-lived or at least intermittent. Another explanation is that sampling the raw signal

at a rate of 1 Hz is too slow to measure high turbulence. A third possibility contends that the limited frequency response of fat-wire probes (approximately 0-20 Hz) simply prevents accurate measurements of strong turbulence.

Only detailed experimental data can resolve the issue. Results from Appendix A confirm that averaging time does affect the shape of the distributions. By shortening the averaging times to 5 minutes, the abrupt cutoff of the distribution lengthens out into a "tail", thereby improving distribution shape. Sampling rate would become more important as averaging periods were shortened to one minute or less. In 1977 Norton and Walters[9] reported reasonable agreement between predicted and measured probability distributions. Their data, also collected with fat-wire probes, calculated turbulence strength for 10-second averages over 15 minute windows in time. These positive results further support averaging time and sampling rate as major factors in the analysis. The data needed to evaluate the performance of fat-wire probes in strong turbulence is now being collected at the AOTF. Atmospheric nonstationarity, which is another consideration, is apparently not the problem because it would smear out the probability distributions. That would be exactly the opposite of the effect observed. The eventual answer might be that the three factors - averaging time, sampling rate and frequency response of fat-wire probes - can each limit the measurement of strong turbulence and affect the shape of probability distributions.

B. POWER SPECTRA

The turbulence values were next analyzed for any possible hidden cyclic behavior, as well as for different power spectral forms according to type of turbulence. The values of the power spectrum and autocovariance function were calculated for 35 different daily profiles, each consisting of a full 24 hours of data. These were divided according to month and type of turbulence to identify any common features.

The power spectrum and the autocovariance values were calculated in the following way [10, 11]: (1) a 48-point discrete Fourier transform was applied to the input data (with the average already removed); (2) a Hamming window was applied as a 3-point convolver; (3) the raw power spectrum was taken to be the "modulus squared" of the resulting sequence; (4) the raw spectrum was averaged over adjacent bands (values) two wide; (5) the spectrum was normalized such that the total power equalled the variance; and (6) the autocovariance was found as the inverse Fourier transform of the power spectrum. Some of these results are plotted in Figures 33-45.

Common features are evident in the plots. Examining the power spectra first, we see that Type I turbulence spectra have the sharpest and strongest central peaks. There is usually at least one small peak in the middle frequencies at about 0.5 hr^{-1}. For Type II turbulence the central peak is wider with somewhat less power, whereas the higher frequencies have more power. For the spectra of Type III turbulence, the central peak is also

wide, with more energy shifted out to the higher frequencies. These features of the power spectra indicate that, for good weather with corresponding "good" turbulence profiles, the C_ξ^2 values are dominated by a low frequency component. This component has a period of approximately 12 hours, which (conveniently) corresponds to a day/night pattern. With cloudier weather, the low frequency component becomes less dominant while the higher frequencies increase in power. The reduction in low frequencies might reflect a lessened change between day and night turbulence. Relying solely on power spectra of sequences of 48 30-minute C_ξ^2 values, though, it is difficult to differentiate the types of turbulence.

Differences are more evident in the autocovariance function. Examining the shape of the autocovariance functions, we see that Type I turbulence is clearly different from the others. For Type I turbulence, the function has a form intermediate between a Gaussian and a triangle function. Relative to other types of turbulence for the same month, Type I turbulence also tends to have stronger autocovariance values. Type II and Type III turbulence exhibit a flatter form for the function, although some of the Type III plots display a distinctive shape resembling the sinc^2 function. The conclusion is that the regular, smooth nature of Type I turbulence profiles is a result of a definite, positive correlation between successive values[12]. Such correlation either deteriorated or never existed for the other turbulence types.

V. SUMMARY

The data has now been presented and briefly discussed. The results, which are specifically applicable to work at the AOTF, should be useful at other locations. Yet, what conclusions can be drawn from all this data?

First, the scheme for classifying turbulence into three basic categories appears reasonable. The three types of turbulence are associated with weather conditions which could almost be termed "good", "fair" or "poor". The standard deviations of the turbulence values for monthly results were highest for the "all weather" combination, still high for the average daytime values of Type II turbulence, but relatively low for daytime values of Type I turbulence. The need for an intermediate turbulence form (Type II) is supported by the analysis of autocovariance functions, which showed a discernible difference between Type I and Type II turbulence in spite of similarities in their profiles.

Type I turbulence exhibits some exceptional features in the monthly profiles. The midday peak is roughly the same over four months. The sunset dip also remains fairly constant. In contrast, turbulence strength at night increases with the warmer months. These findings should be interesting to investigators studying turbulence from a heat budget standpoint.

Although the probability distributions do not display the predicted lognormal shape, reasons are offered which might explain the discrepancy. The experimental curves are valid within the limitations apparently imposed by the manner in which the data were collected and reduced.

Other conclusions might be drawn from the data, but they are left to

the reader. Hopefully, this report will not mark the only use of the data. An attempt has been made to present enough data to allow immediate use by others who could not otherwise invest the required time and resources.

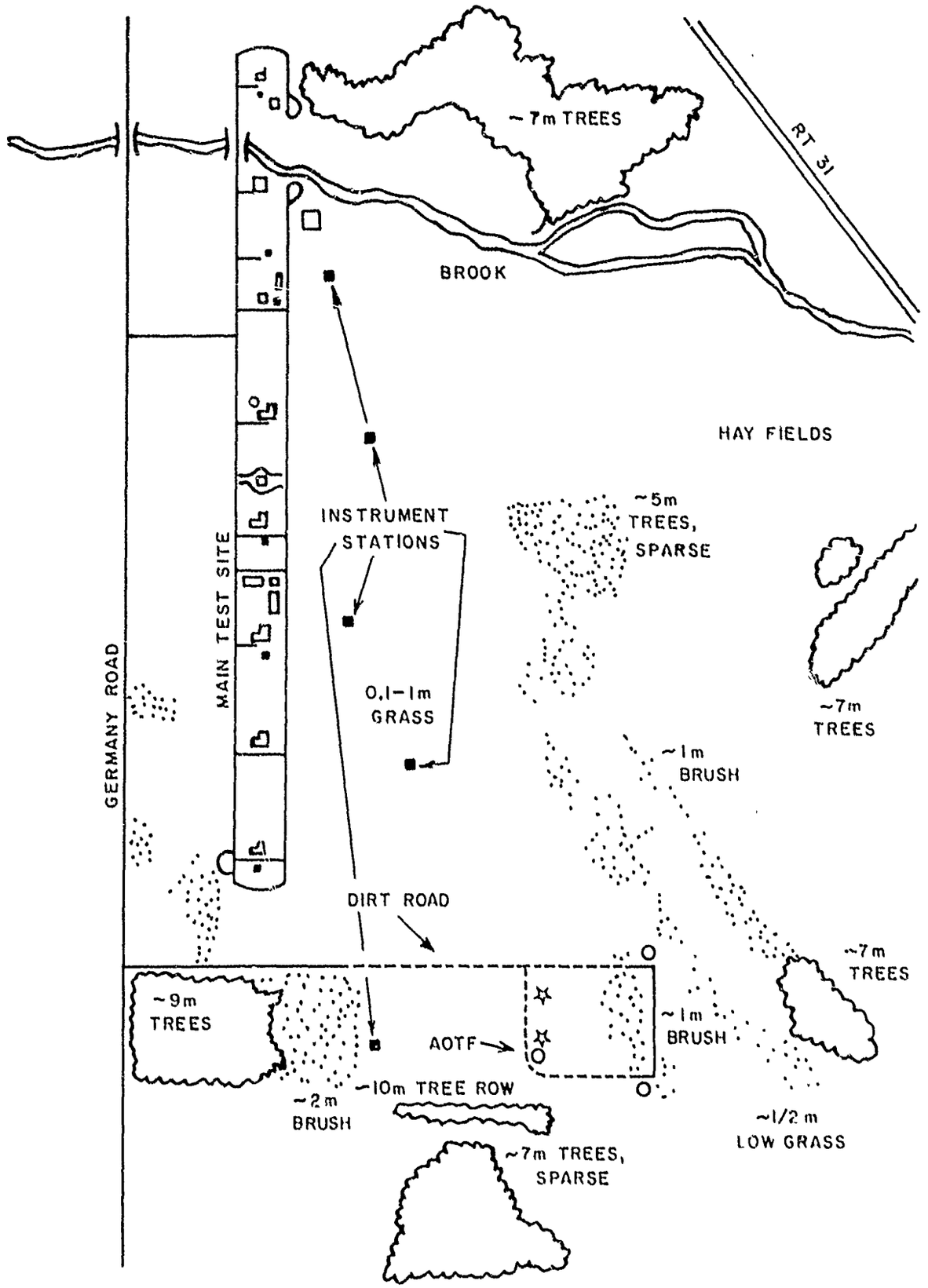

Figure 1. Terrain around the AOTF. Instrument towers: ☆

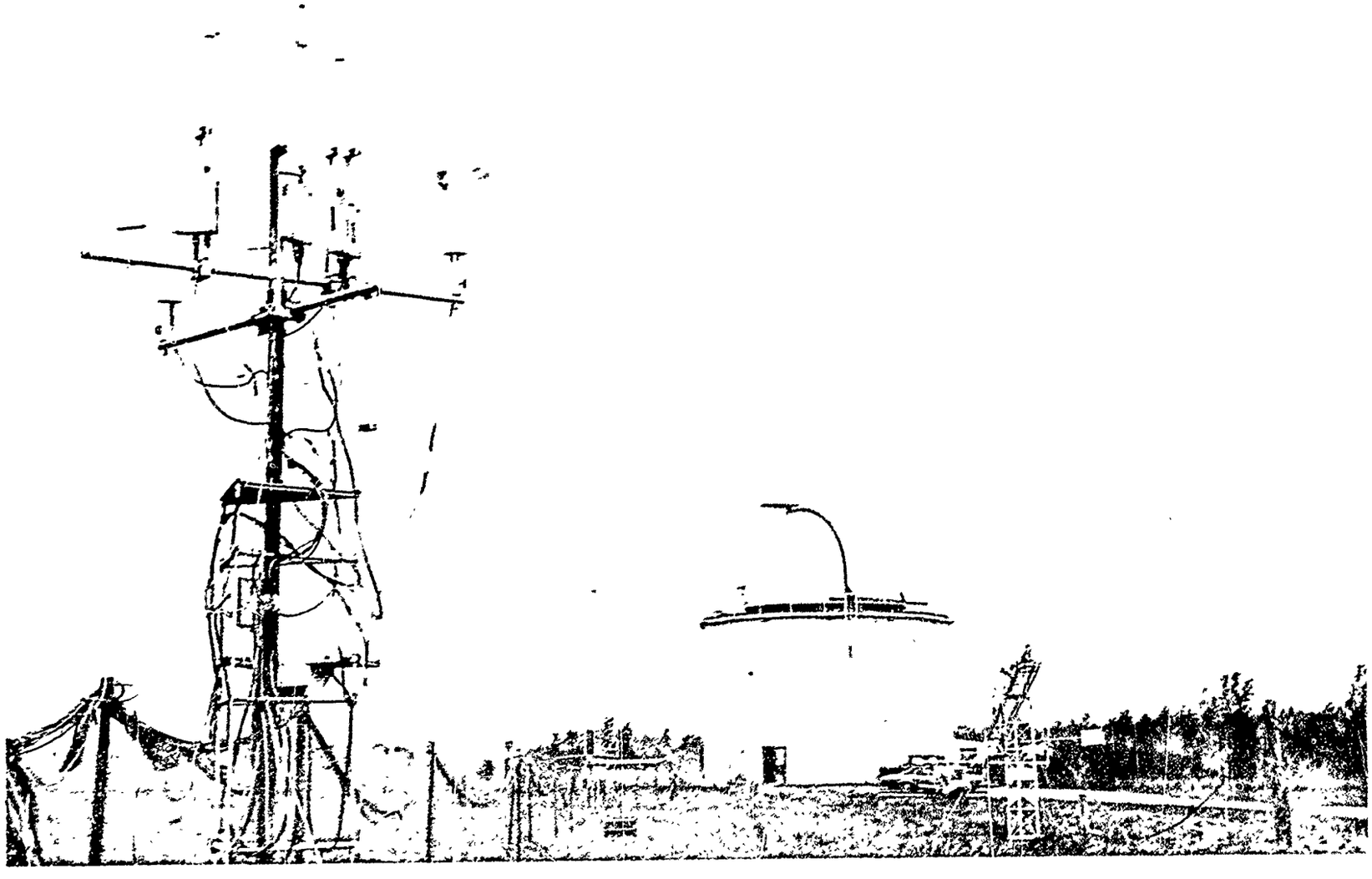

Figure 2. Instrument tower.

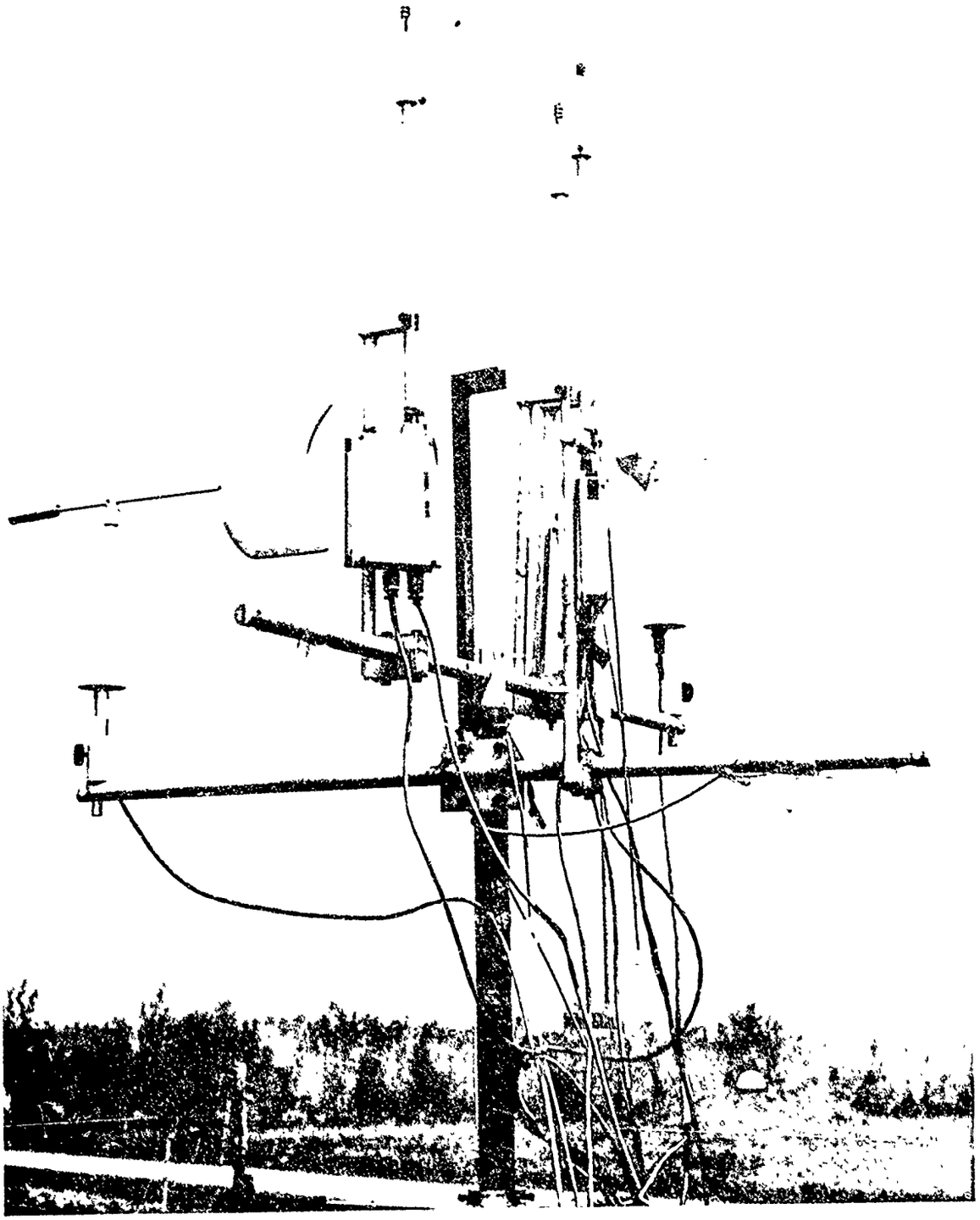

Figure 3. Microturbulence probes.

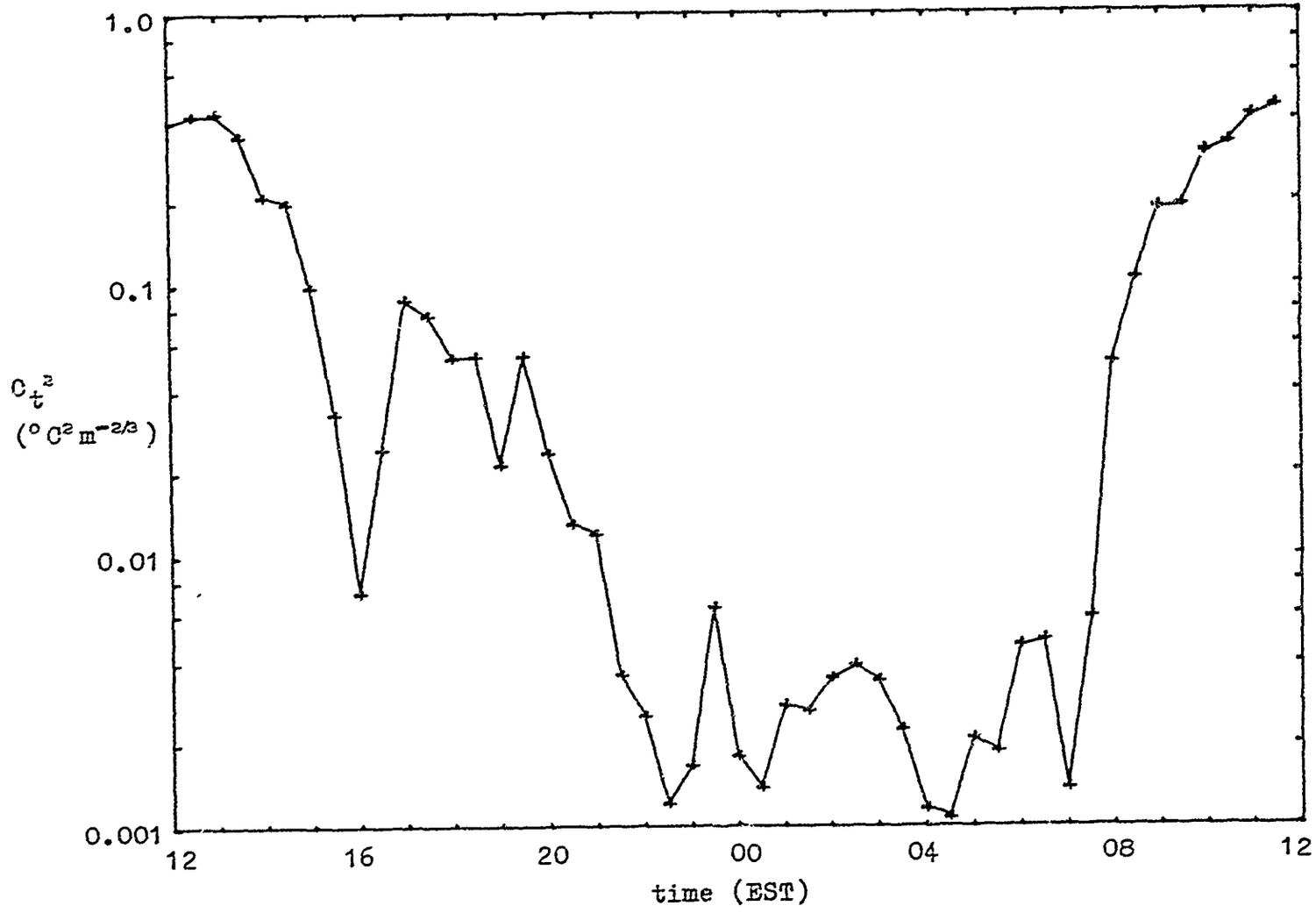

Figure 4. Example of Type I turbulence (1 Feb 75).

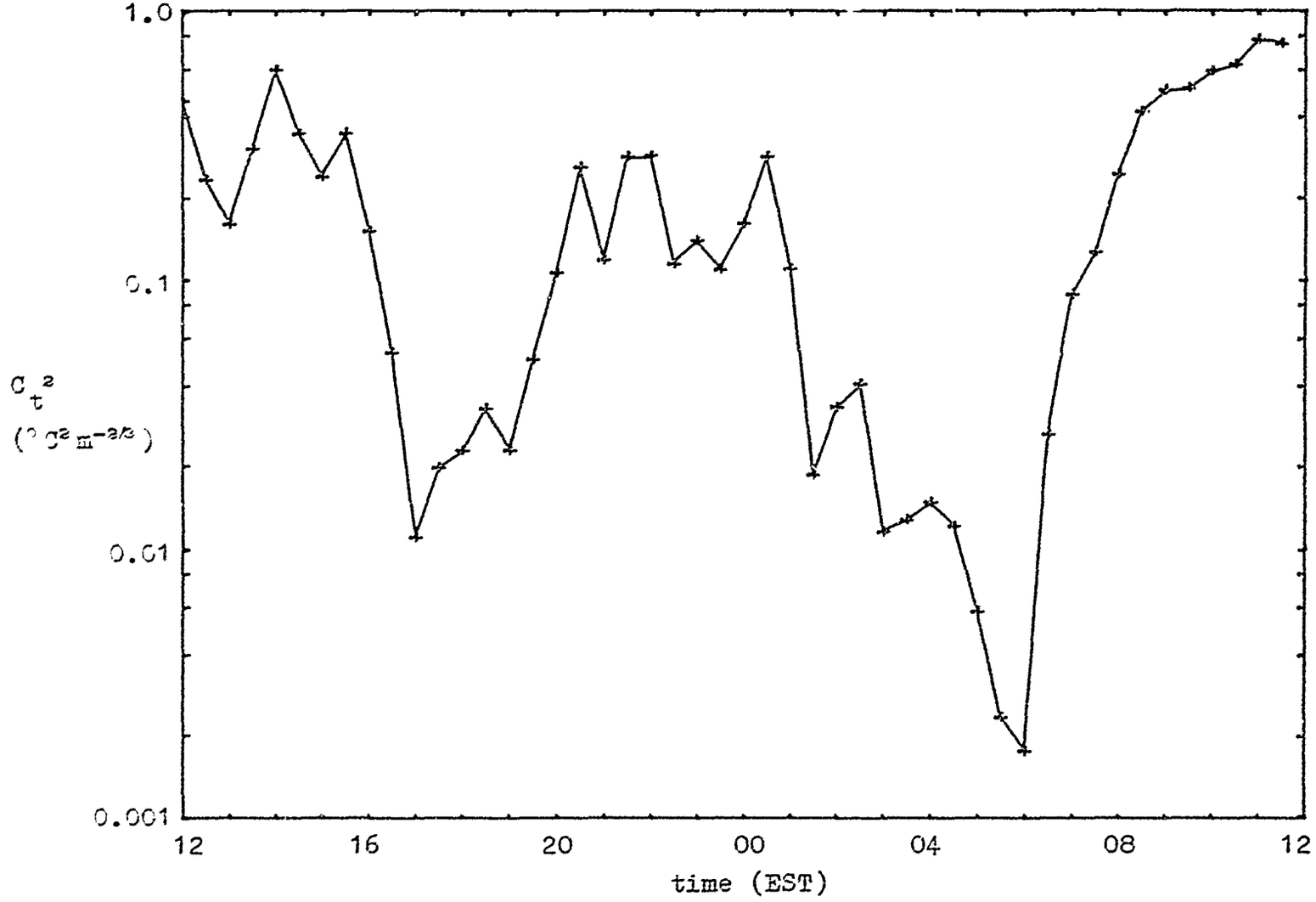

Figure 5. Example of Type II turbulence (29 Apr 75).

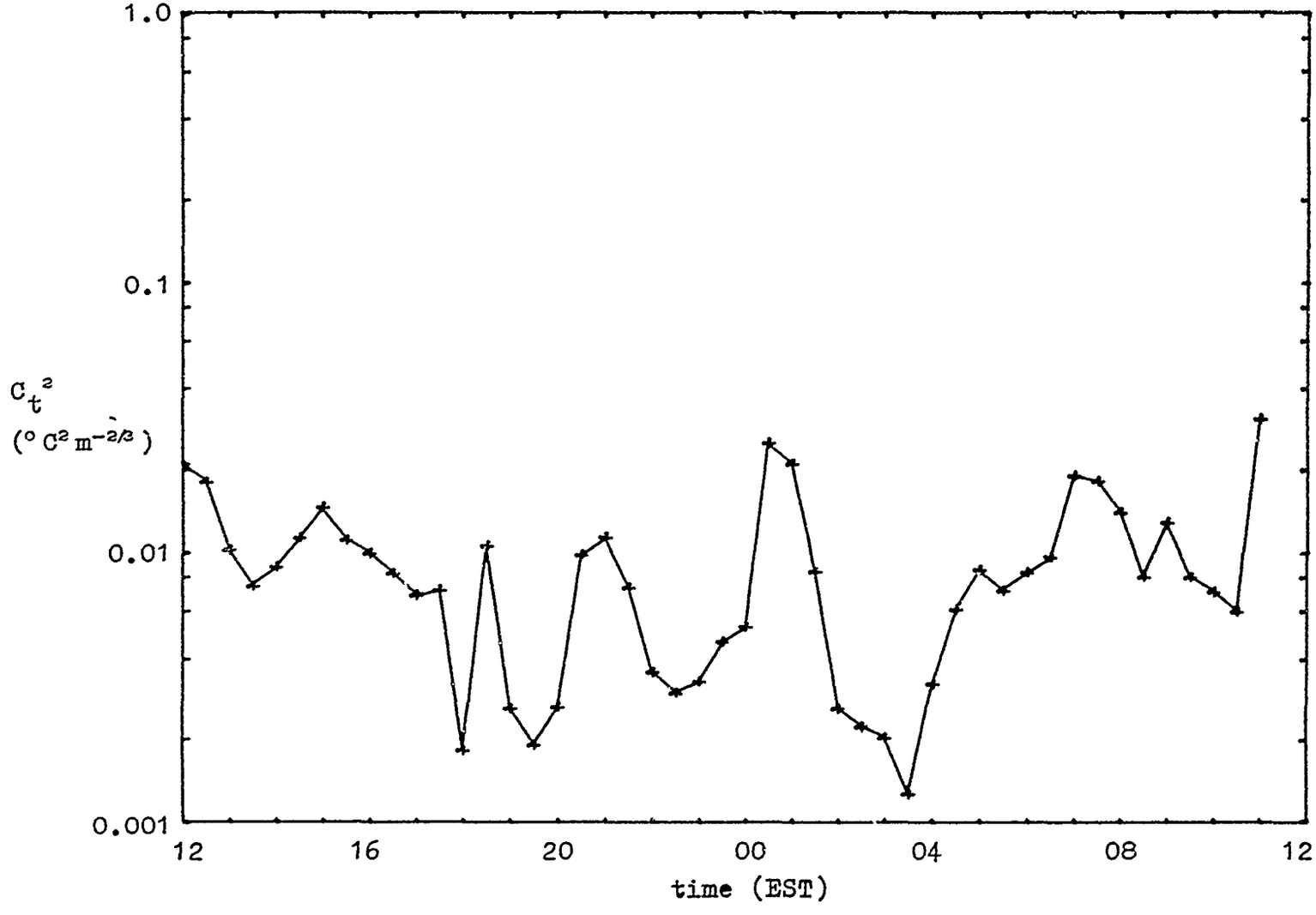

Figure 6. Example of Type III turbulence (20 Feb 75).

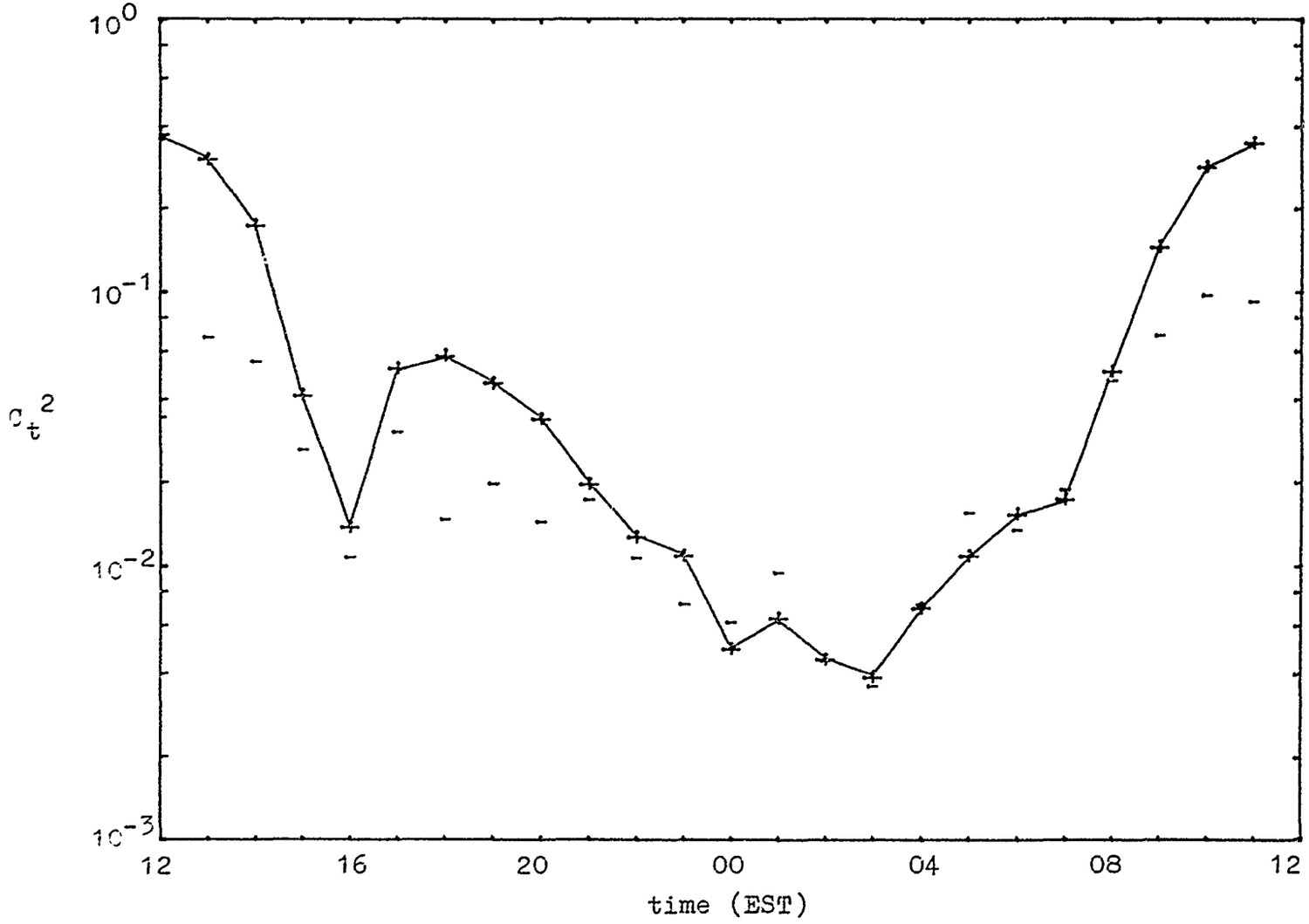

Figure 7. Mean (+) and std. dev. (-) for Type I turbulence: February 1975.

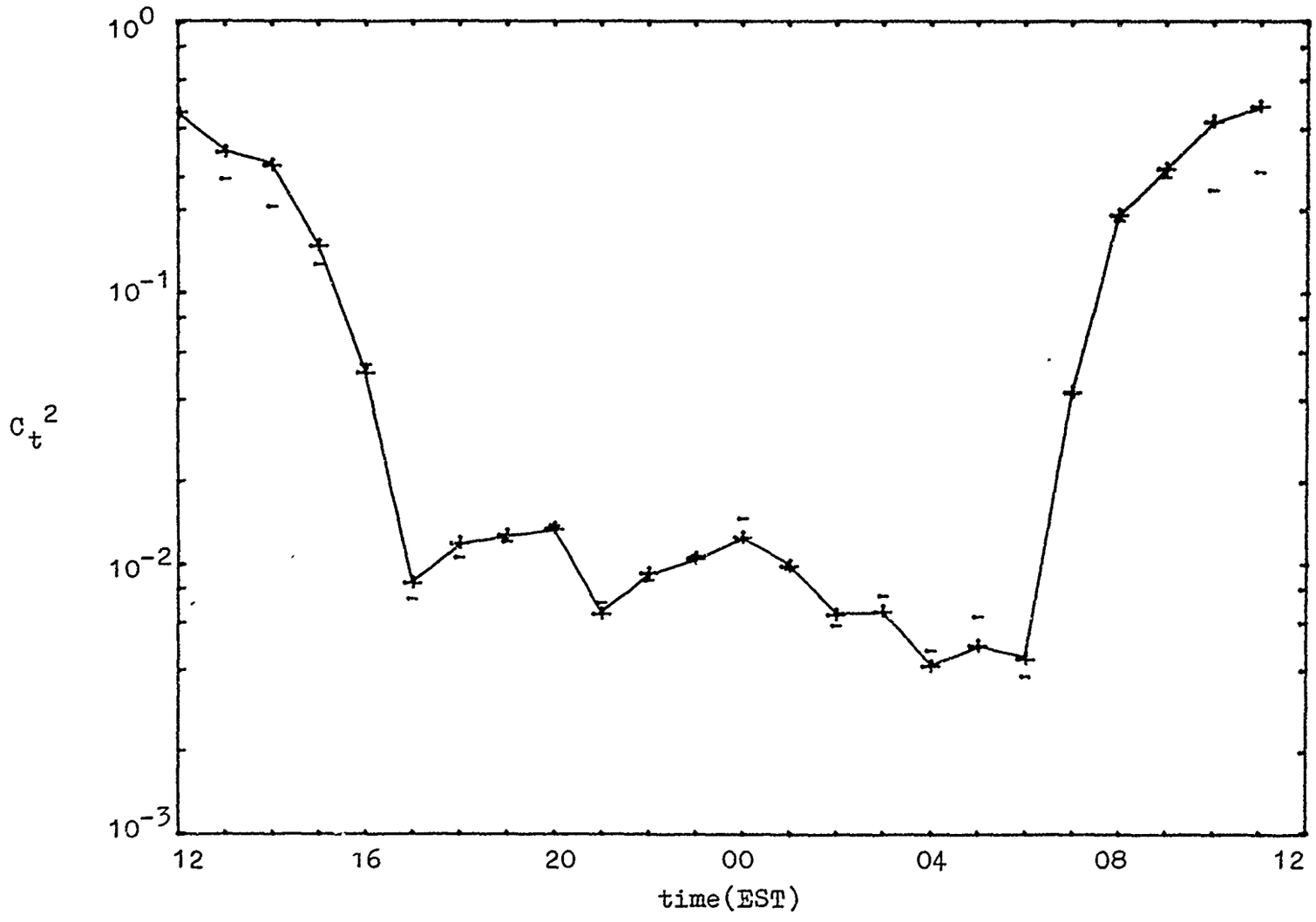

Figure 8. Mean (+) and std. dev. (-) for Type I turbulence: March 1975.

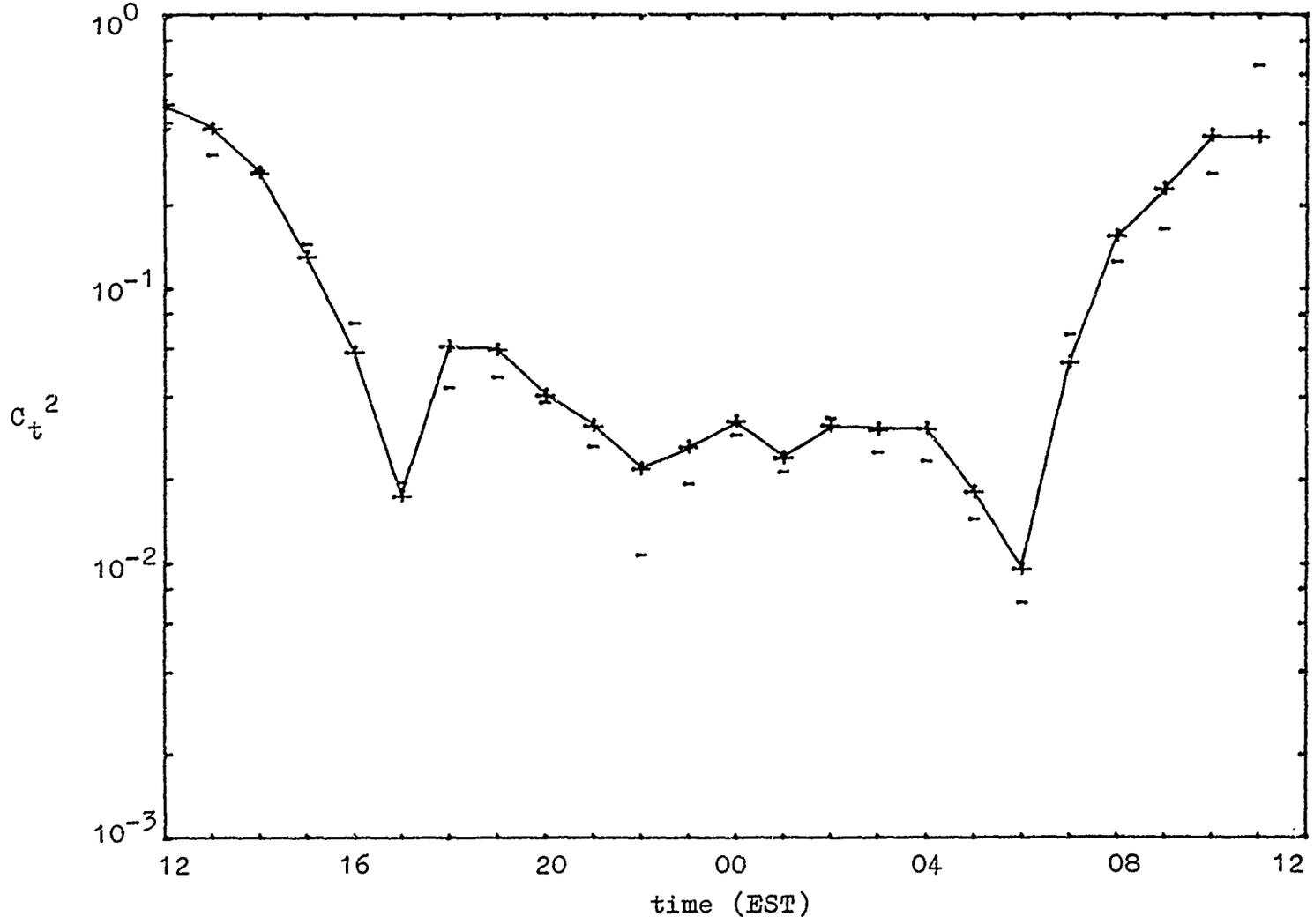

Figure 9. Mean (+) and std. dev. (-) for Type I turbulence: April 1975.

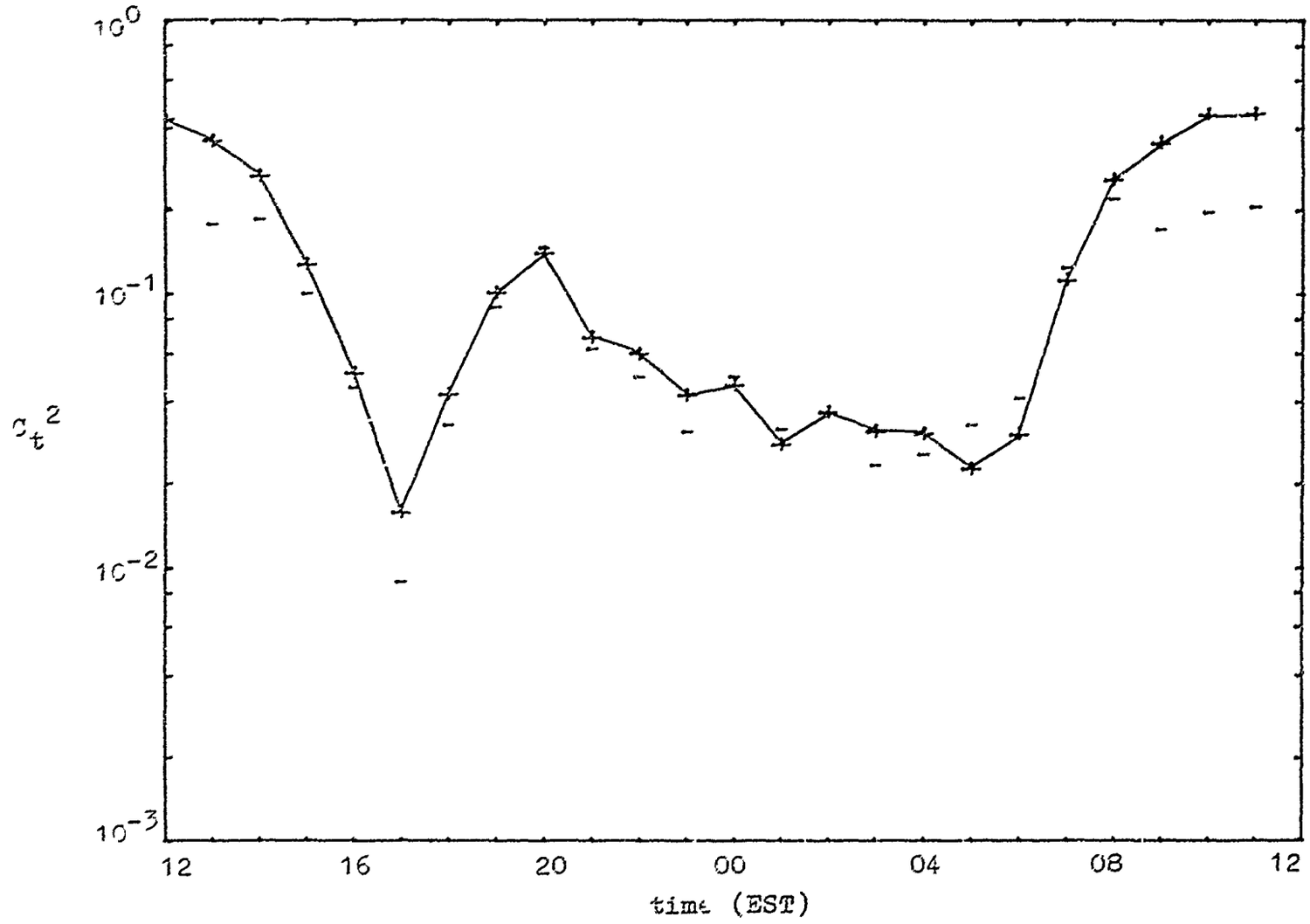

Figure 10. Mean (+) and std. dev. (-) for Type I turbulence: May 1975.

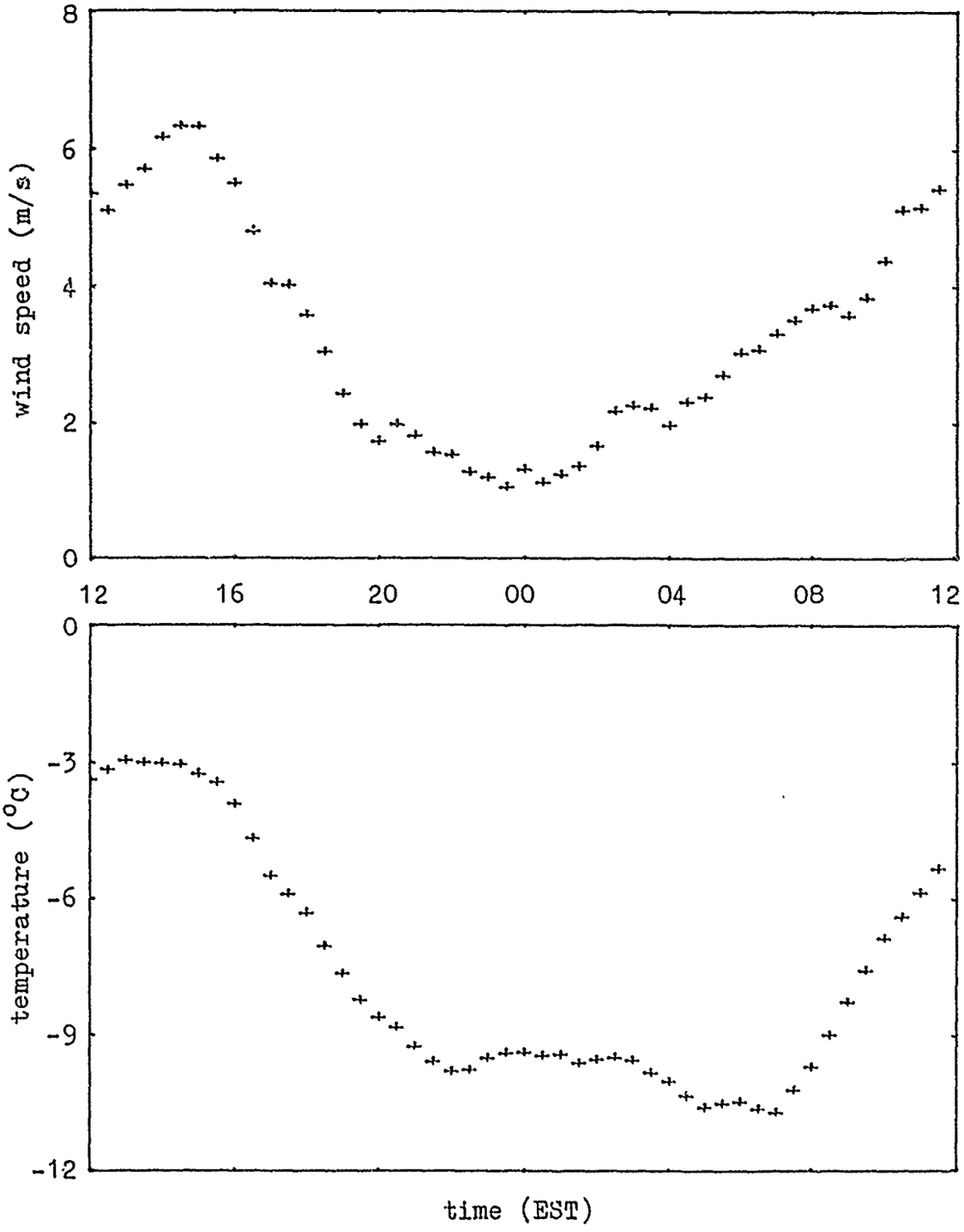

Figure 11. Average wind speed and ambient temperature recorded during periods of Type I turbulence: February 1975.

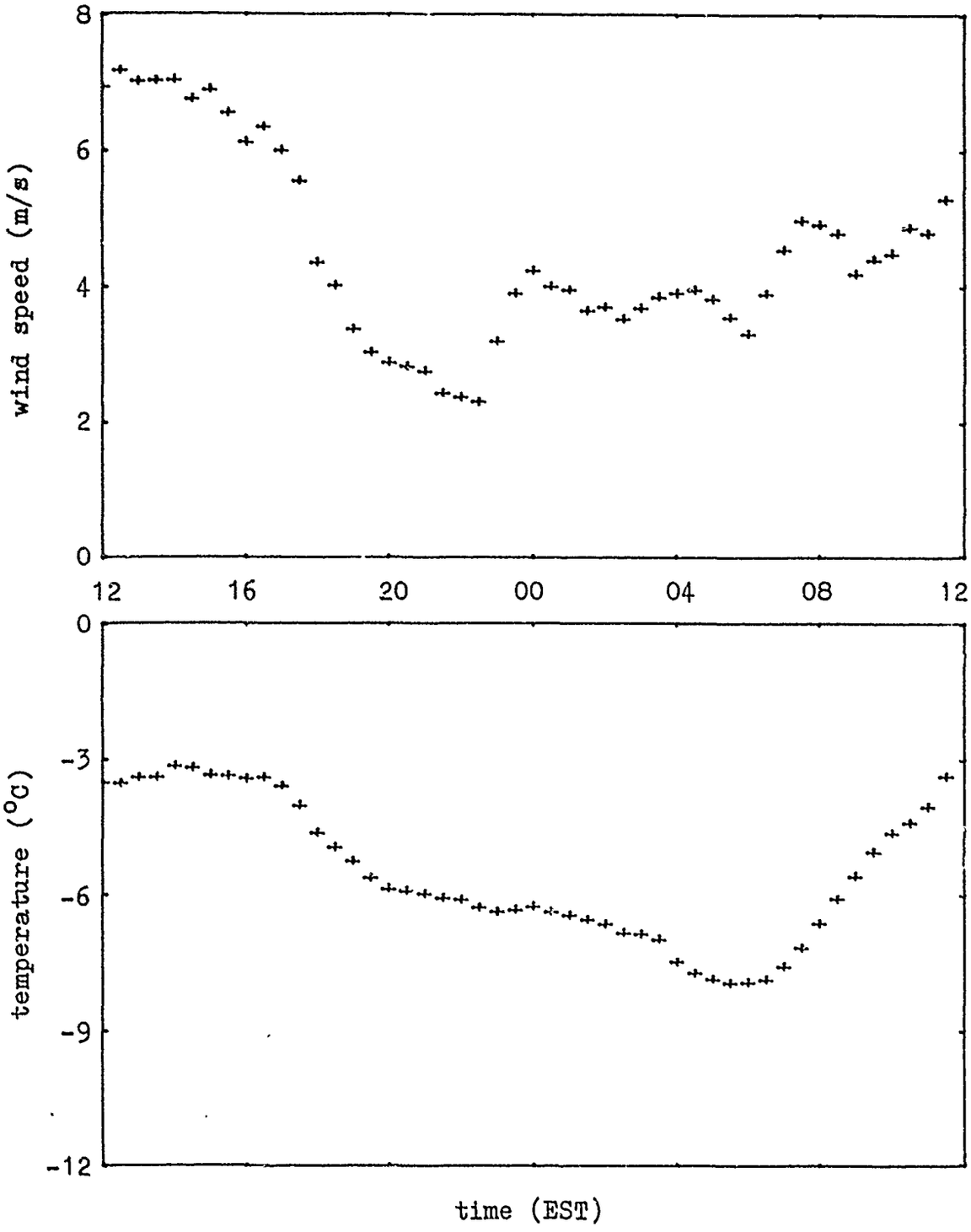

Figure 12. Average wind speed and ambient temperature recorded during periods of Type I turbulence: March 1975.

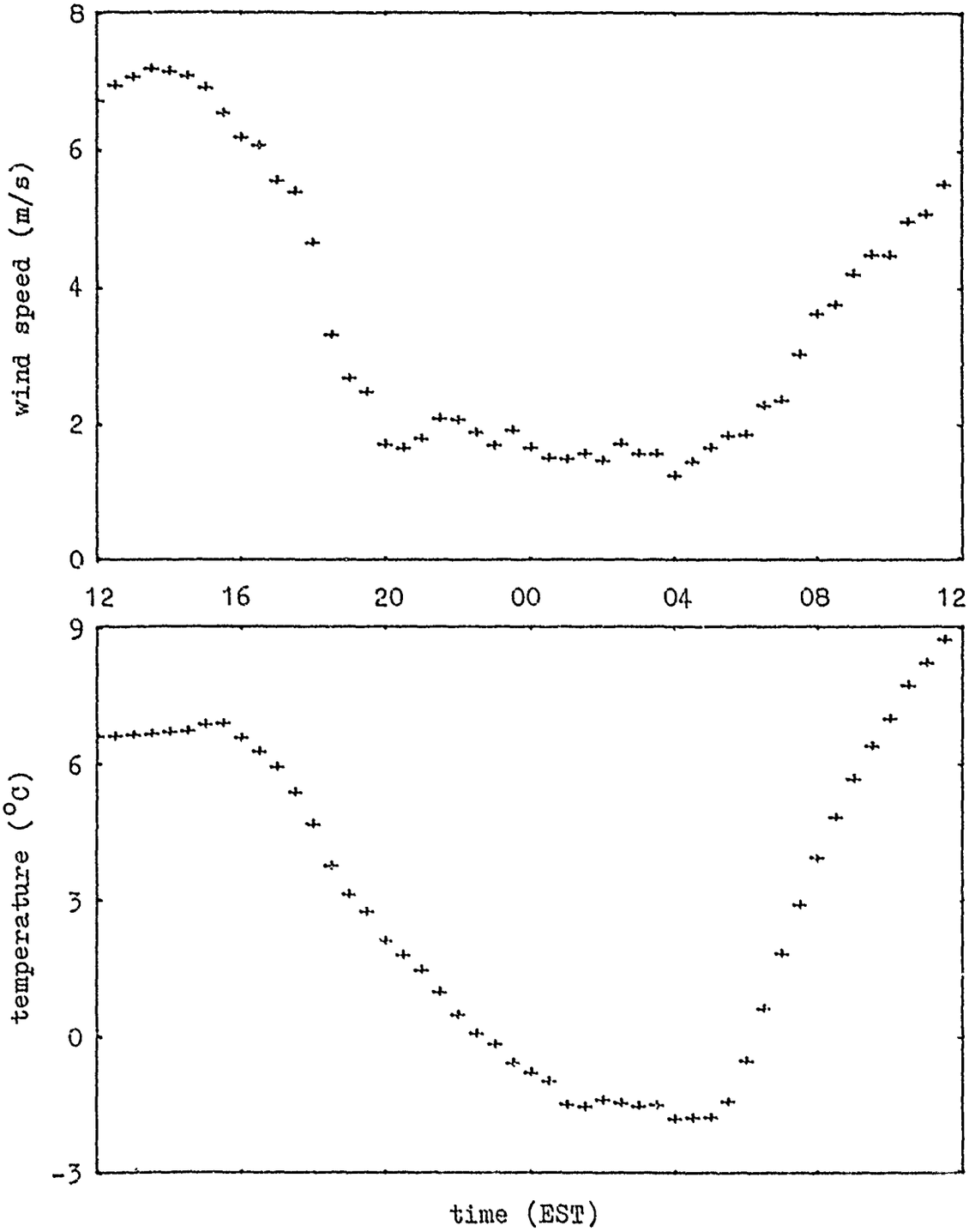

Figure 13. Average wind speed and ambient temperature recorded during periods of Type I turbulence: April 1975.

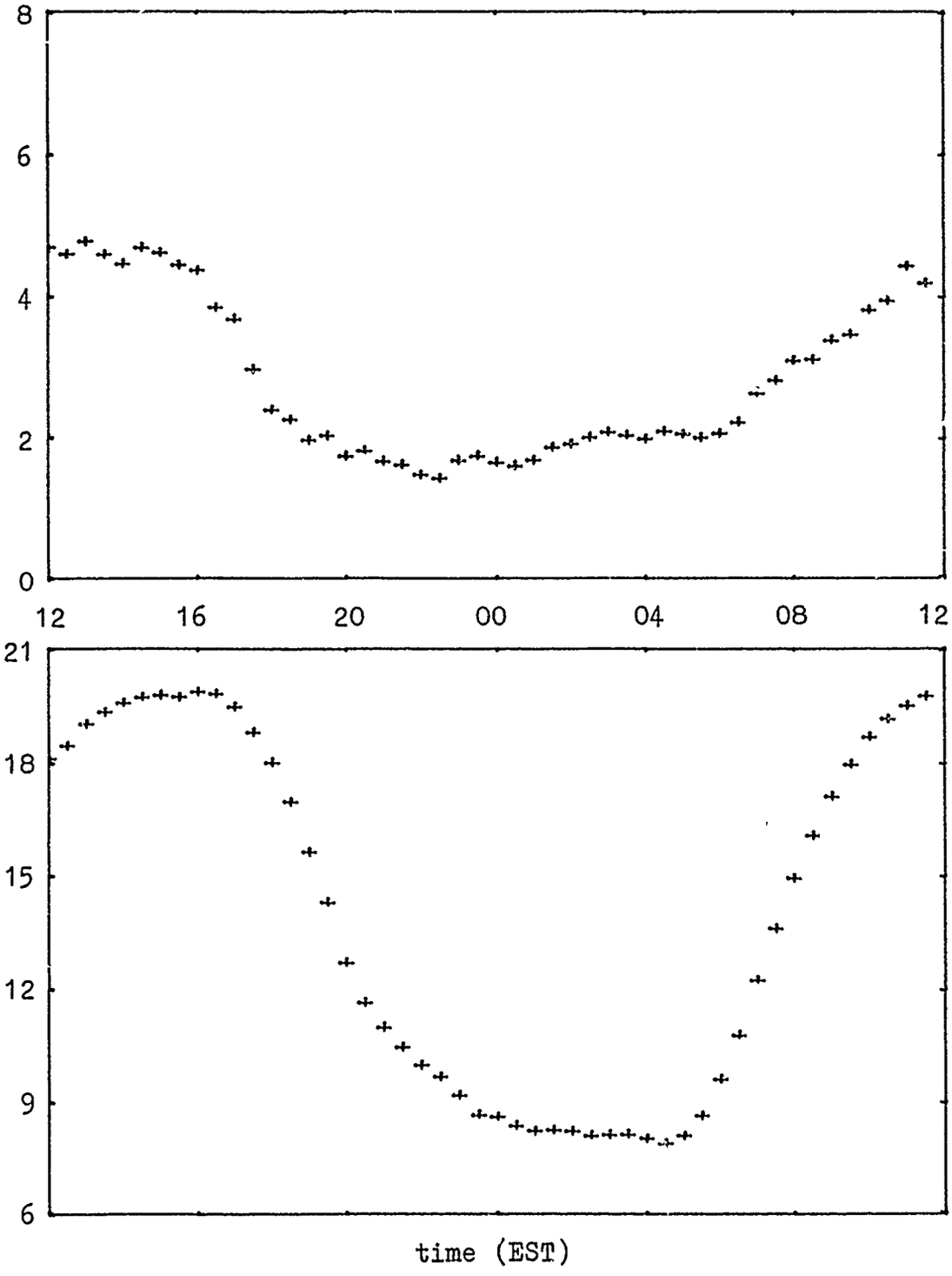

Figure 14. Average wind speed and ambient temperature recorded during periods of Type I turbulence: May 1975.

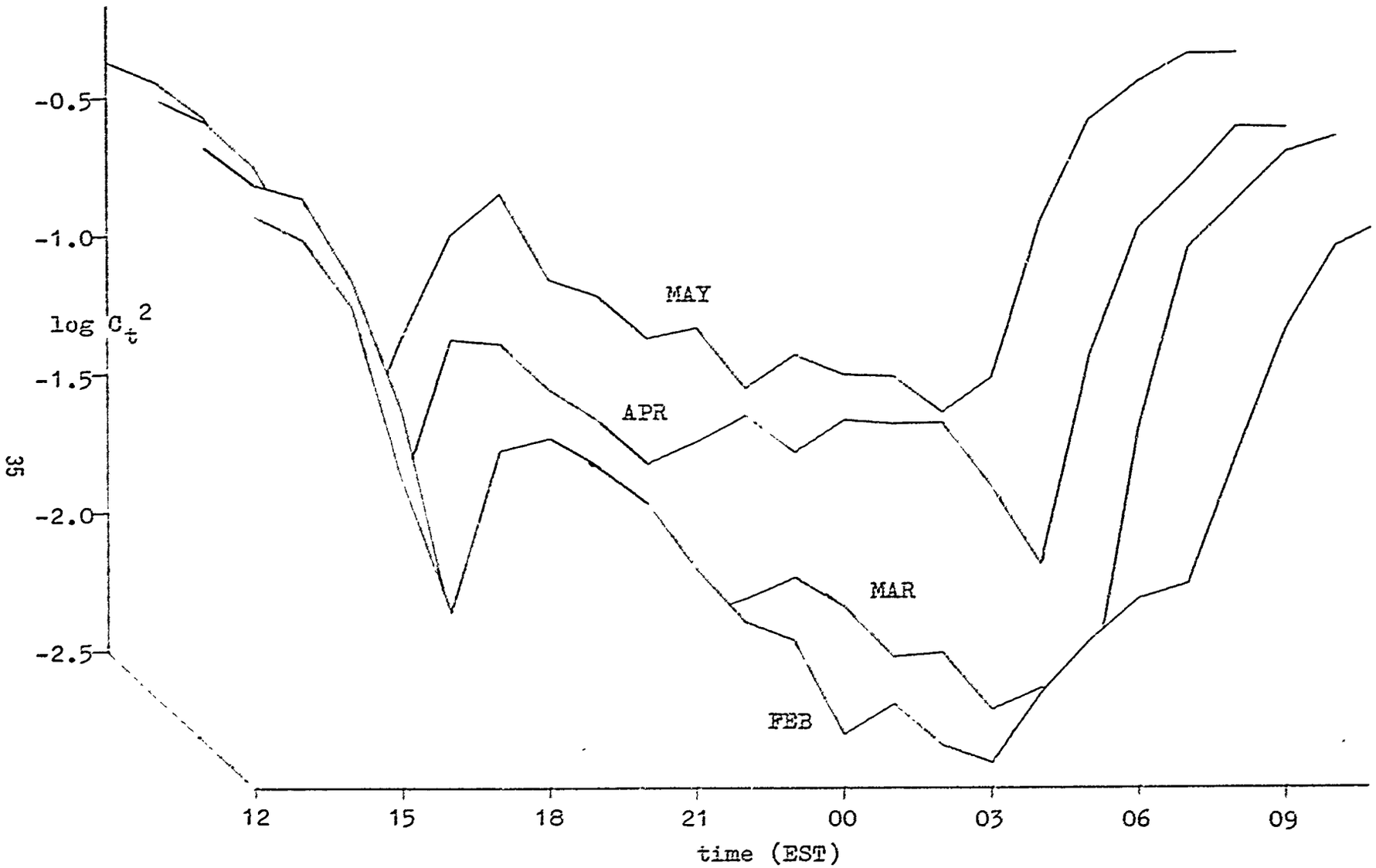

Figure 15. Mean values of Type I turbulence: February - May 1975.

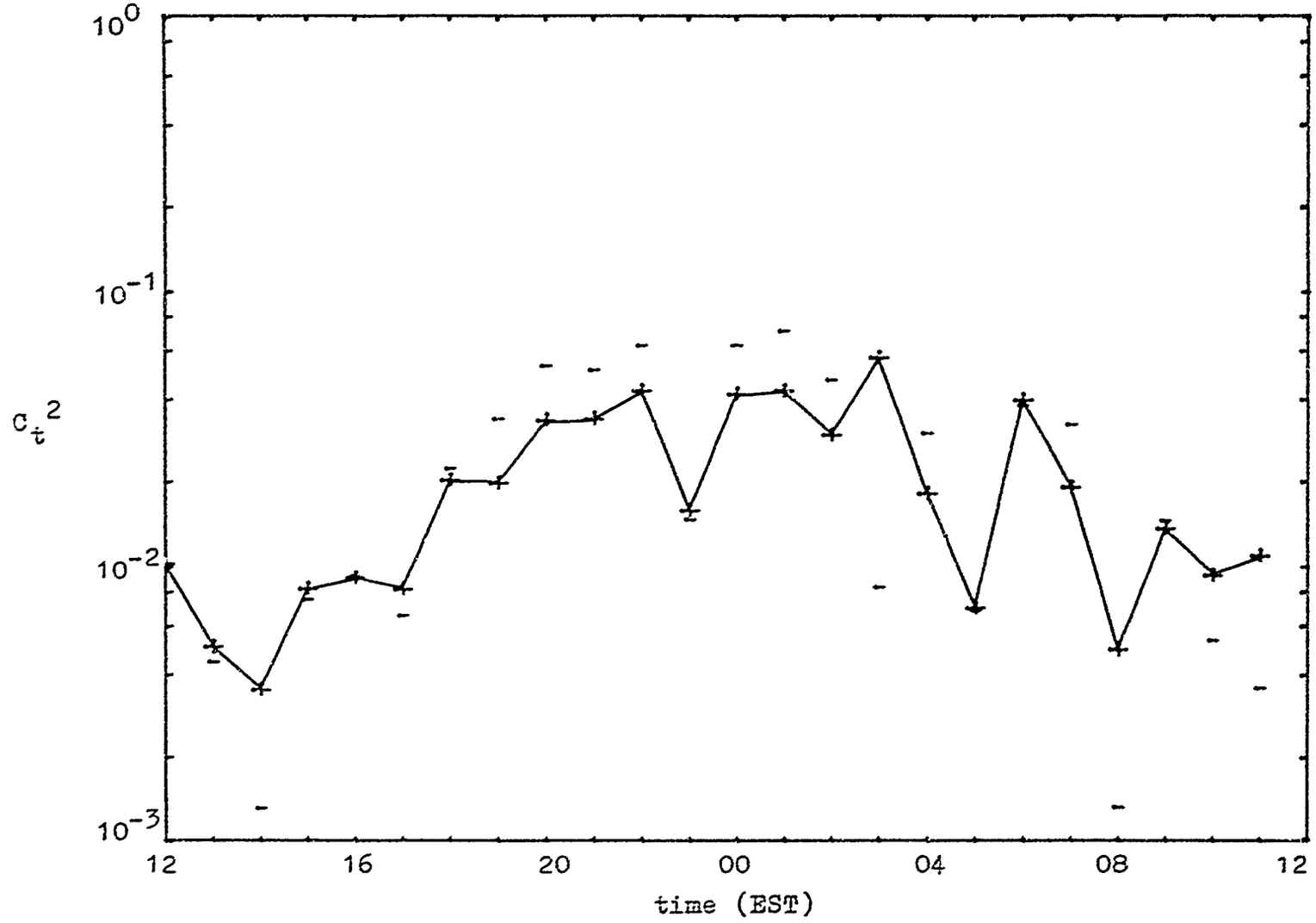

Figure 16. Mean (+) and std. dev. (-) for Type II turbulence: February 1975.

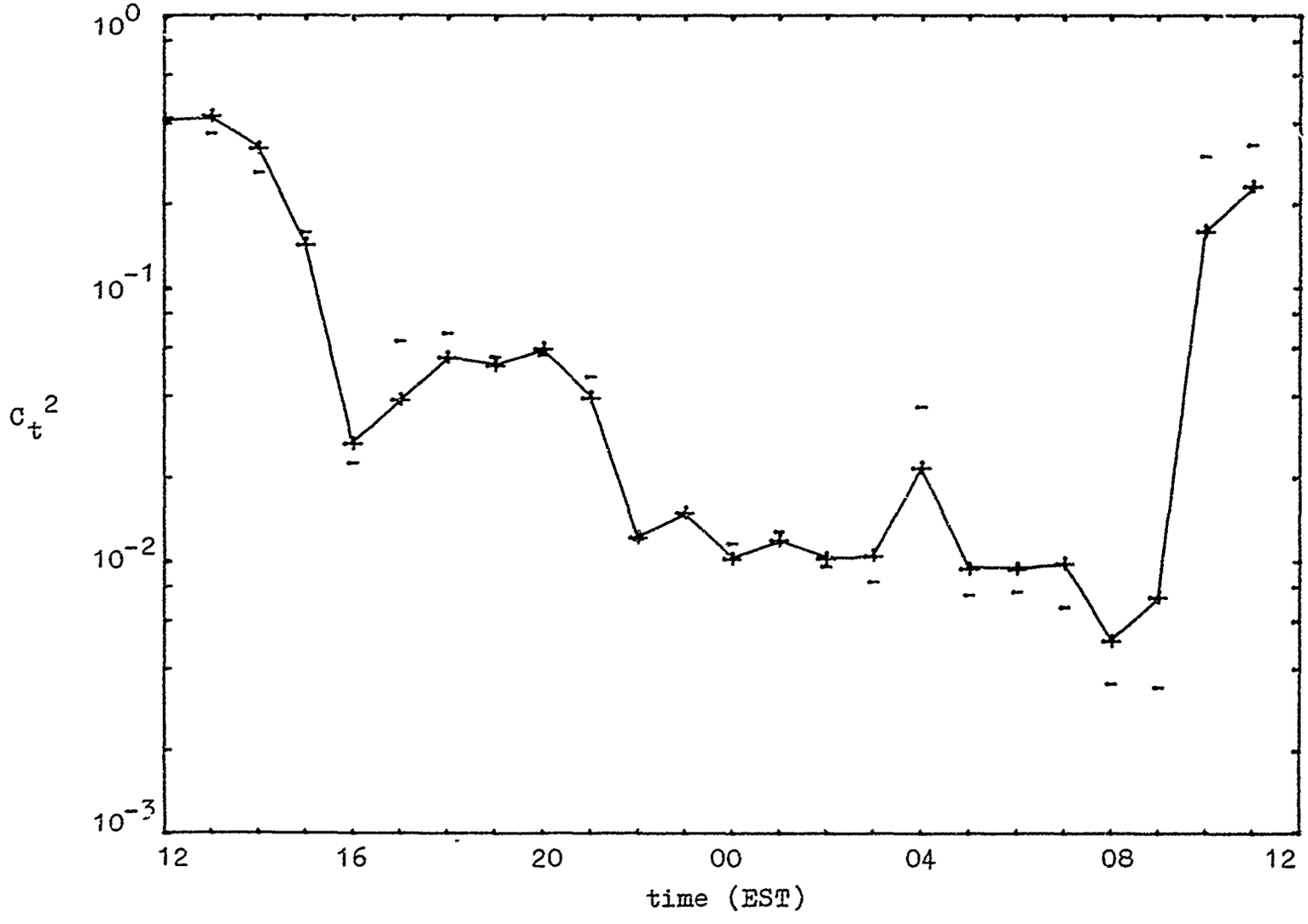

Figure 17. Mean (+) and std. dev. (-) for Type II turbulence: March 1975.

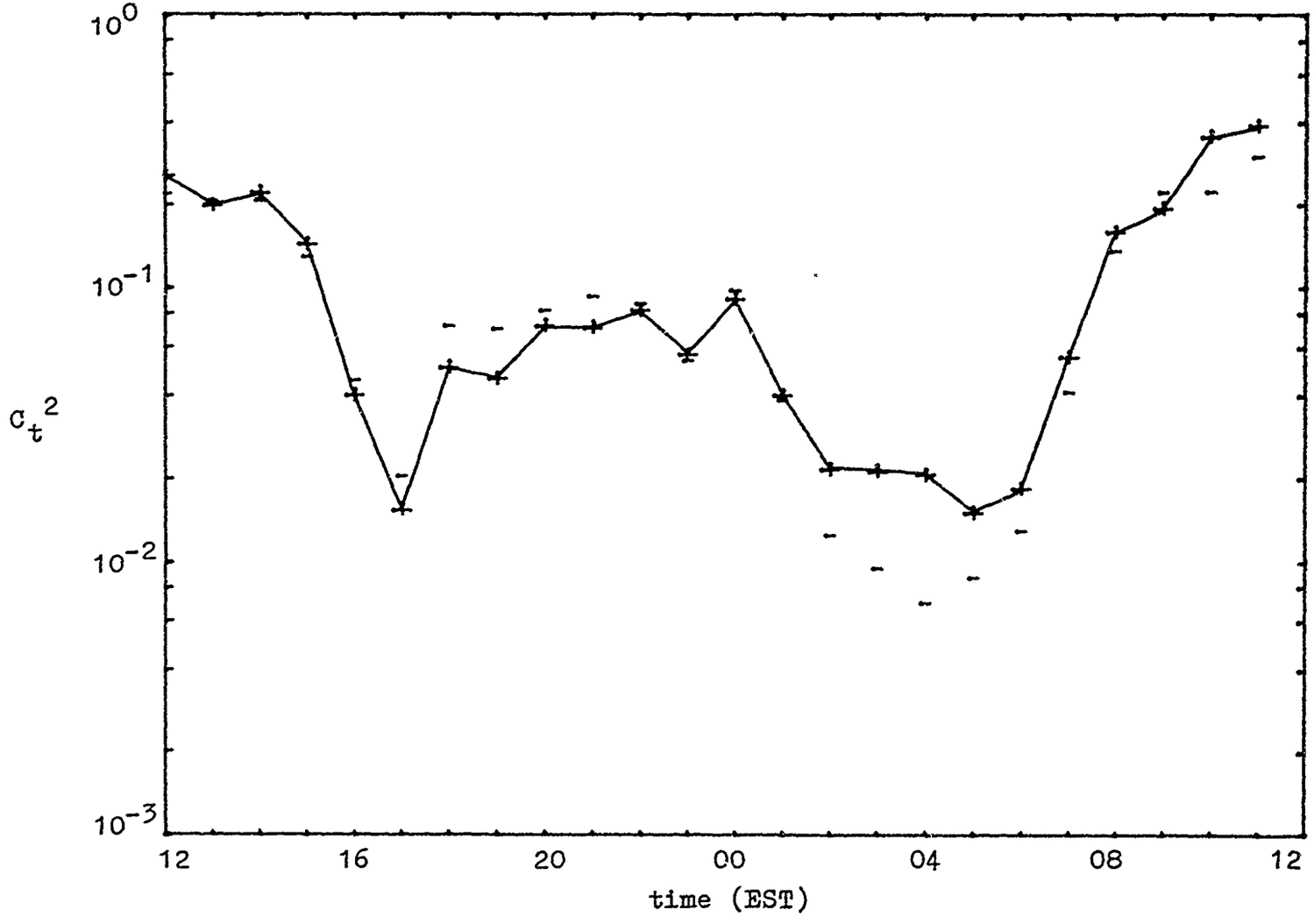

Figure 18. Mean (+) and std. dev. (-) for Type II turbulence: April 1975.

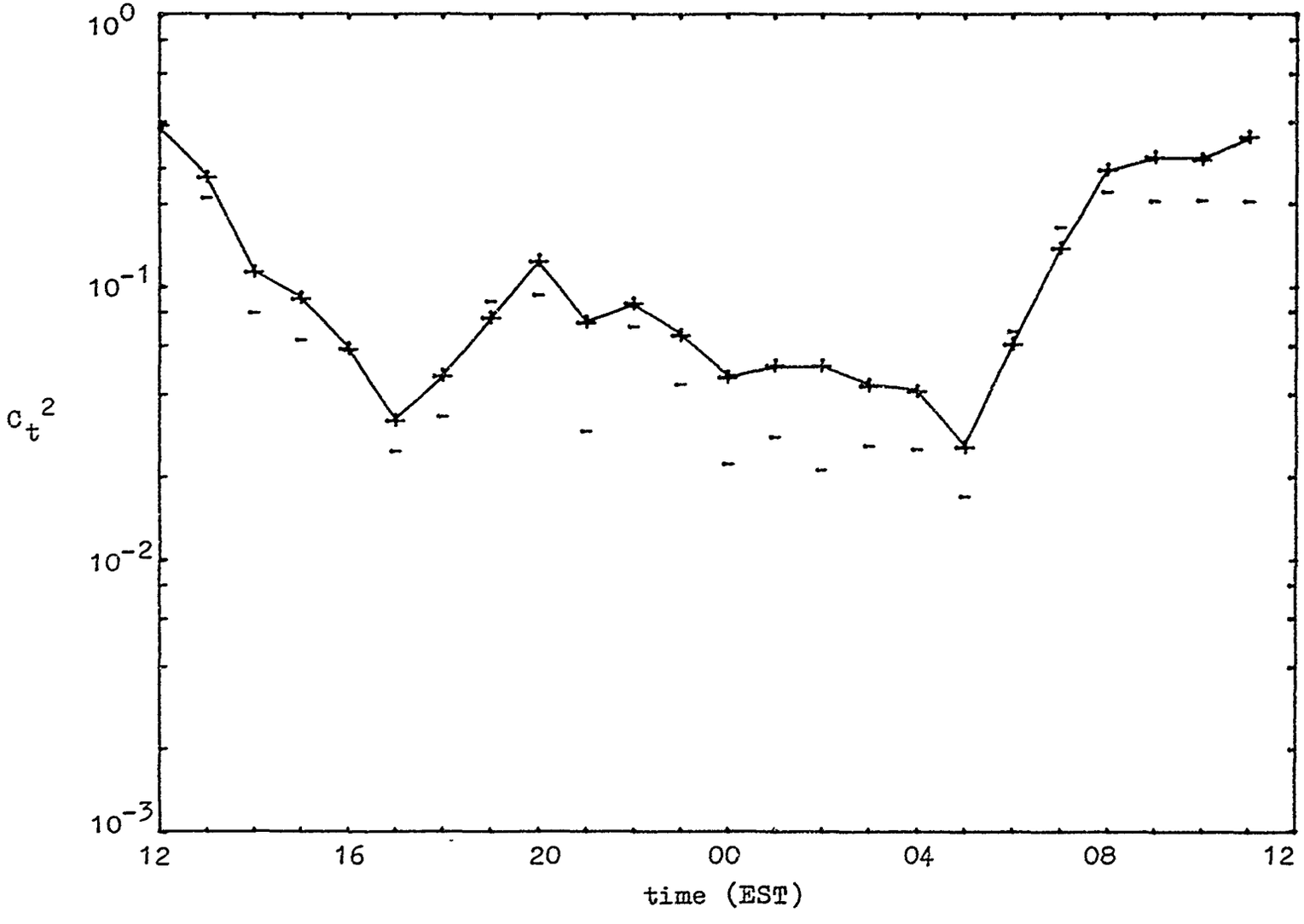

Figure 19. Mean (+) and std. dev. (-) for Type II turbulence: May 1975.

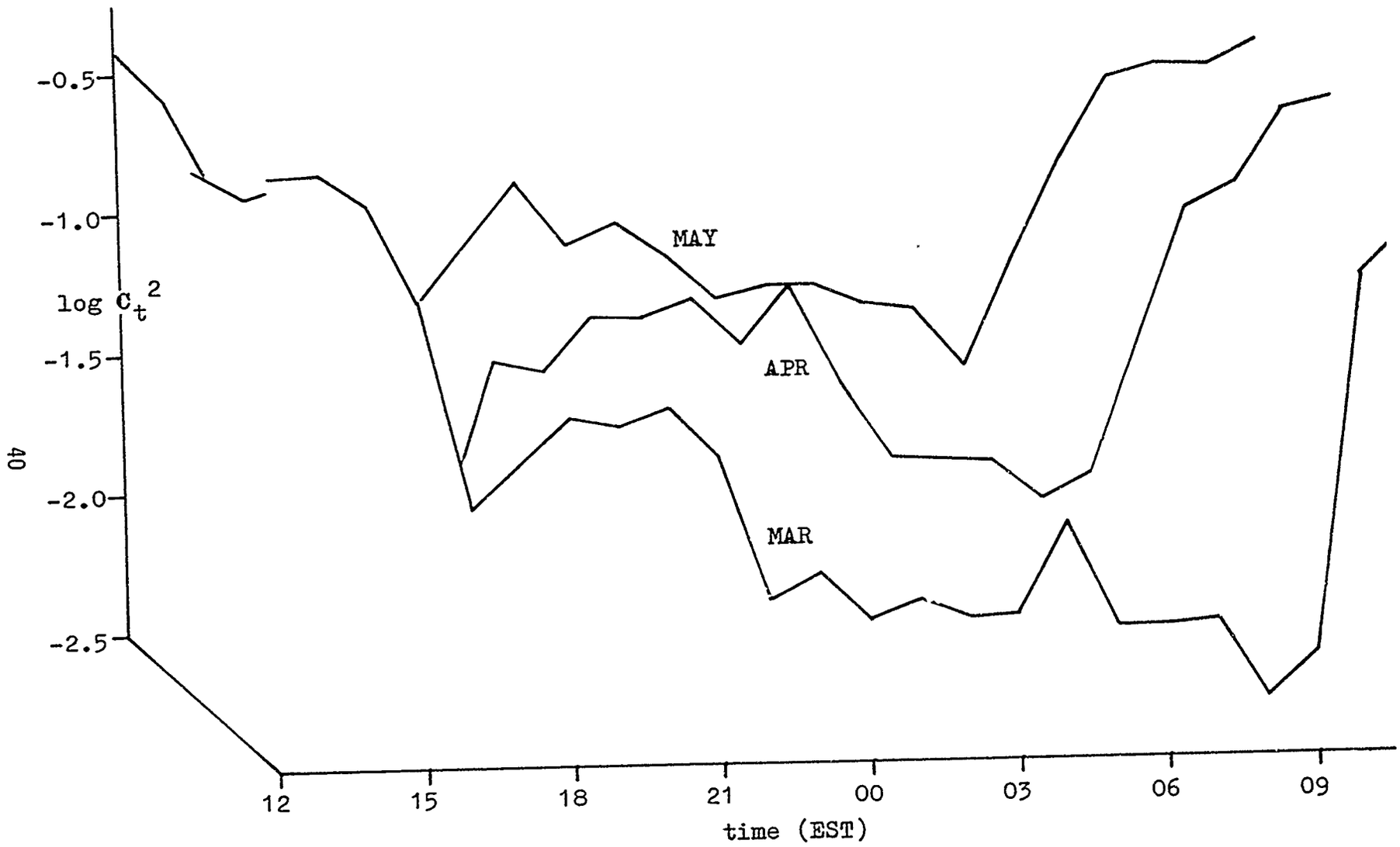

Figure 20. Mean values of Type II turbulence: March - May 1975.

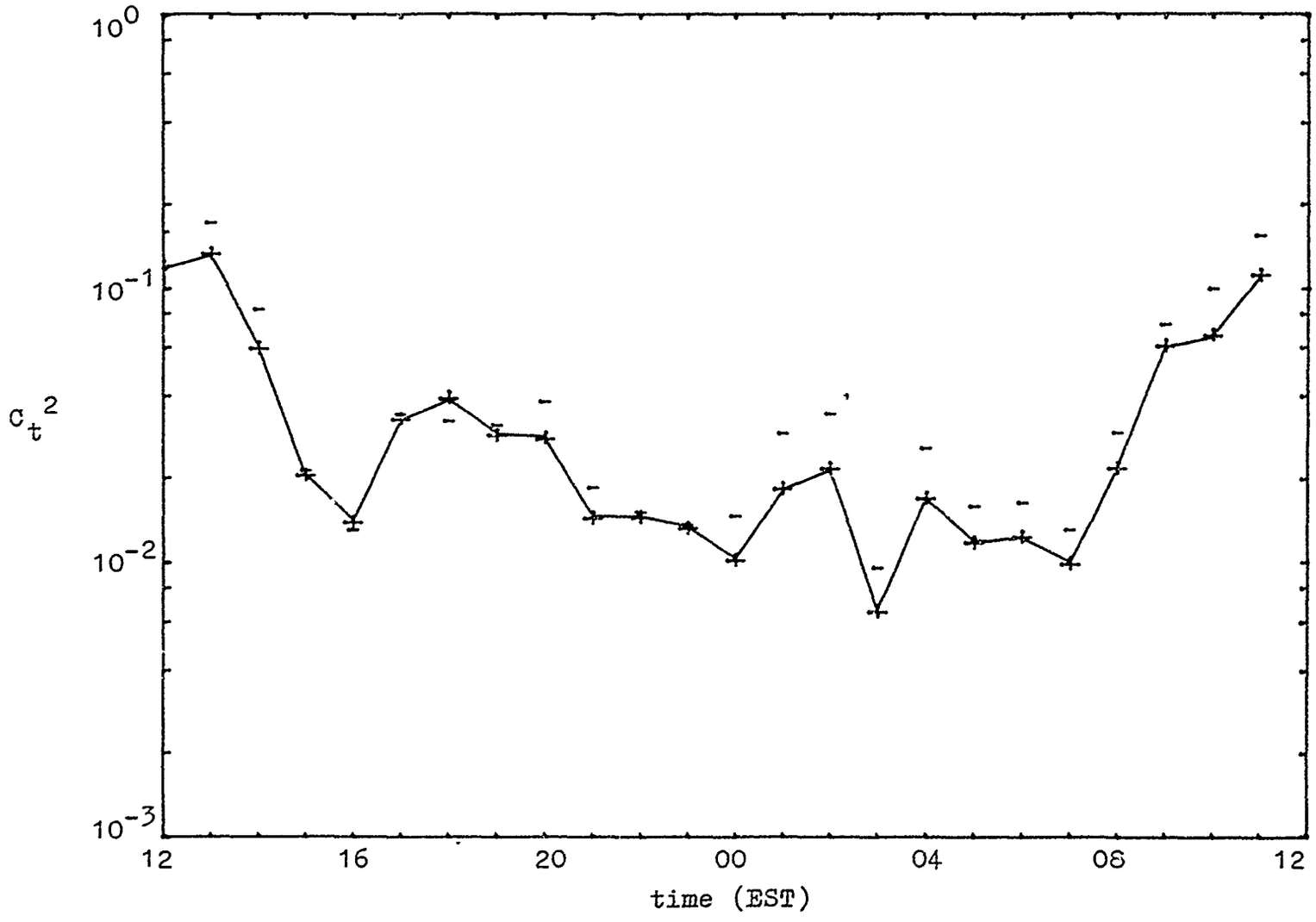

Figure 21. Mean (+) and std. dev. (-) for "all weather": February 1975.

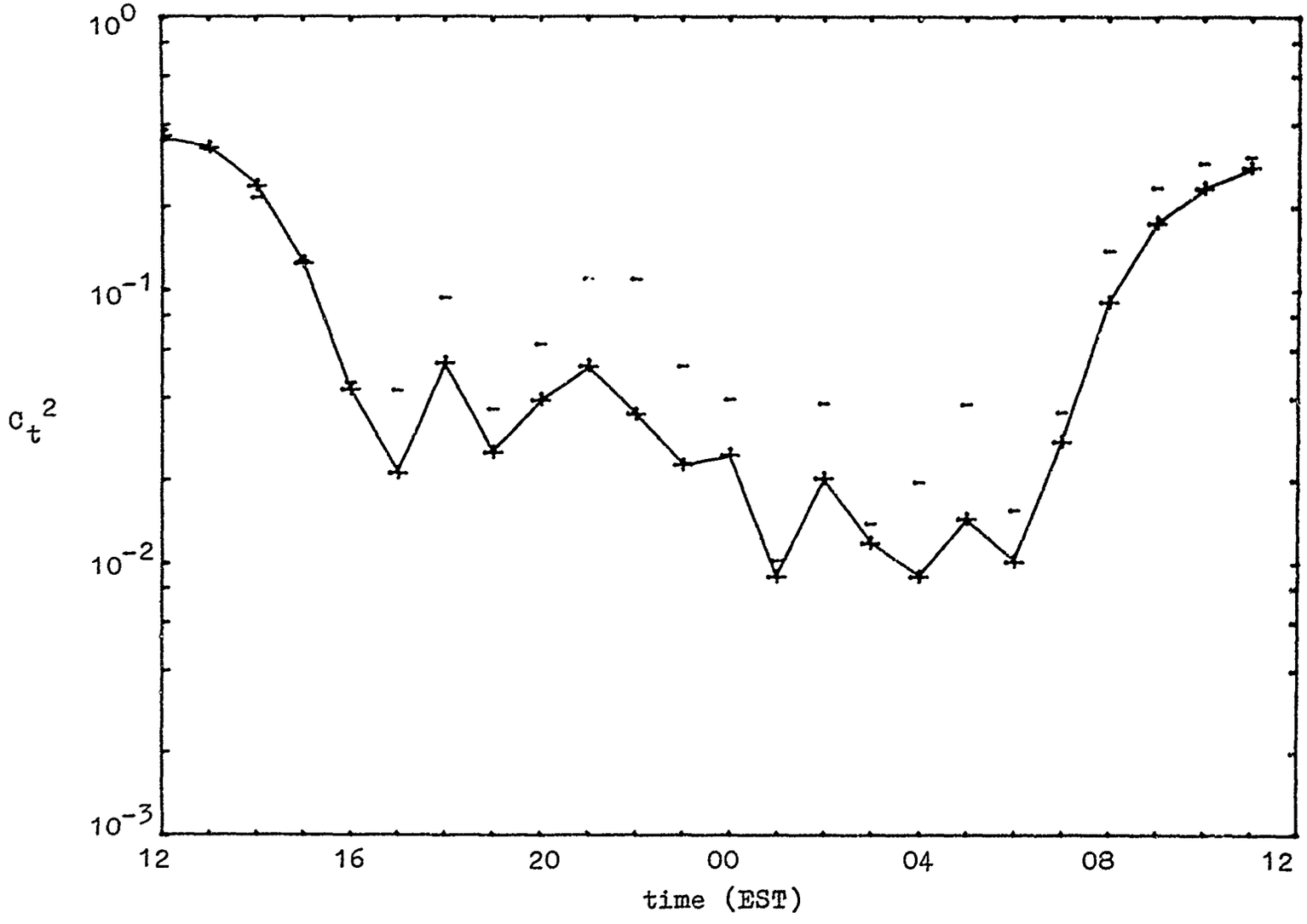

Figure 22. Mean (+) and std. dev. (-) for "all weather": March 1975.

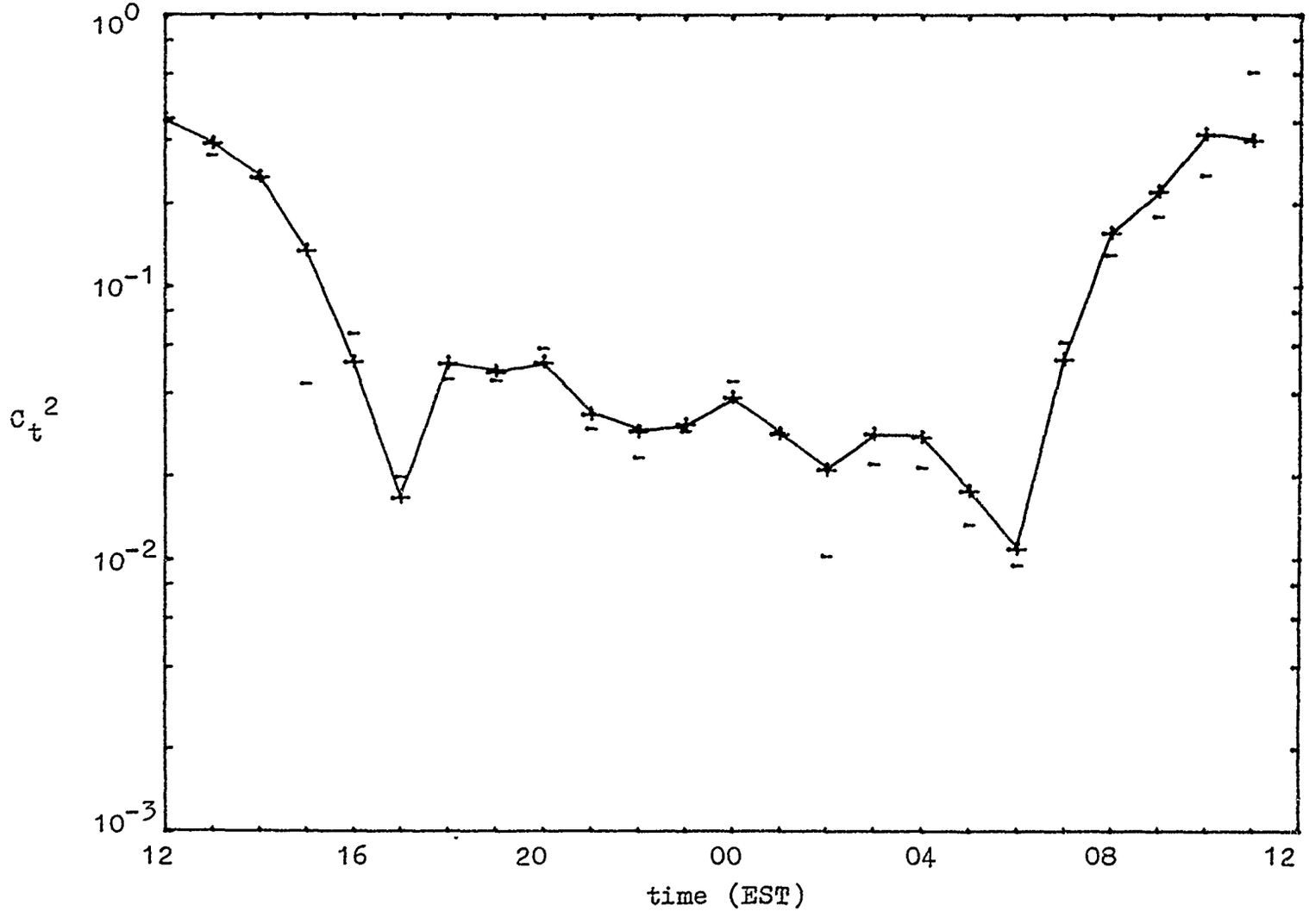

Figure 23. Mean (+) and std. dev. (-) for "all weather": April 1975.

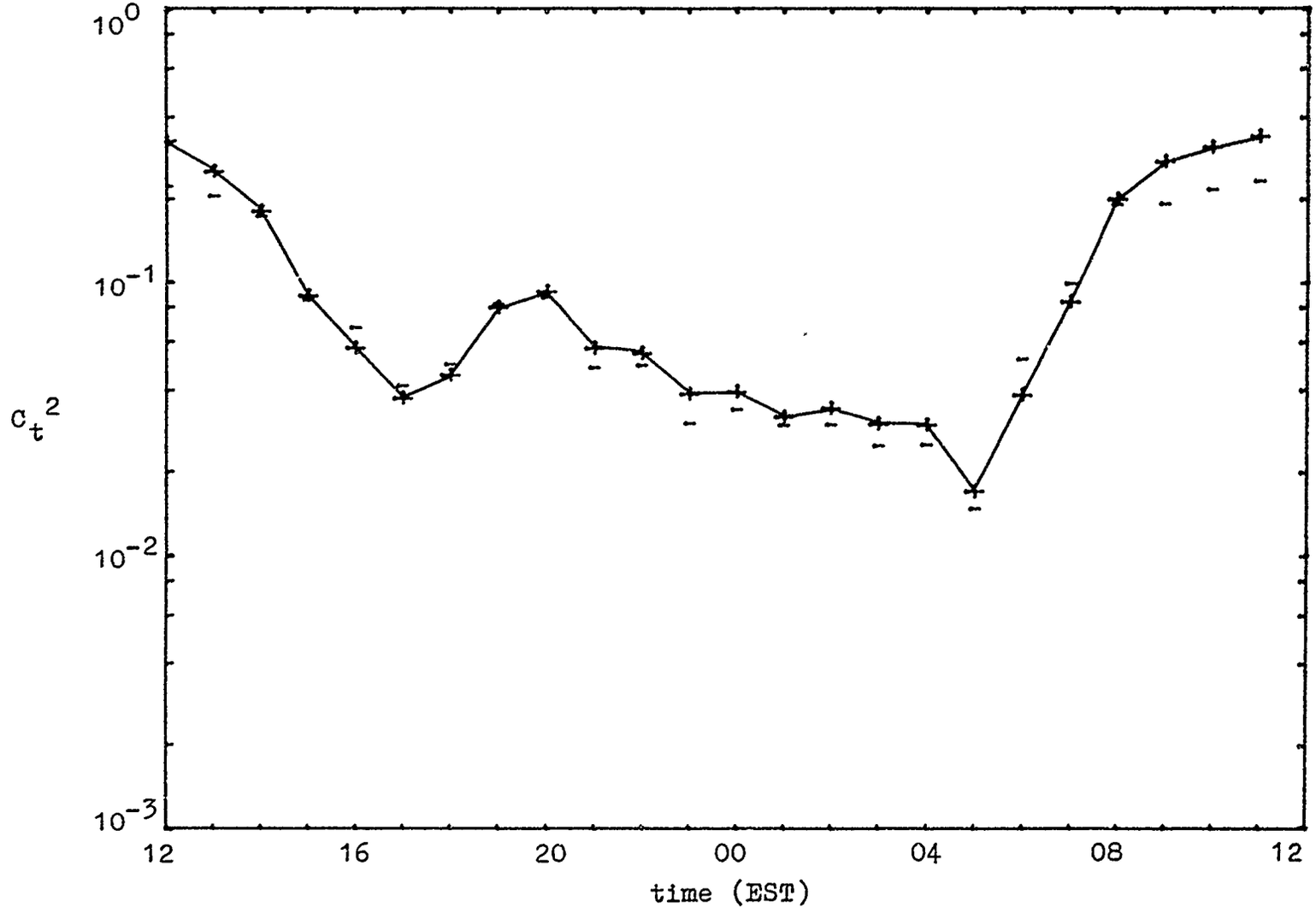

Figure 24. Mean (+) and std. dev. (-) for "all weather": May 1975.

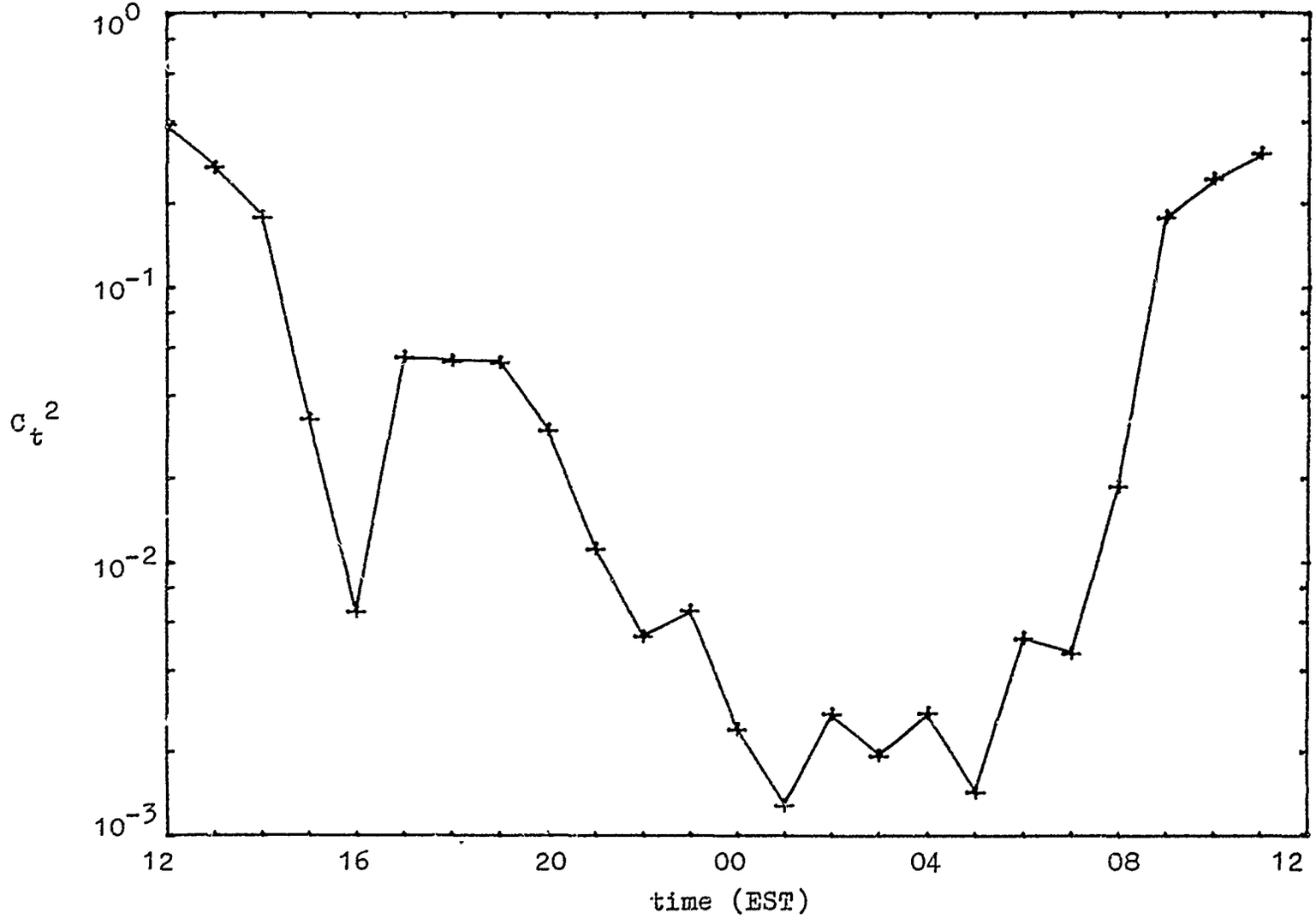

Figure 25. Median values for Type I turbulence: February 1975.

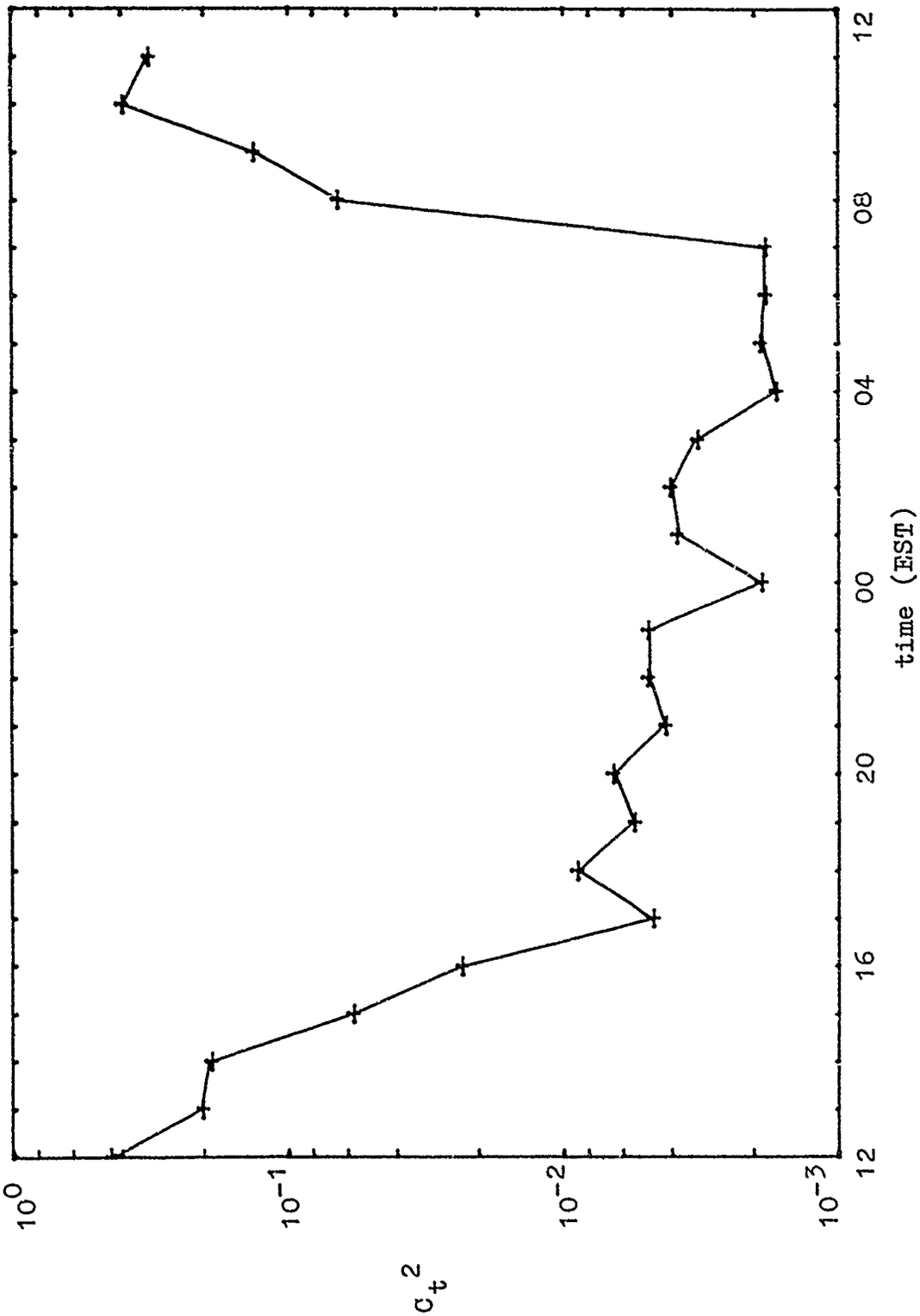

Figure 26. Median values for Type I turbulence: March 1975.

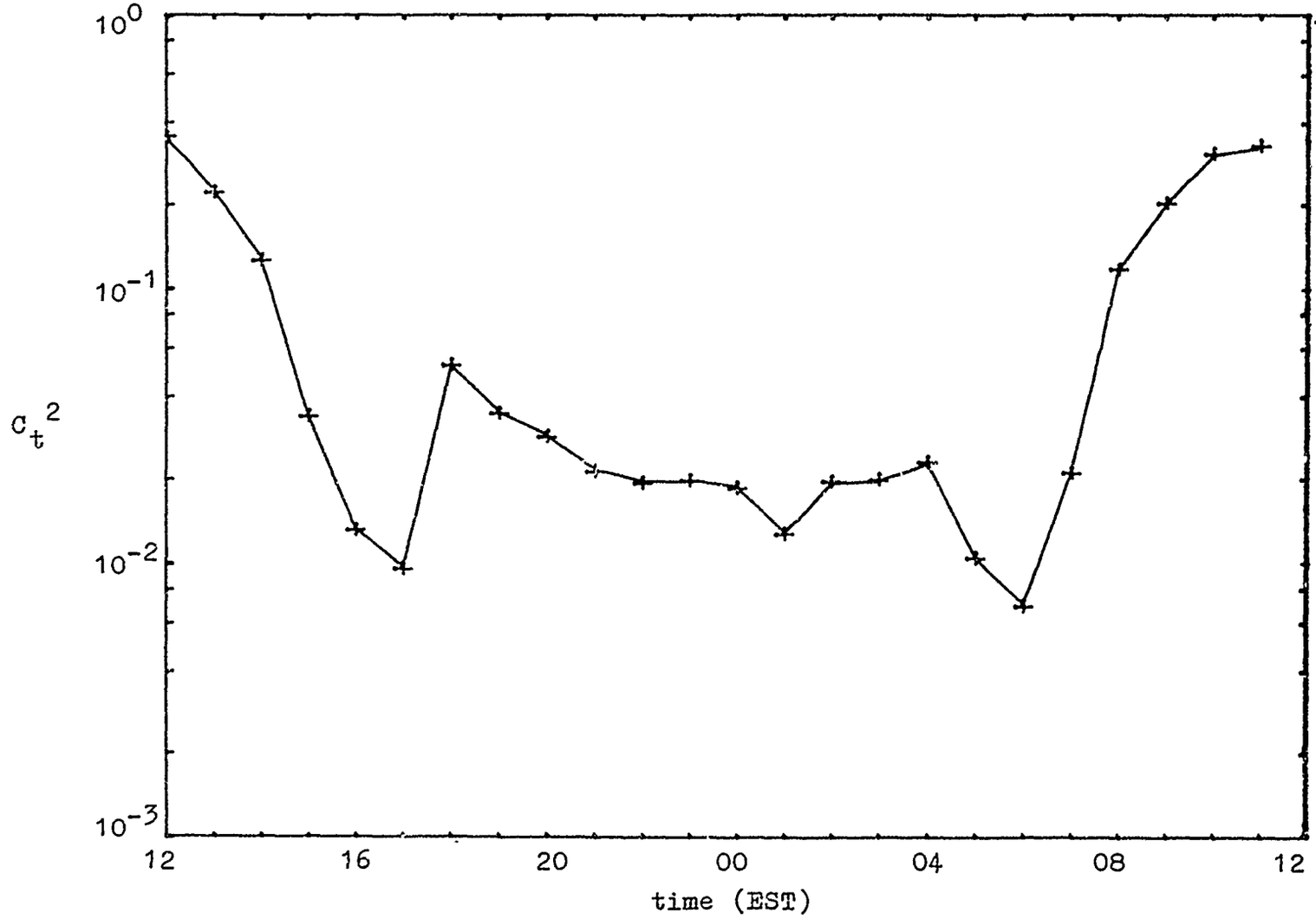

Figure 27. Median values for Type I turbulence: April 1975.

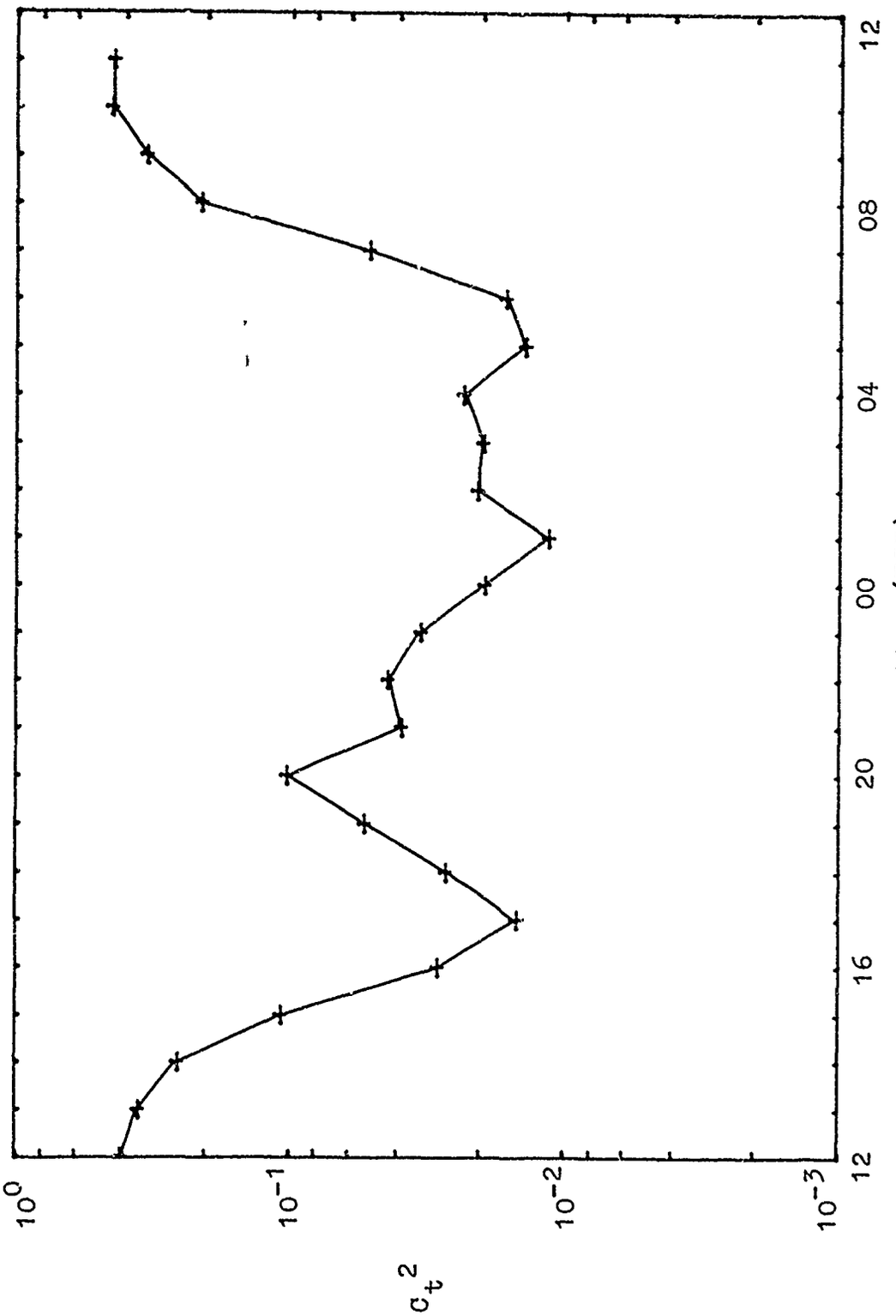

Figure 28. Median values for Type I turbulence: May 1975.

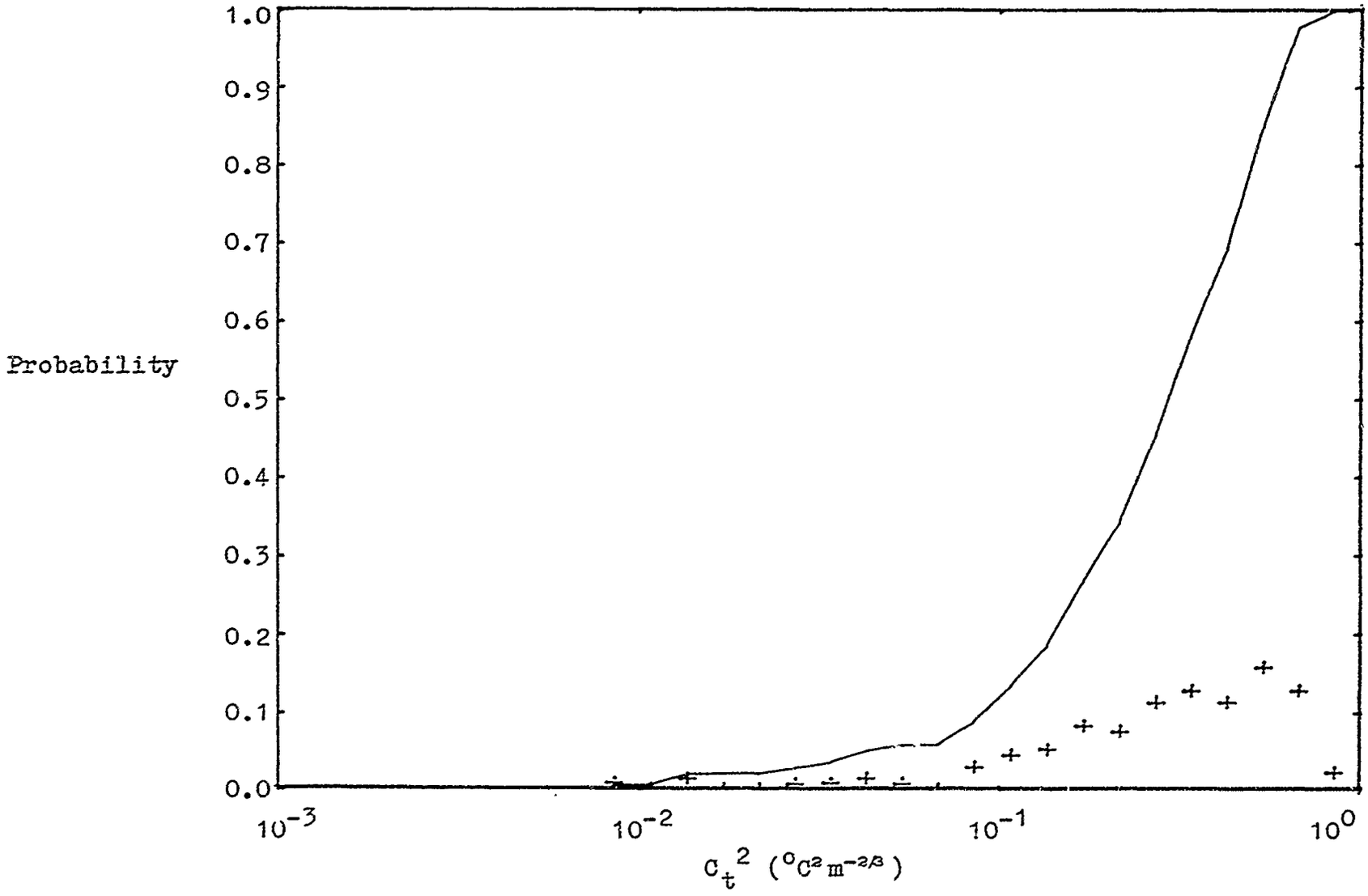

Figure 29. Discrete probability (+) and cumulative probability (solid line) of turbulence strength (Type I only): May 1975, daytime values.

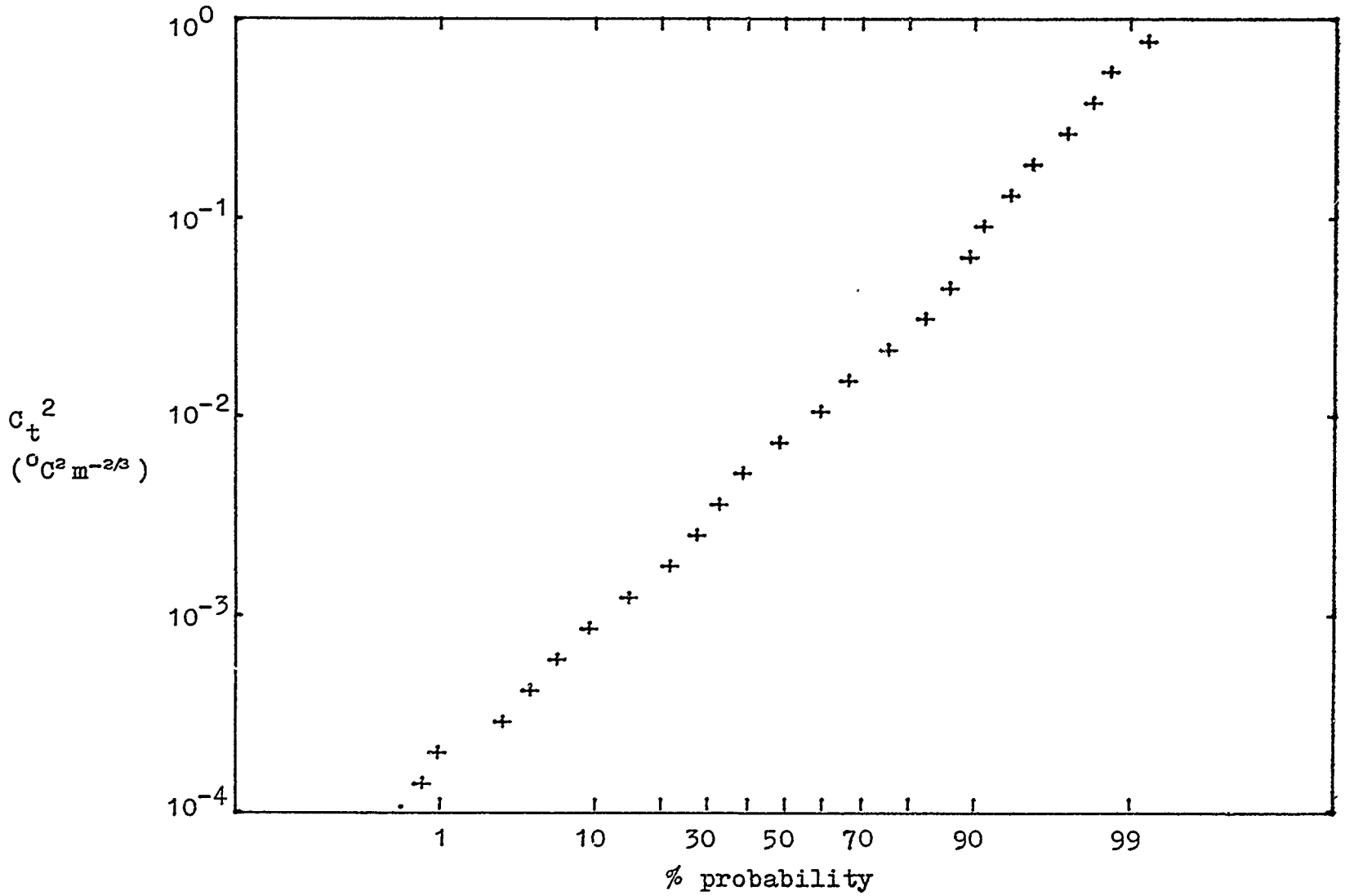

Figure 30. Cumulative probability function for "all weather": March 1975, night values.

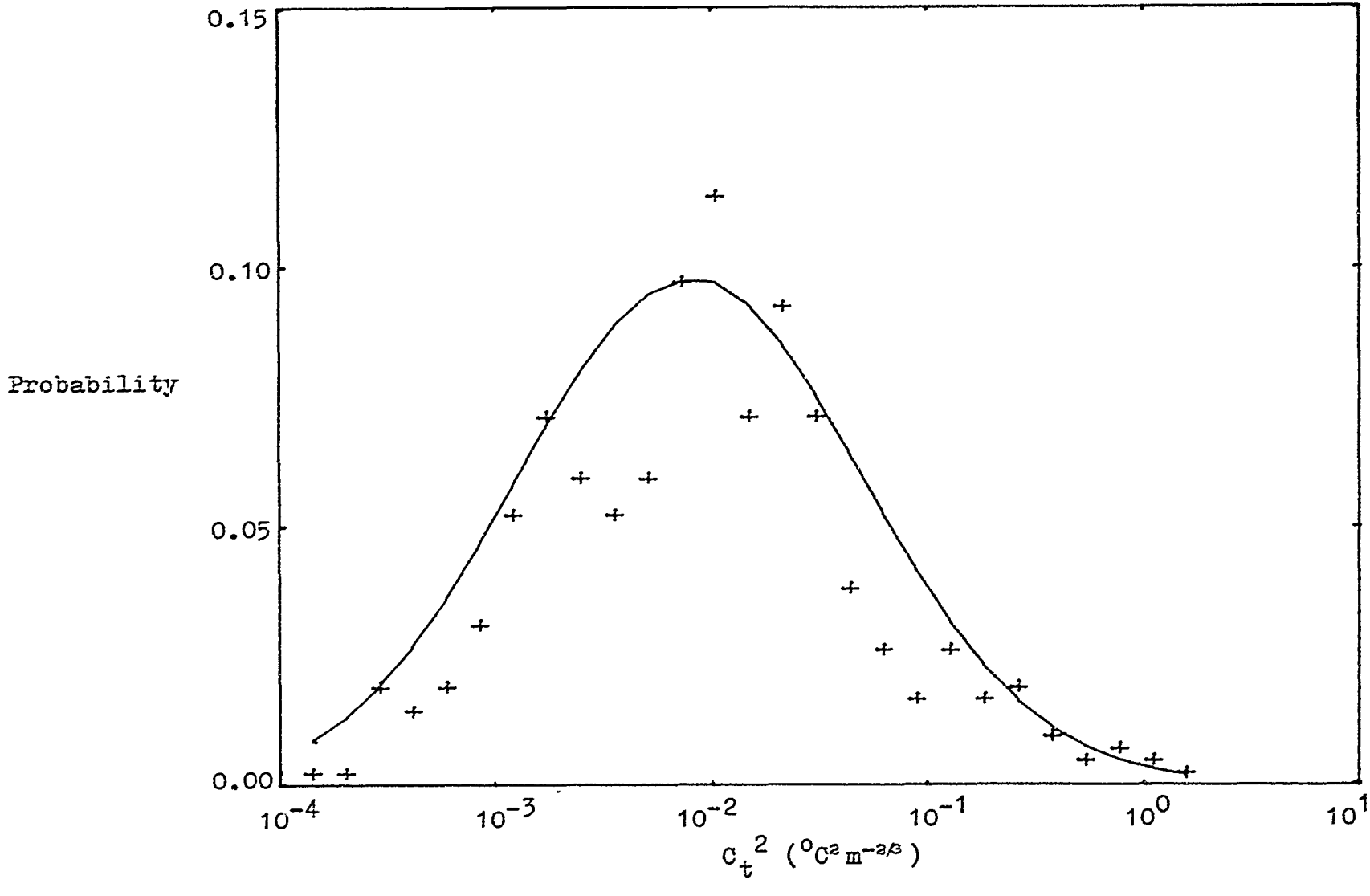

Figure 31. "All weather" turbulence values (March 1975, night values) compared to its Gaussian fit (solid line).

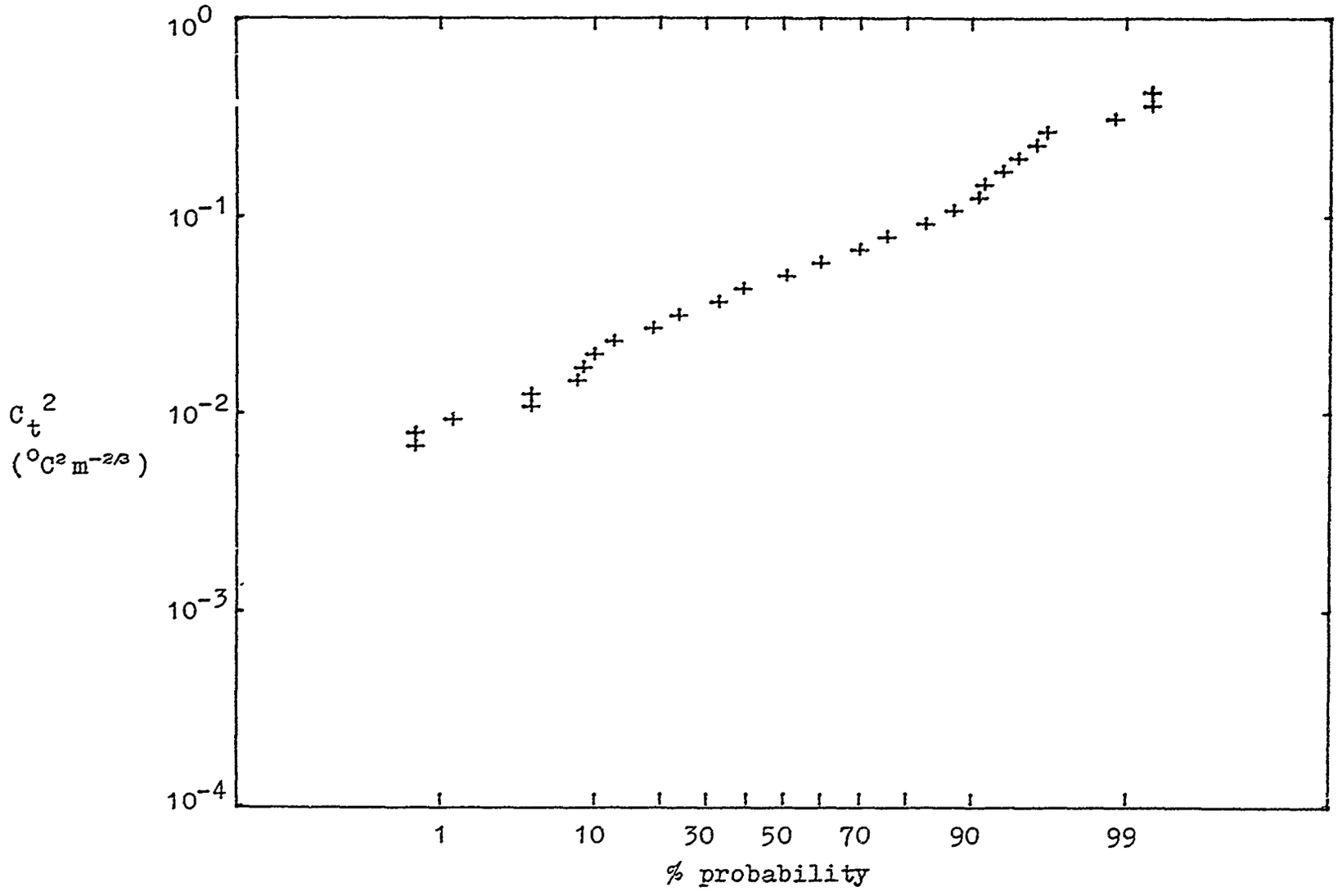

Figure 32. Cumulative probability function for Type II turbulence: May 1975, night values.

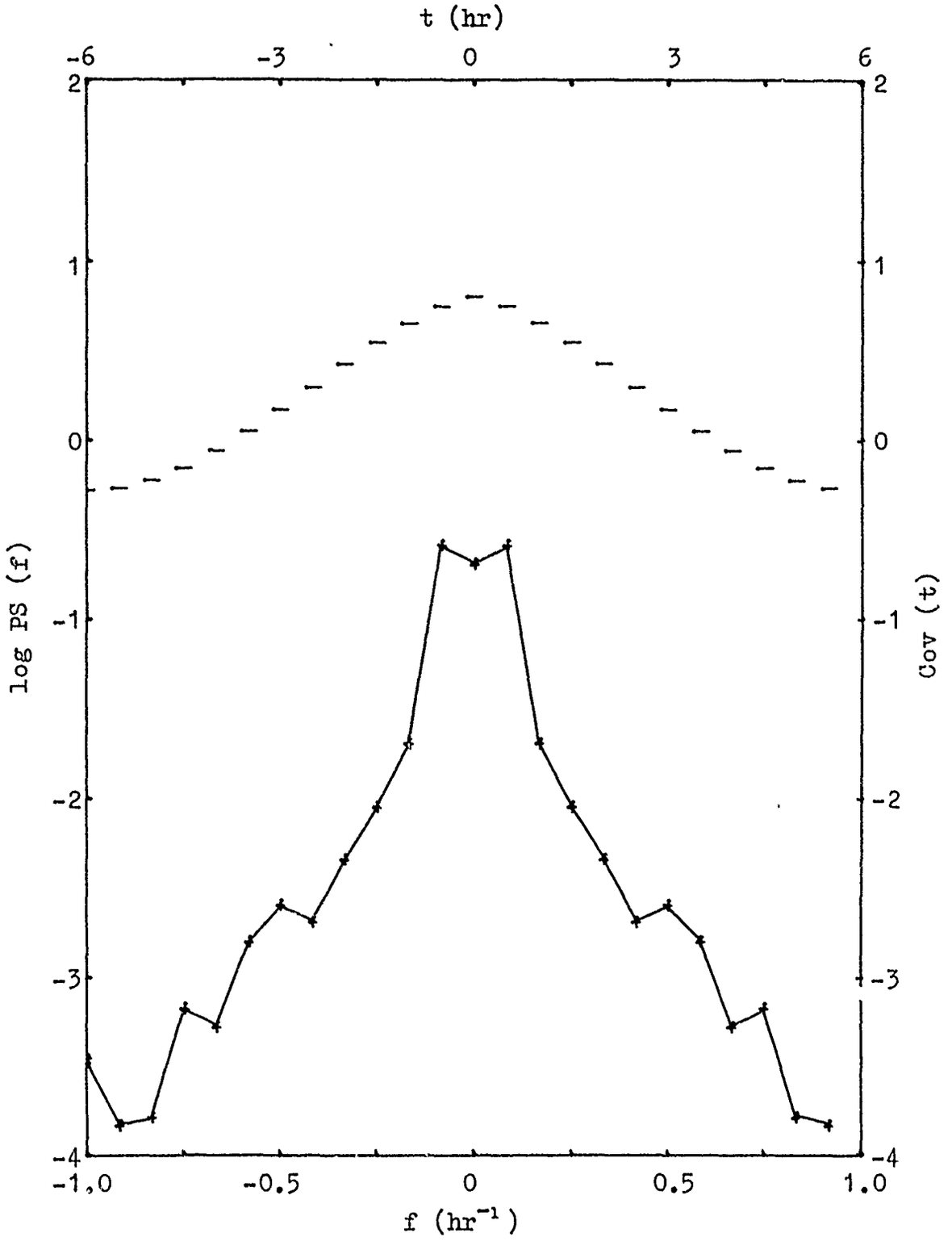

Figure 33. Power spectrum (+) and autocovariance function (-) for 1 Feb 75 (Type I).

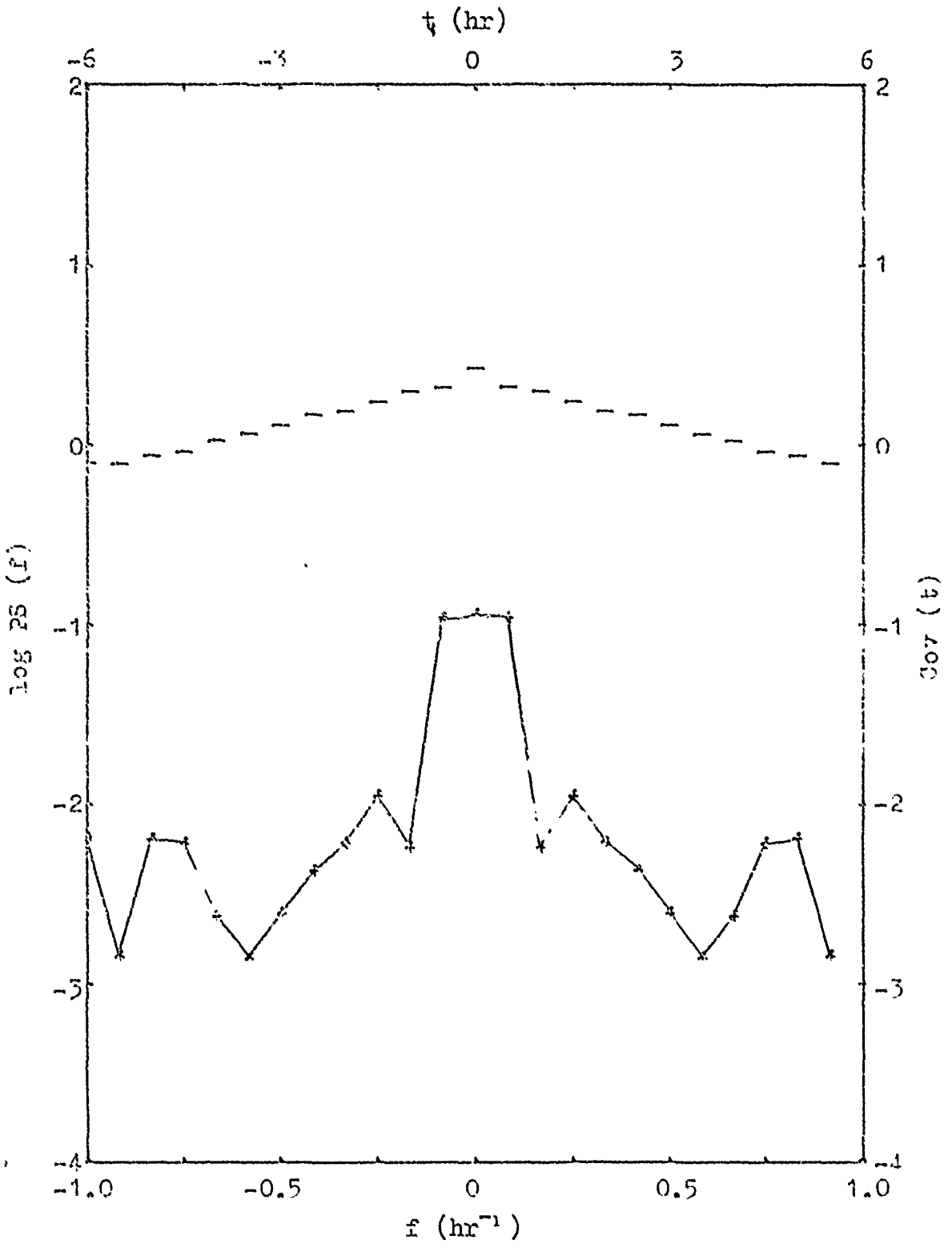

Figure 34. Power spectrum (+) and autocovariance function (-) for 7 Feb 75 (Type II, abnormal).

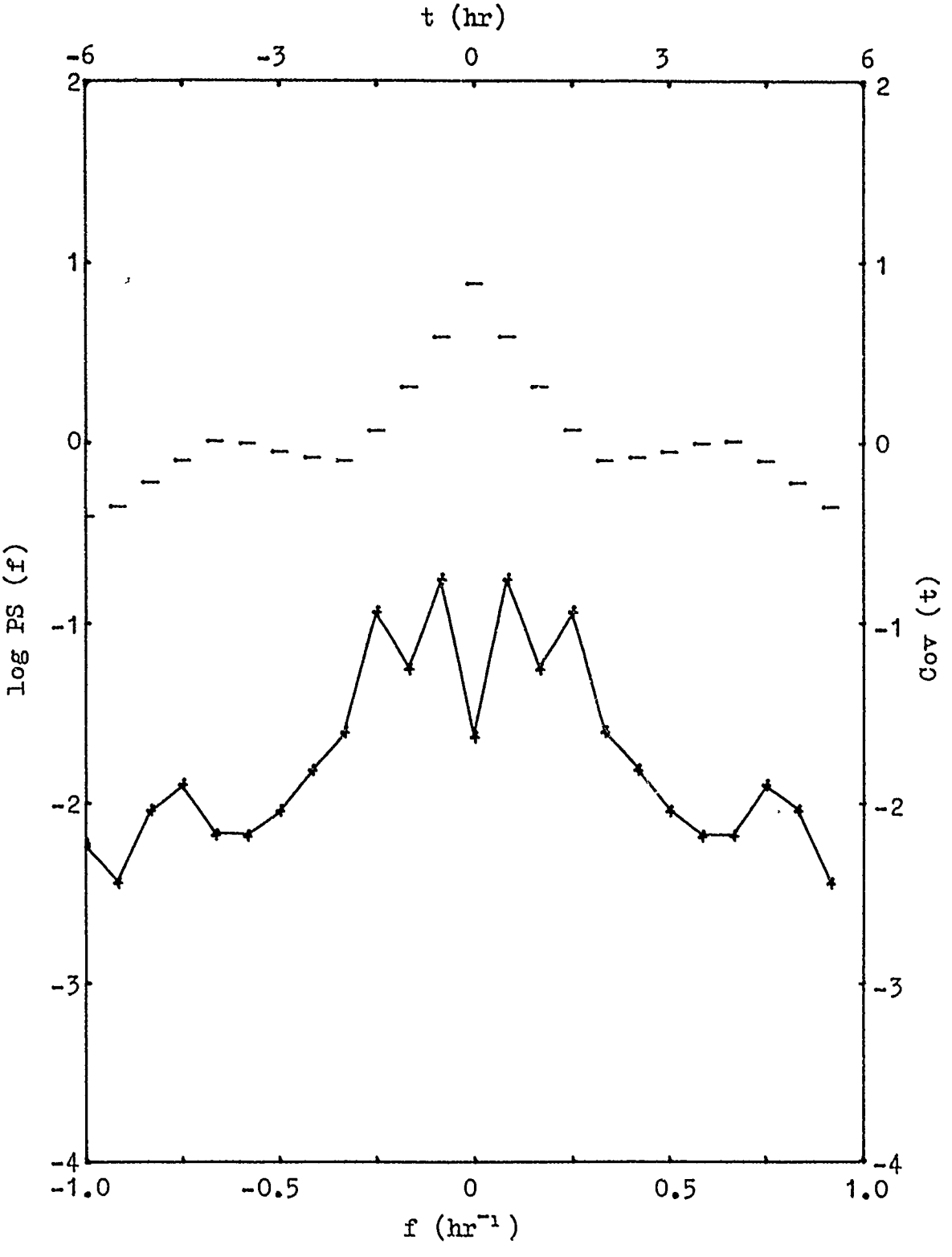

Figure 35. Power spectrum (+) and autocovariance function (-) for 11 Feb 75 (Type III, typical).

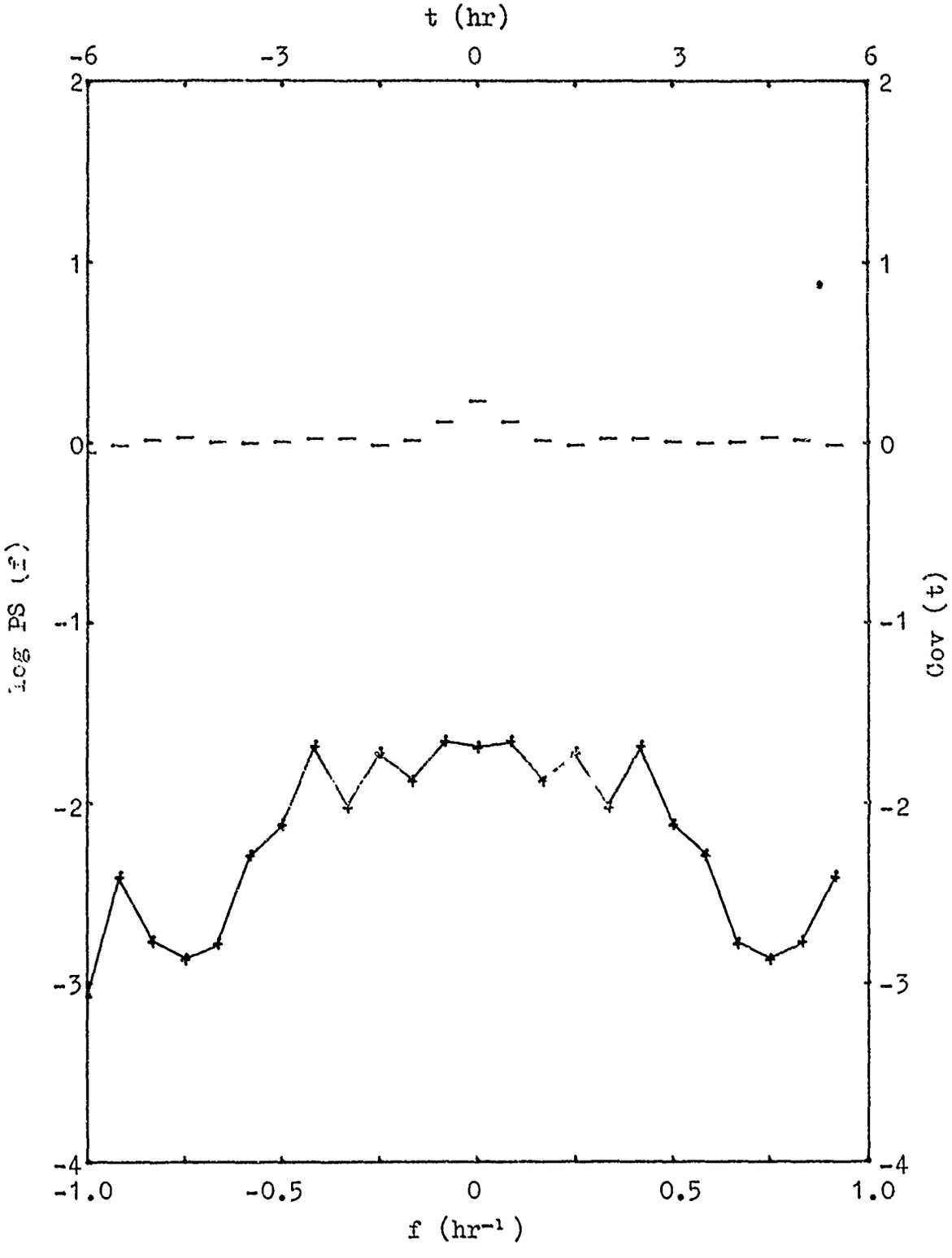

Figure 36. Power spectrum (+) and autocovariance function (-) for 19 Feb 75 (Type III, unusual).

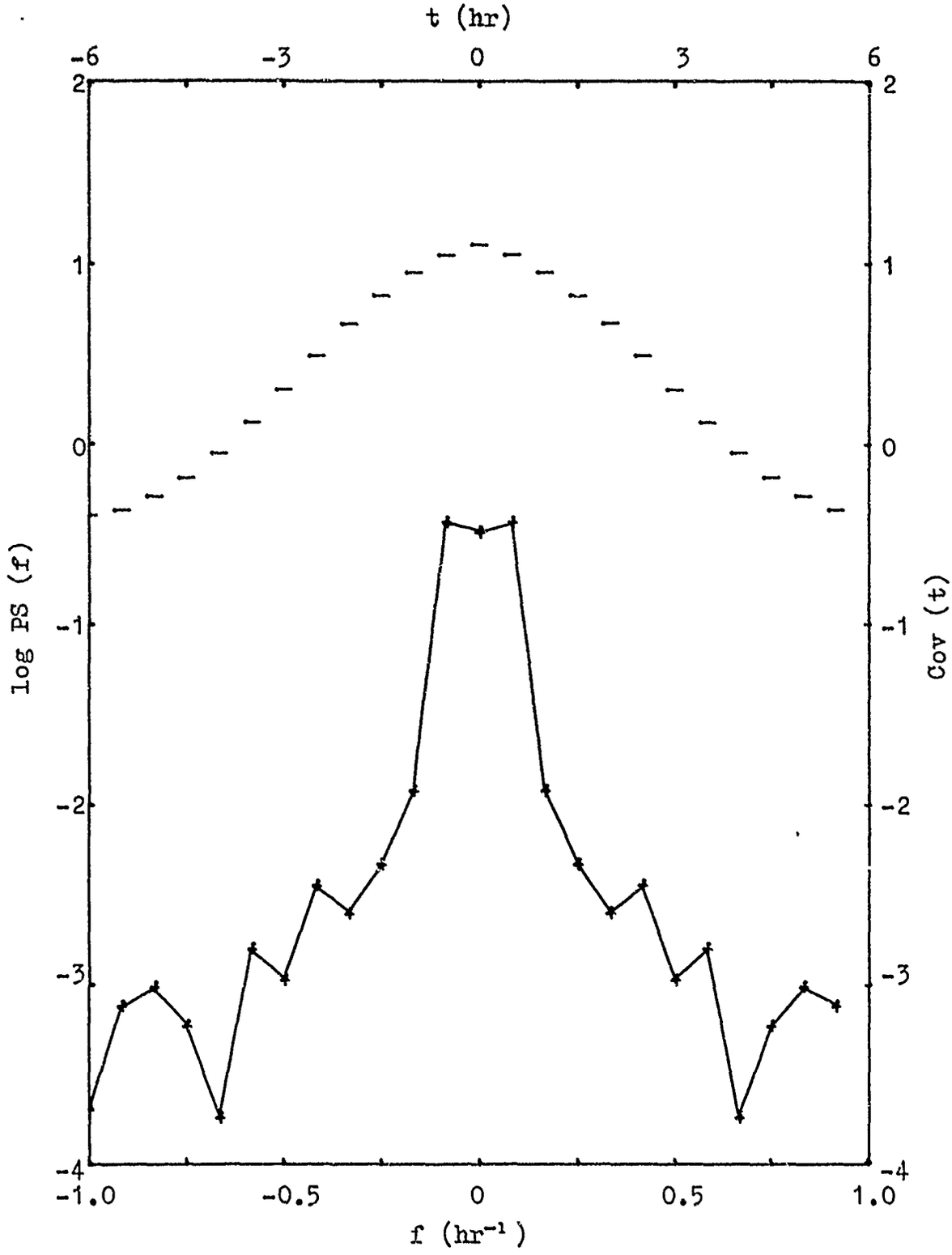

Figure 37. Power spectrum (+) and autocovariance function (-) for 8 Mar 75 (Type I).

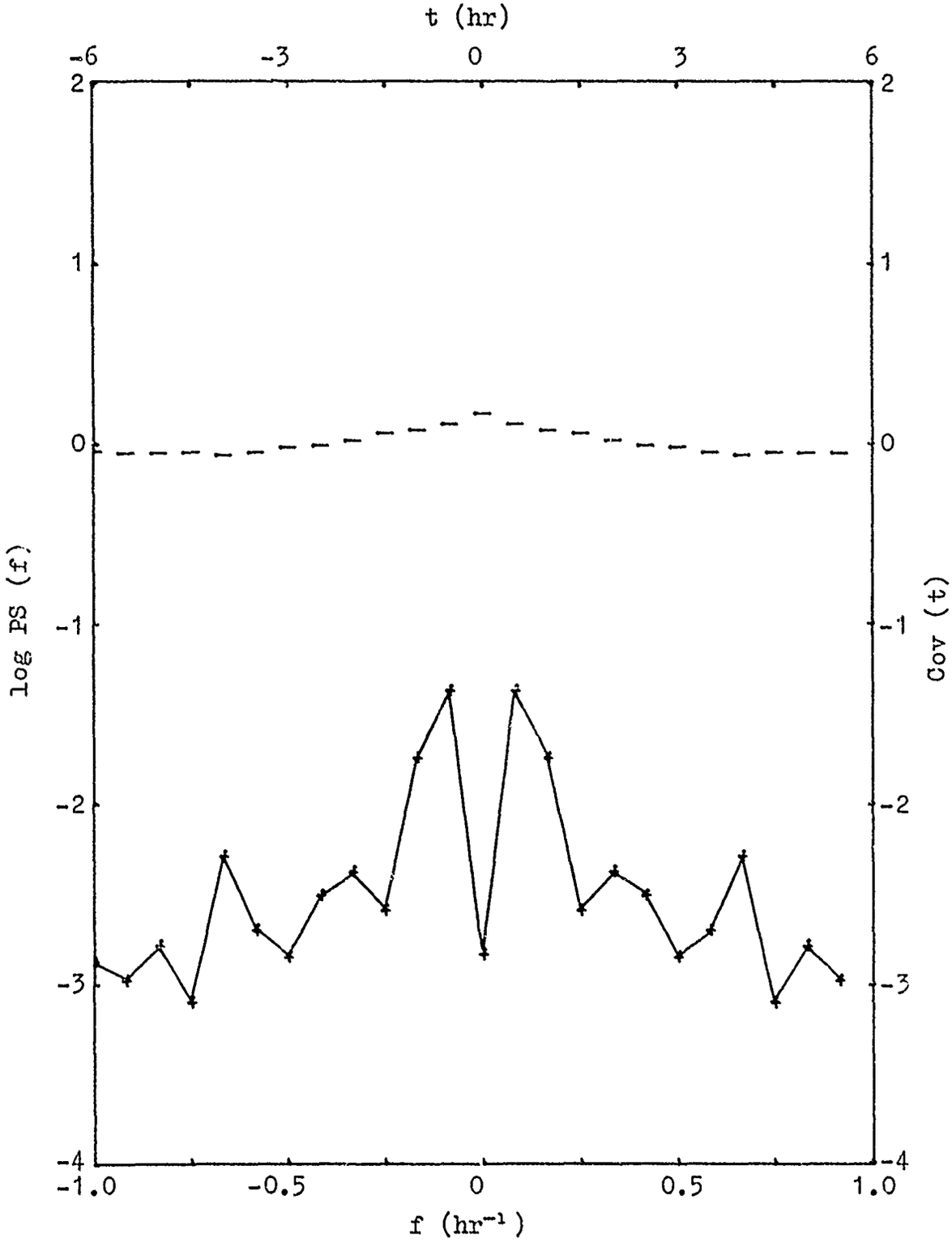

Figure 38. Power spectrum (+) and autocovariance function (-) for 6 Mar 75 (Type II).

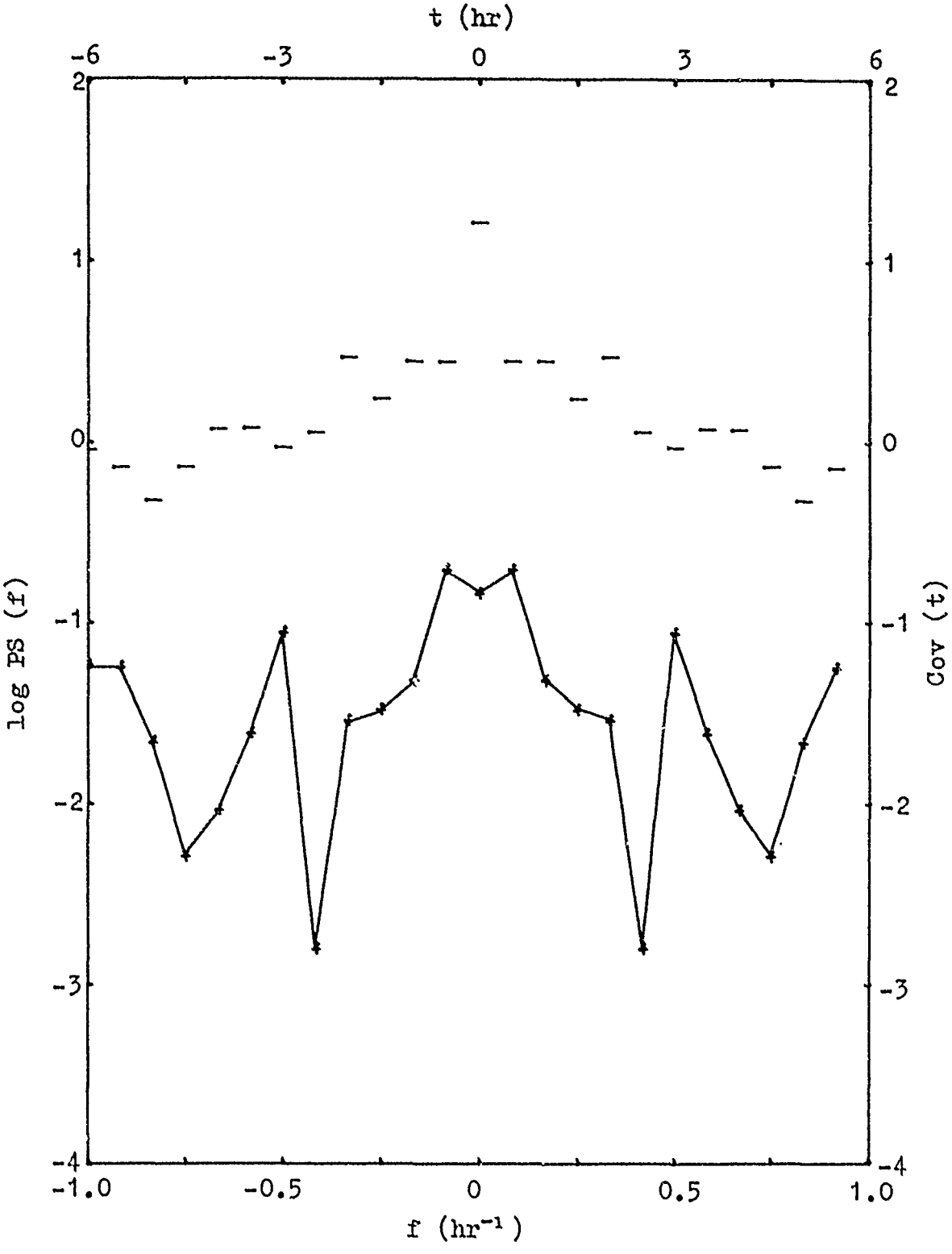

Figure 39. Power spectrum (+) and autocovariance function (-) for 16 Mar 75 (Type III).

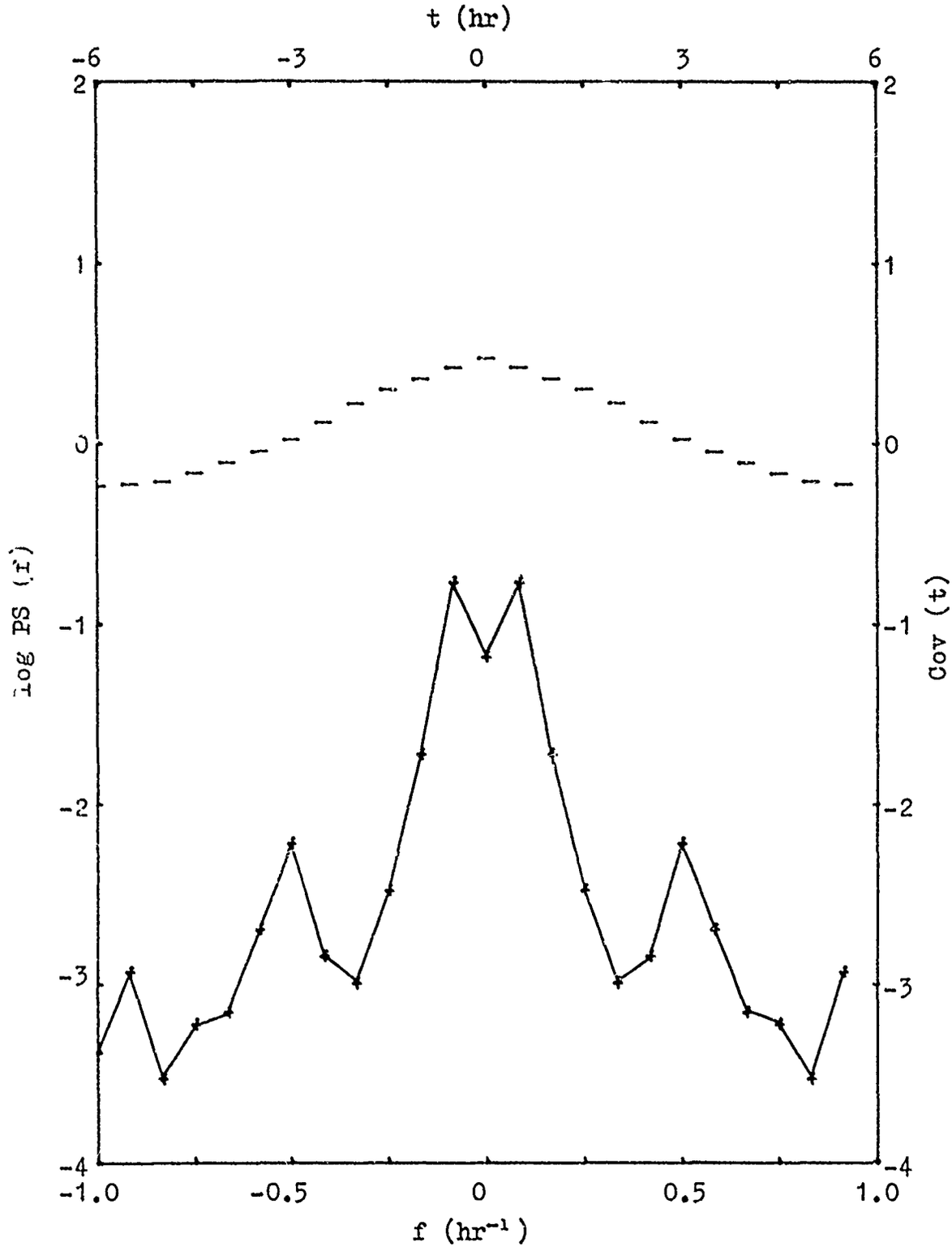

Figure 40. Power spectrum (+) and autocovariance function (-) for 10 Apr 75 (Type I).

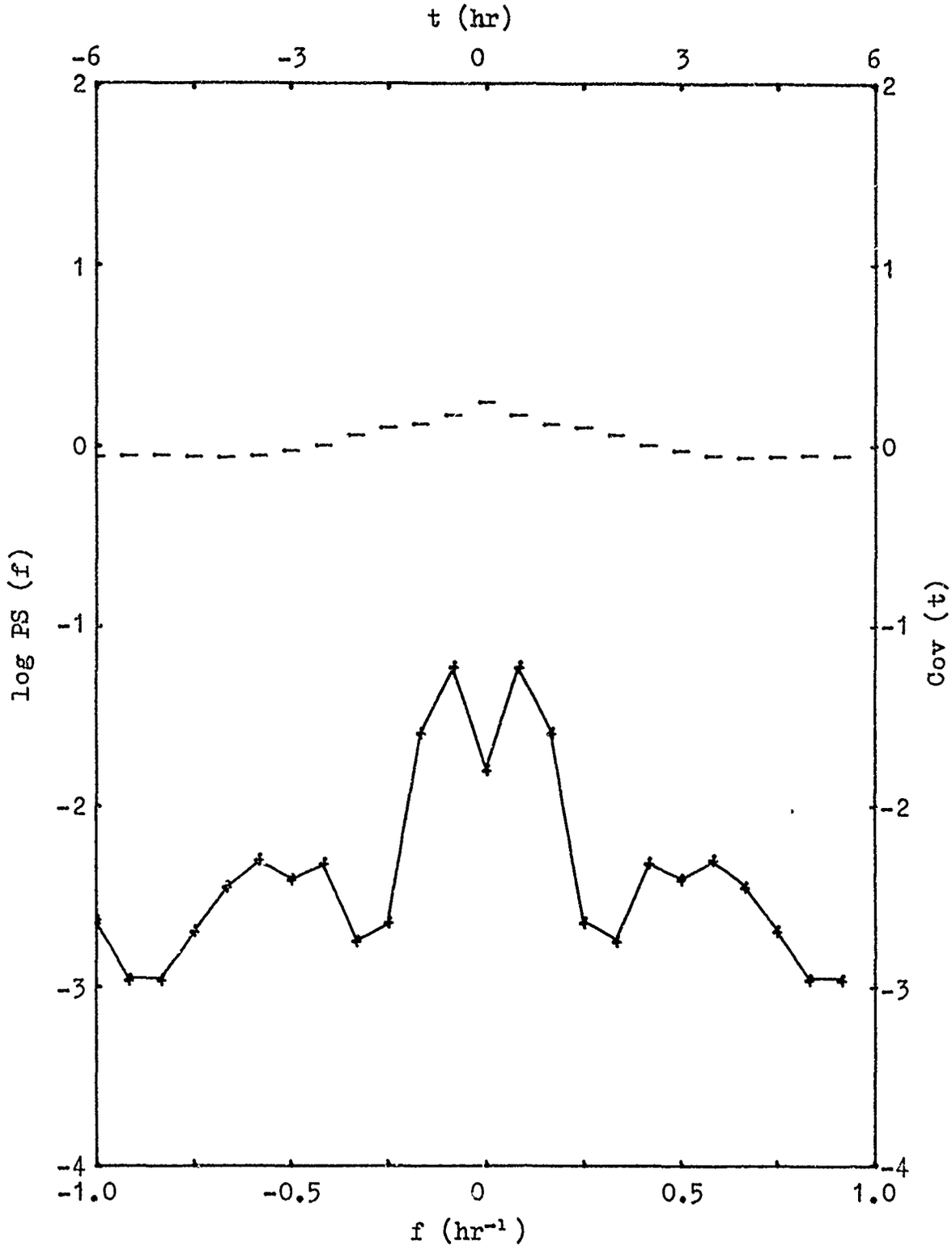

Figure 41. Power spectrum (+) and autocovariance function (-) for 17 Apr 75 (Type II).

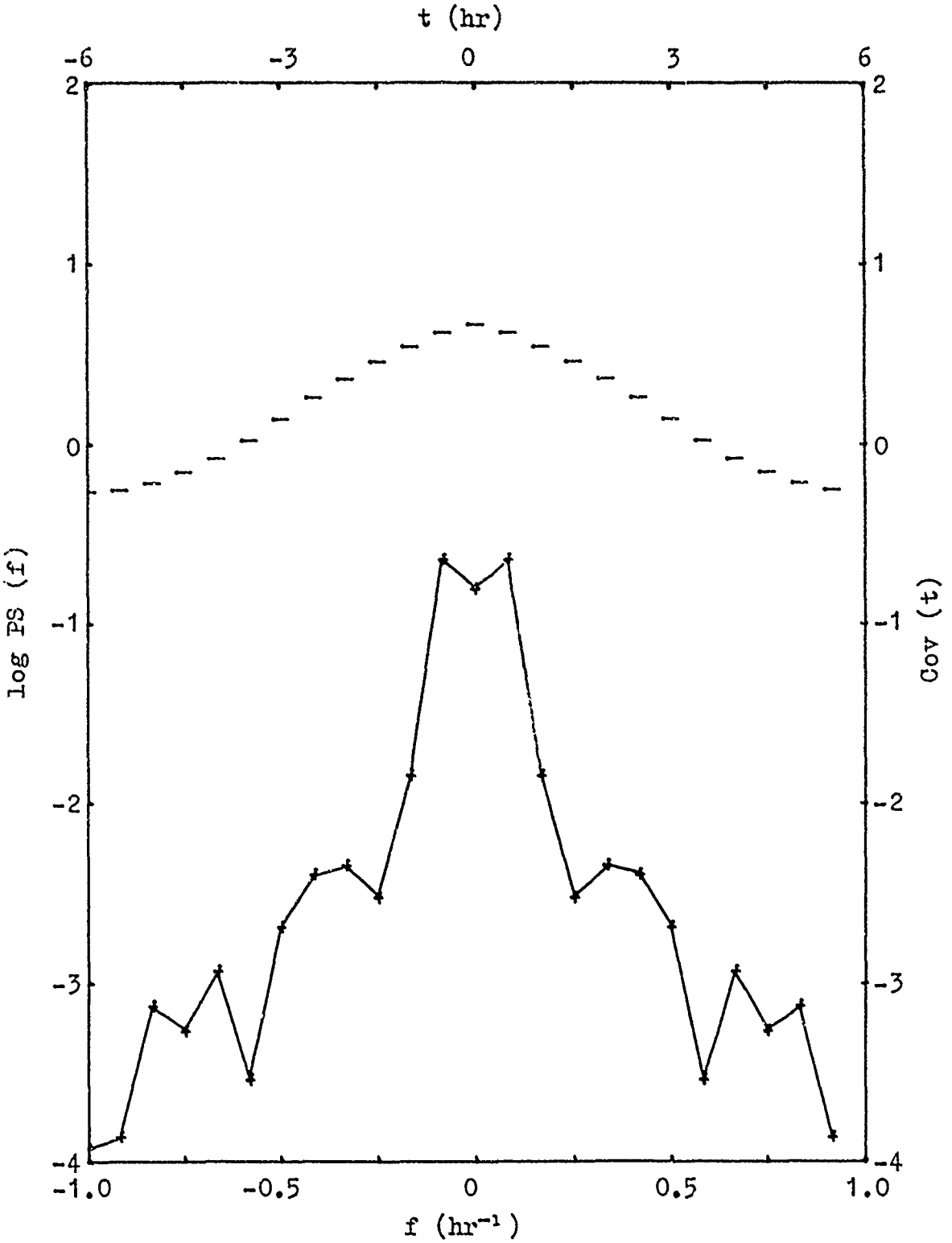

Figure 42. Power spectrum (+) and autocovariance function (-) for 2 May 75 (Type I).

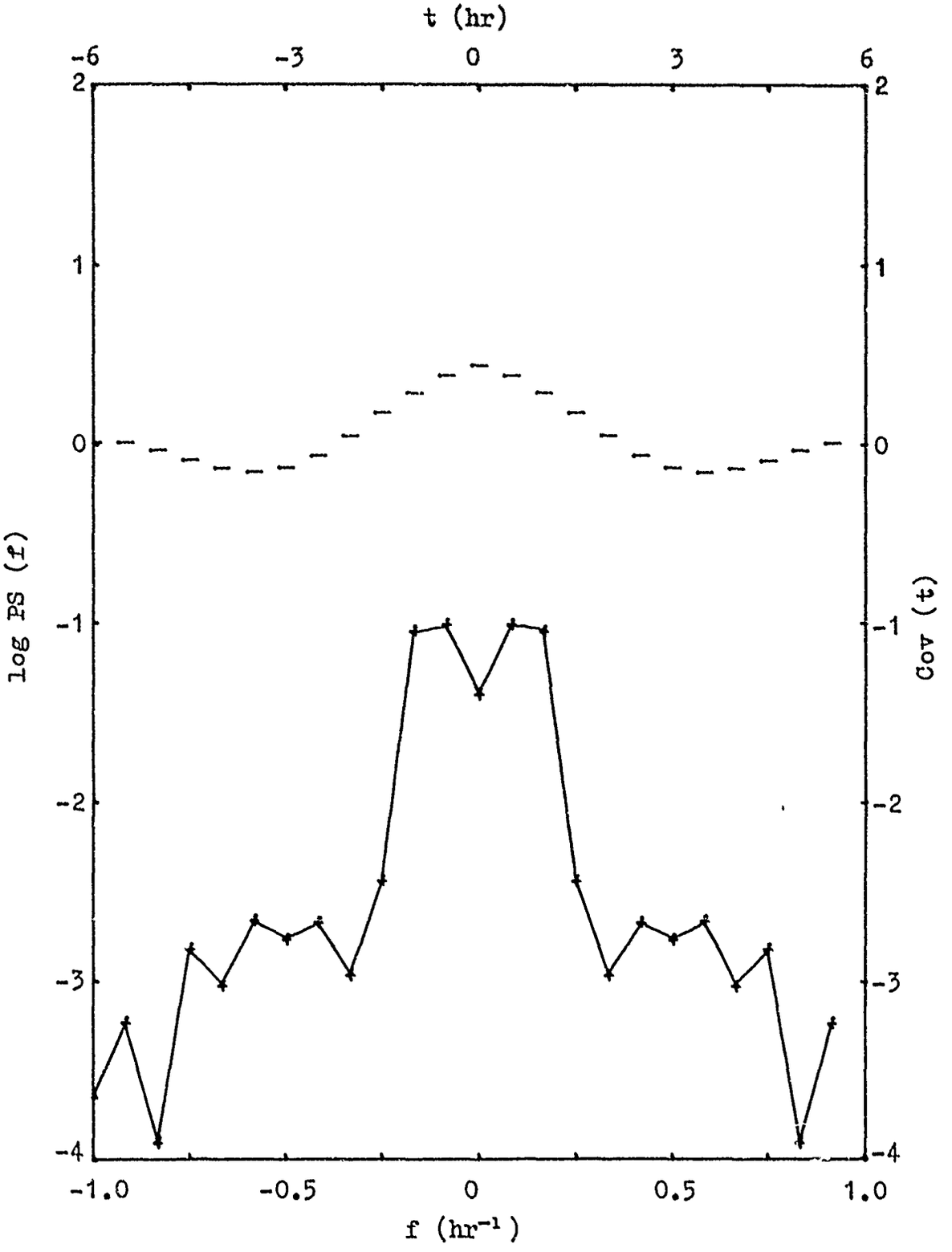

Figure 43. Power spectrum (+) and autocovariance function (-) for 4 May 75 (Type I).

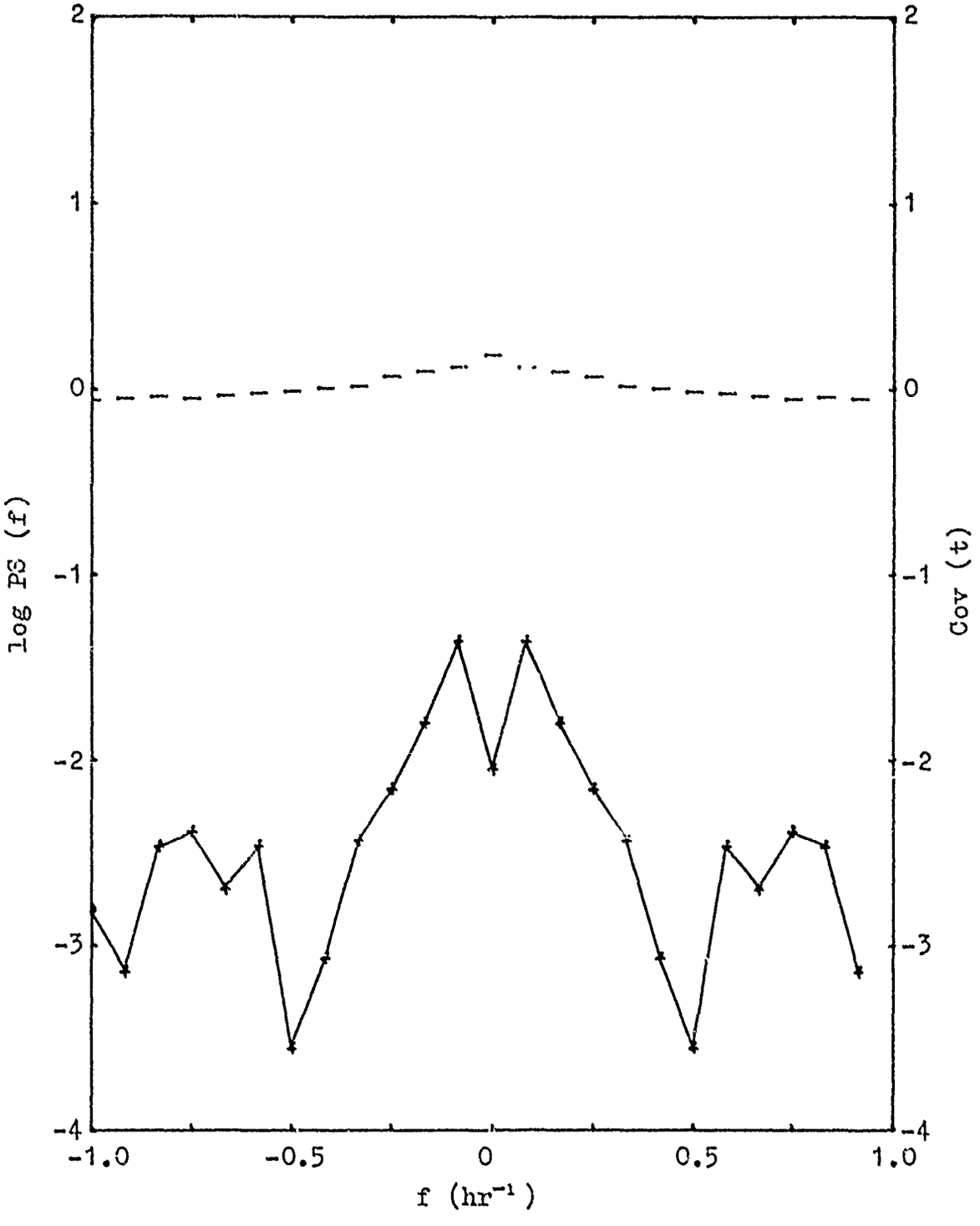

Figure 44. Power spectrum (+) and autocovariance function (-) for 24 May 75 (Type II).

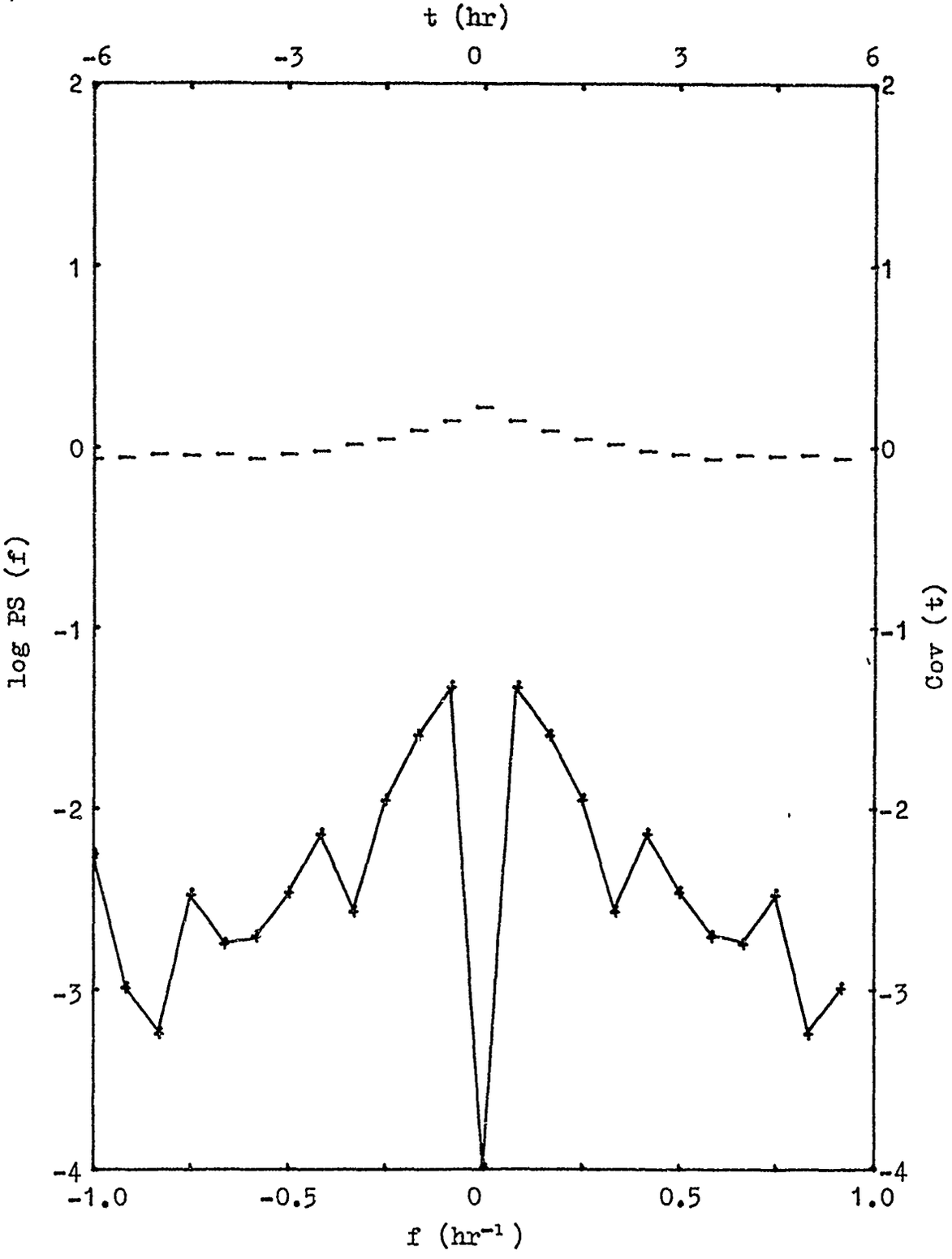

Figure 45. Power spectrum (÷) and autocovariance function (-) for 30 May 75 (Type III).

TABLE 1. CFLOS PROBABILITY (%)

Month	Time (LST) 03-05	09-11	15-17	21-23
Jan	33	35	35	35
Feb	38	39	38	39
Mar	42	40	38	44
Apr	46	40	41	48
May	51	45	46	54
Jun	56	51	51	61
Jul	61	54	55	65
Aug	59	52	56	65
Sep	60	52	55	62
Oct	59	50	53	59
Nov	38	34	35	38
Dec	33	32	34	34

Note: Viewing angle is 90° elevation.

TABLE 2. LEGEND FOR WEATHER CONDITIONS

O	Clear skies
θ	Scattered clouds (<50%)
⊖	Broken cloud cover (50-99%)
@	Overcast (100%)
WX	Cloud cover not observable
R	Rain
S	Snow
L	Drizzle
F	Fog
H	Haze
K	Smoke
T	Thunder
Z_	Freezing ...
_W	... Shower
B_	Blowing ...
+	(heavy)
-	(light)

TABLE 3. WEATHER - FEBRUARY 1975

Date	Sky	Precipitation	Snow Depth
(Type I Turbulence)			
31 Jan	θ to ⊖, @	some SW-	<1 cm
1 Feb	O, θ		<1
2	θ	some SW-	<1
3	O; later ⊖		<1
(Type II Turbulence)			
6 Feb	@	frequent S-, F	22-25 cm
7	@	frequent SW-, BS	25
8	@	SW-, S-, BS	25-27
18	@	F, R-, L-, SW-	15-10
("Quiet Turbulence")			
4 Feb	@	late SW-, S-	<1-5 cm
5	@	S-, F	12-21
(Type III Turbulence)			
8 Feb	@	late SW-	25-27 cm
9	@ to O to @, ⊖	S-, SW-	27-30
10	@	SW-, S-	30-33
11	⊖, @ to O to @	S-, SW-, F	33-35
12	@, ⊖, θ, WX	late SW-,SW+,BS,SW	35-50
13	WX, ⊖, @	SW-	50-55
19	@	SW-	10
20	@		10
26	mostly @	SW-	<1
27	mostly @	SW-	<1
28	mostly @	SW-, T, SW	<1

TABLE 5. WEATHER - APRIL 1975

Date	Sky	Precipitation	Snow Depth
(Type I Turbulence)			
8 Apr	@ to O to θ		2 cm
9	θ,O to ⊖,@		<1
10	@ to O, θ		<1
11	O, θ		<1
14	θ to @		<1
15	@		0
16	@, ⊖to O		0
21	θ to O to θ		0
22	θ to O		0
23	O to @	some RW-	0
28	⊖, @		0
(Type II Turbulence)			
1 Apr	@		2 cm
2	@	S-	2-5
17	O to @	some RW-	0
29	⊖		0
30	⊗, ϧ to @	late R-	0

TABLE 4. WEATHER - MARCH 1975

Date	Sky	Precipitation	Snow Depth
(Type I Turbulence)			
4 Mar	θ, brief ⊖,@,O	some SW-	2 cm
7	⊖, @	SW-, R-	2
8	θ, O		2
9	θ, O to ⊖, @		2
10	@	S-	2
13	⊖, O to @		<1
26	@ to O	some SW-	0
27	O to θ, ⊖		0
(Type II Turbulence)			
5 Mar	@	SW-, S, S-	<1-7 cm
6	@	S-	4
11	θ, ⊖, @		<1
18	@	late RW-	<1
25	@	L, F, SW-	<1
28	⊖to @		0
31	@		2
(Type III Turbulence)			
14 Mar	@	SW-, S-	<1-7 cm
15	⊖ to O to @		7-5
16	@ to O		<1
17	O to @		<1
20	@ to O		<1
21	θ to @	ZRW-	0
22	@	R-, L-	0
23	θ to @	late R-	0
24	@, some ⊖,θ	F, brief RW-	0
28	@	late ZR-, F	0
29	@	F	0

TABLE 6. WEATHER - MAY 1975

Date	Sky	Precipitation	Snow Depth
(Type I Turbulence)			
2 May	⊖ to O,θ,⊖,@		O all month
3	θ, ⊖ to @		
4	@	early R-	
5	⊖ to O to θ,@		
9	θ to O to θ		
10	θ to O to θ		
11	θto @		
14	⊖,@ to θ to @		
16	⊖, @ to θ	H, F	
19	θ to O to @	H	
21	⊖		
(Type II Turbulence)			
7 May	θto O		
13	⊖ to O to @	some T	
22	θ, ⊖, @, O	F, H	
23	⊖ to O to ⊖	F, H	
24	⊖,some O,θ,@	early TRW-	
25	θ, ⊖		
27	@ to O,some ⊖		
28	O to θ		
29	⊖, θ	late RW-	
(Type III Turbulence)			
1 May	@	RW-, F	
6	@	RW-, R-, F	
12	@	RW-, F	
17	⊖ to @		
18	@	F, H	

(continued)

TABLE 6. (continued)

Date	Sky	Precipitation	Snow Depth
20 May	@ to ⊖to @	H, F	0 all month
21	⊖	H	
26	@, ⊖	late RW-	
30	@	F, some TRW-	
31	@	TRW-, RW-, H, F	

TABLE 7. STATISTICS FOR LOG C_t^2 (TYPE I TURBULENCE)

Month	Time	# Pts	Mean	Std Dev	Skew	Kurtosis
Feb	night	72	-2.1293	0.5818	-0.0193	1.8721
	day	59	-0.7599	0.4071	-1.4601	4.7501
	dusk	28	-1.5885	0.4554	-0.7393	2.3638
	dawn	32	-2.2593	0.6082	-0.0373	2.2389
Mar	night	157	-2.3290	0.6027	-0.2786	2.1450
	day	109	-0.7031	0.5226	-0.8821	3.0298
	dusk	63	-1.8647	0.6043	0.5247	2.4447
	dawn	56	-2.3422	0.6345	0.3018	2.4577
Apr	night	180	-1.6654	0.4278	-0.3780	2.9456
	day	150	-0.7913	0.6151	-0.8924	3.1236
	dusk	70	-1.5856	0.5569	0.1467	2.0468
	dawn	77	-1.7922	0.5187	0.2501	3.1293
May	night	198	-1.4911	0.5369	-0.1877	2.3367
	day	138	-0.5602	0.3703	-1.5192	5.9714
	dusk	77	-1.5285	0.4634	-0.2176	2.9851
	dawn	85	-1.6567	0.5986	0.0812	2.5258

TABLE 9. STATISTICS FOR LOG C_t^2 ("ALL WEATHER")

Month	Time	# Pts	Mean	Std Dev	Skew	Kurtosis
Feb	night	303	-2.1218	0.6750	0.0603	2.3967
	day	244	-1.6349	0.7631	0.2102	2.1841
	dusk	117	-1.8117	0.5895	-0.2495	2.6038
	dawn	136	-2.2997	0.7113	-0.0420	2.3398
Mar	night	425	-2.0482	0.7496	0.1822	3.1892
	day	294	-1.1210	0.8219	-0.3946	1.9218
	dusk	160	-1.7303	0.6911	0.0951	2.2917
	dawn	163	-2.1935	0.7008	0.2681	3.3321
Apr	night	249	-1.6394	0.5079	-0.2778	3.3083
	day	206	-0.8155	0.6286	-0.8228	2.9301
	dusk	98	-1.6653	0.6370	-0.0915	2.4126
	dawn	101	-1.7850	0.5109	0.1018	3.0319
May	night	501	-1.5387	0.5728	-0.6395	3.1334
	day	373	-0.8524	0.6315	-1.1269	3.6039
	dusk	197	-1.5110	0.5412	-0.3310	3.0026
	dawn	199	-1.7145	0.6337	-0.2969	3.0355

TABLE 10. MEAN SQUARED ERRORS

Turbulence	Time	Skew	Kurtosis
Type I	night	0.0640	0.6115
	day	1.5036	2.9771
	dusk	0.2227	0.4055
	dawn	0.0404	0.2787
	all	0.4576	1.0682
Type II	night	0.1630	0.3202
	day	0.4582	0.8739
	dusk	0.0338	0.7141
	dawn	0.1362	0.2361
	all	0.1977	0.5361
"All Weather"	night	0.1307	0.1282
	day	0.5367	0.5494
	dusk	0.0473	0.3421
	dawn	0.0430	0.1371
	all	0.1894	0.2664

REFERENCES

1. Lawrence, R. S., G.R. Ochs and S.F. Clifford, "Measurements of Atmospheric Turbulence Relevant to Optical Propagation," J. Opt. Soc. Am., 60, 826 (1970).

2. Cloud-Free Line-of-Sight Probabilities for Selected Surveillance Sites, Report 7232 (USAF Environmental Technical Applications Center, Washington, D.C., Feb 1974).

3. Greenwood, Darryl P., and Donald O. Tarazano, A Proposed Form for the Atmospheric Microtemperature Spatial Spectrum in the Input Range, RADC-TR-74-19 (Available NTIS, Washington, D.C., Feb 1974). (776294)

4. Greenwood, Darryl P., and David B. Youmans, A Fine-Wire Microtemperature Probe for Atmospheric Measurements, RADC-TR-75-240 (Available NTIS, Washington, D.C., Dec 1975).(A019277)

5. Greenwood, Darryl P., and James L. Spencer, Frequency Response of Fat-Wire Probes, unpublished technical memo (Rome Air Development Center, Griffiss AFB, NY, Feb 1975).

6. Jayne, Richard A., and Donald H. Foley, Data Processing Support to Laser Propagation Program, RADC-TR-74-284 (Available NTIS, Washington, D.C., Oct 1974).(A001089)

7. Strohbehn, John W., "Optical Propagation Through the Turbulent Atmosphere," in Progress in Optics, Vol. IX 73-122 (North-Holland Publishing Company, Amsterdam, 1971).

8. Greenwood, Darryl P., private communication.

9. Norton, C.L. and D.L. Walters, "Statistics of Thermal Turbulence Data at White Sands Missile Range," Digest, Topical Meeting on Optical Propagation Through Turbulence, Rain and Fog, O.S.A., Paper PD2, August 1977.

10. Oppenheim, Alan V., and Ronald W. Schafer, Digital Signal Processing (Prentice-Hall, Inc., New Jersey, 1975).

11. Greenwood, Darryl P., Subprogram Documentation (University of Texas, Austin, 1971).

12. Box, George E.P., and Gwilym M. Jenkins, Time Series Analysis: Forecasting and Control (Holden-Day, Inc., San Francisco, 1976).

APPENDIX A - AVERAGING TIMES

I. THE EFFECT OF AVERAGING TIMES ON THE TURBULENCE PROFILE

Late in the experiment a question arose concerning averaging times. The question originally came up with respect to unexpected results in the probability distributions, but it was also unknown what effect the long averaging time had on the characteristics of the diurnal profile, especially on the magnitude of the sunset dip. The 30-minute time period for evaluating turbulence levels from raw data had been specifically chosen to "smooth out" the effects of turbulence intermittency.

The 48-hour period beginning 1400 EST, 9 May 1975, was studied to determine the effect of averaging time on profile shape. This particular period was picked because it was the longest segment of raw data collected under good weather conditions still available at the time of this analysis. Good weather conditions were required because they gave the "best" turbulence profiles. The strong peaks in the nighttime turbulence were an interesting byproduct of the choice, but not a determining factor. The raw data were reduced to 5-minute periods in addition to the usual 30-minute periods (see Figures A1 and A2).

Comparing Figures A1 and A2, one immediately sees that the longer averaging period effectively low-pass filters the data. The result is helpful for observing trends, but it appears that the sharper spikes and dips in turbulence are lost. The longer time averages tend to follow the spikes more closely than the dips of the shorter time periods. The item of interest, the sunset dip, changes substantially between the two averaging periods. For 5-minute periods, its values are 1.6×10^{-3} and 2.0×10^{-3} $^{\circ}C^{2}\,m^{-2/3}$ (for 9 May and 10 May, respectively), versus 30-minute values

of 4.8×10^{-3} and 1.25×10^{-2} $^{\circ}C^{2} m^{-2/3}$. The daytime turbulence values are not affected as much, but several spikes stronger than $1.0^{\circ}C^{2} m^{-2/3}$ are "lost" in the longer averages.

II. THE EFFECT OF AVERAGING TIMES ON PROBABILITY DISTRIBUTIONS

The probability distributions calculated from 30-minute averages of raw data did not exhibit the lognormal shape predicted for daytime Type I turbulence. Three possible reasons were hypothesized, of which one was the length of the averaging period. To examine this possibility, a 70-hour period of data, collected under good weather conditions beginning at 1400 EST on 9 May 1975, was analyzed.

The raw data were reduced to 5-periods, from which the usual probability distributions were calculated. The statistics for log C_t^2 are given below:

	mean	std	skewness	kurtosis	# pts
night	-1.5331	0.6258	-0.1130	2.0511	324
day	-0.5803	0.3407	-0.6906	3.5373	240
dusk	-1.6161	0.5379	-0.4286	2.1706	126
dawn	-1.5624	0.6247	-0.3880	2.2358	144

The numbers suggest that the daytime distribution was significantly improved by using 5-minute averages, whereas the nighttime distribution flattened, almost to the point of becoming a perfect uniform distribution (compare Figures A3 and A4 with C10 and C11). The cumulative probability distributions of the 840 consecutive 5-minute values and the month of 30-minute values have been plotted on a probability scale in Figures A5-A8. Figure A5 has the characteristic shape of a uniform distribution. A comparison of Figures A5 and A8 shows that the distribution for the 5-minute values lies much closer to a straight line (a Gaussian distribution). It appears, then,

that the long 30-minute periods do limit the ability to "observe" strong turbulence.

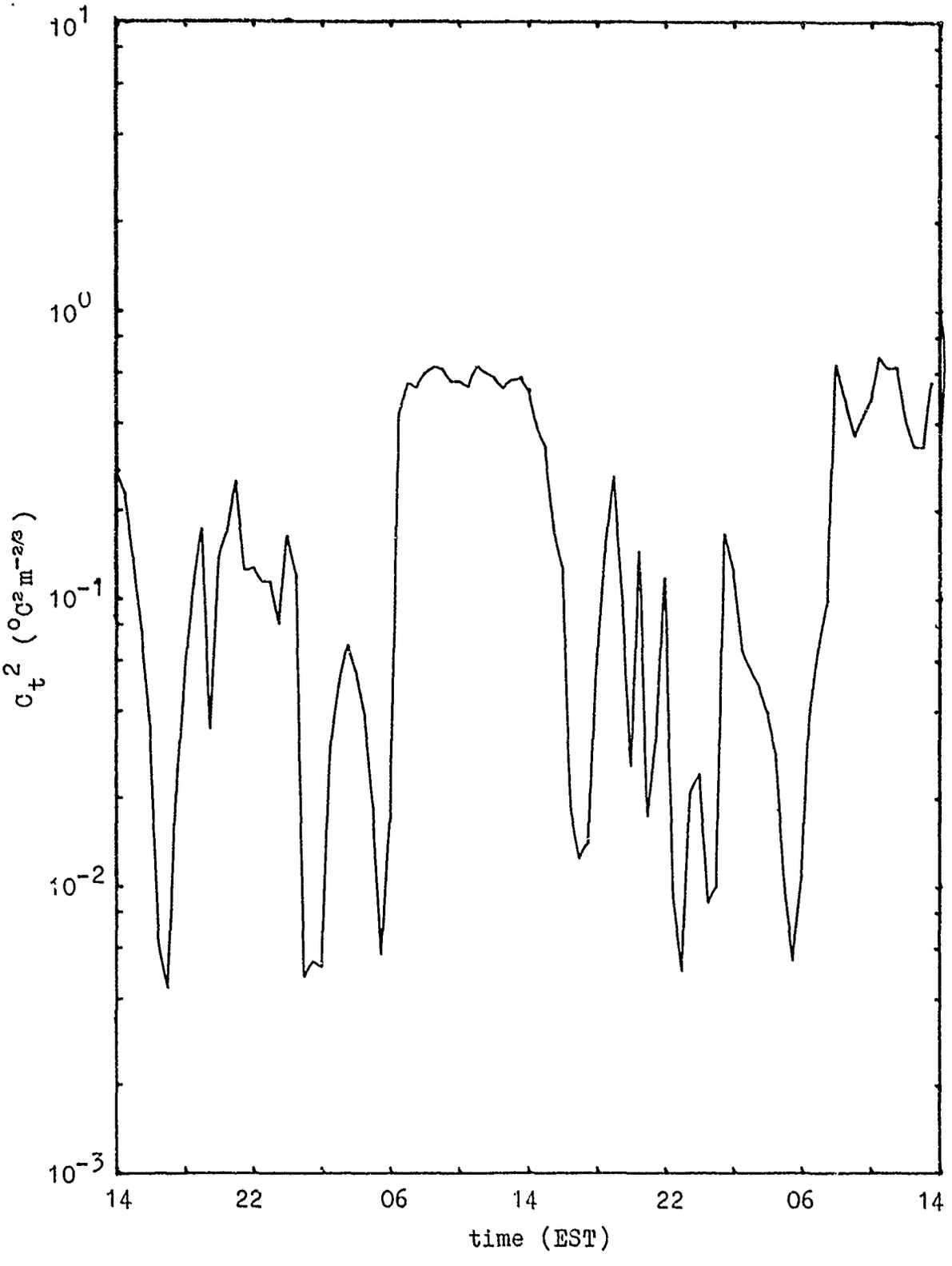

Figure A1. Turbulence values for 9-11 May 75: 30-minute averages.

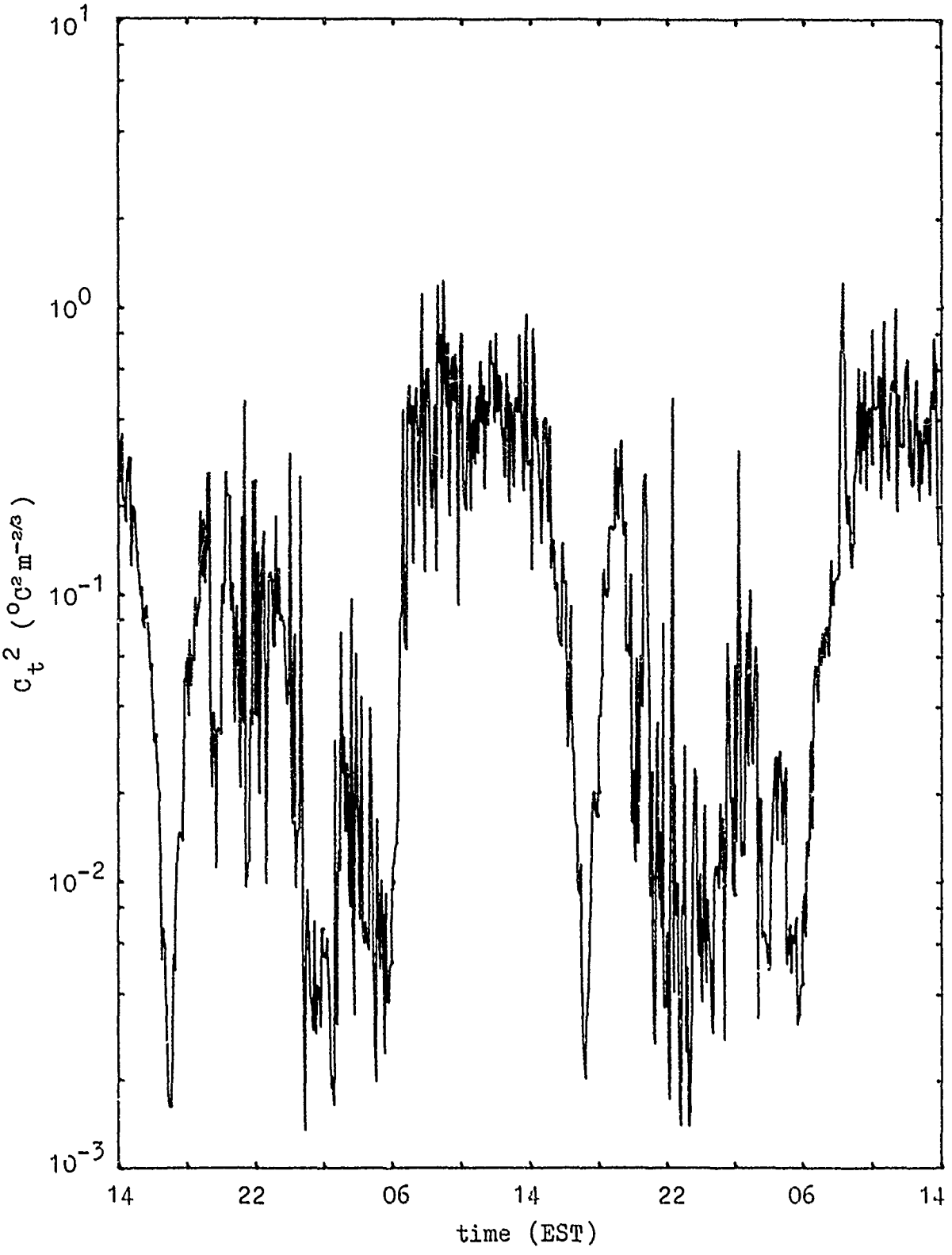

Figure A2. Turbulence values for 9-11 May 1975: 5-minute averages.

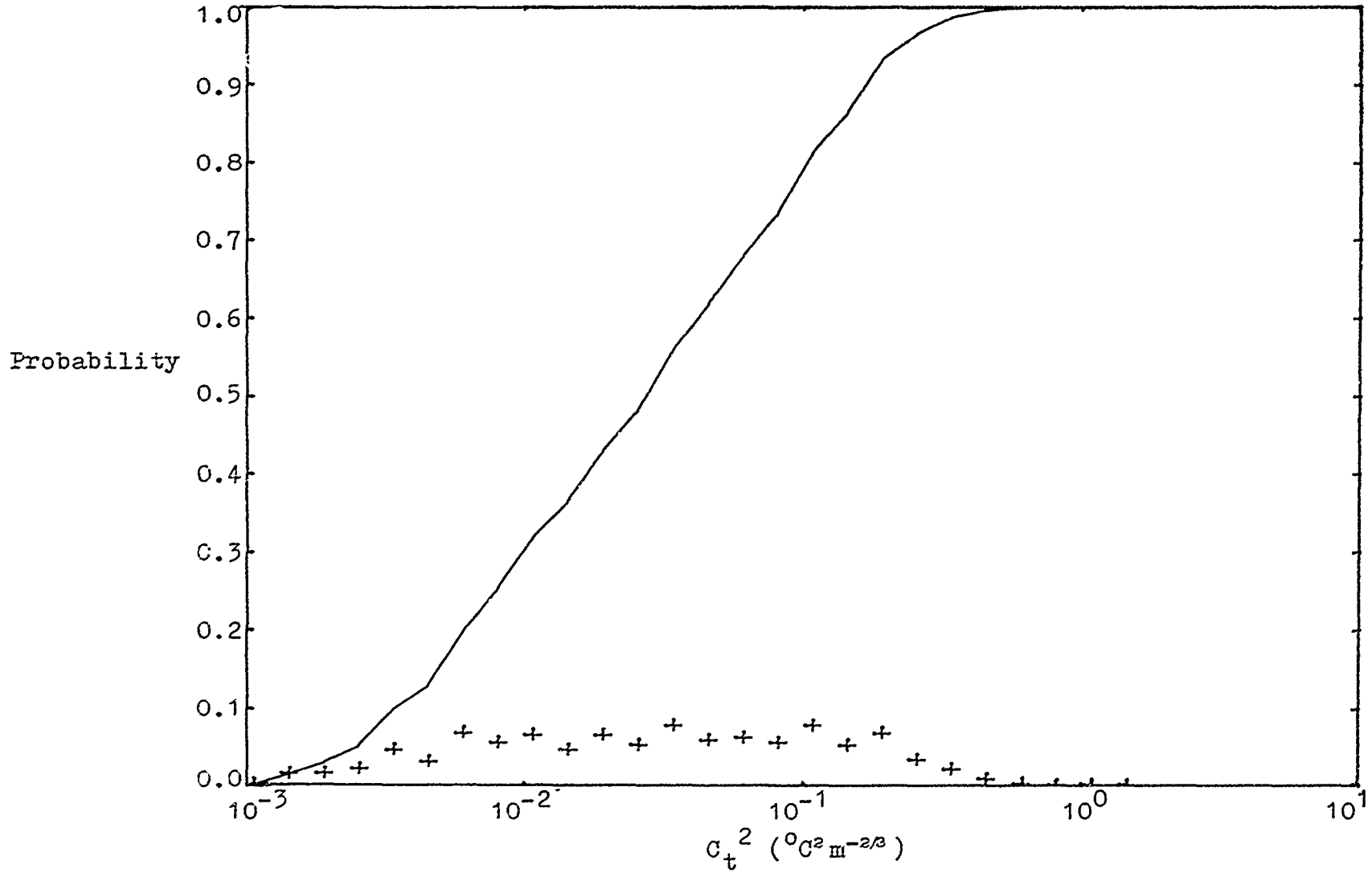

Figure A3. Discrete probability (+) and cumulative probability (solid line) of turbulence for 9-11 May 1975 (night values): 5-minute averages.

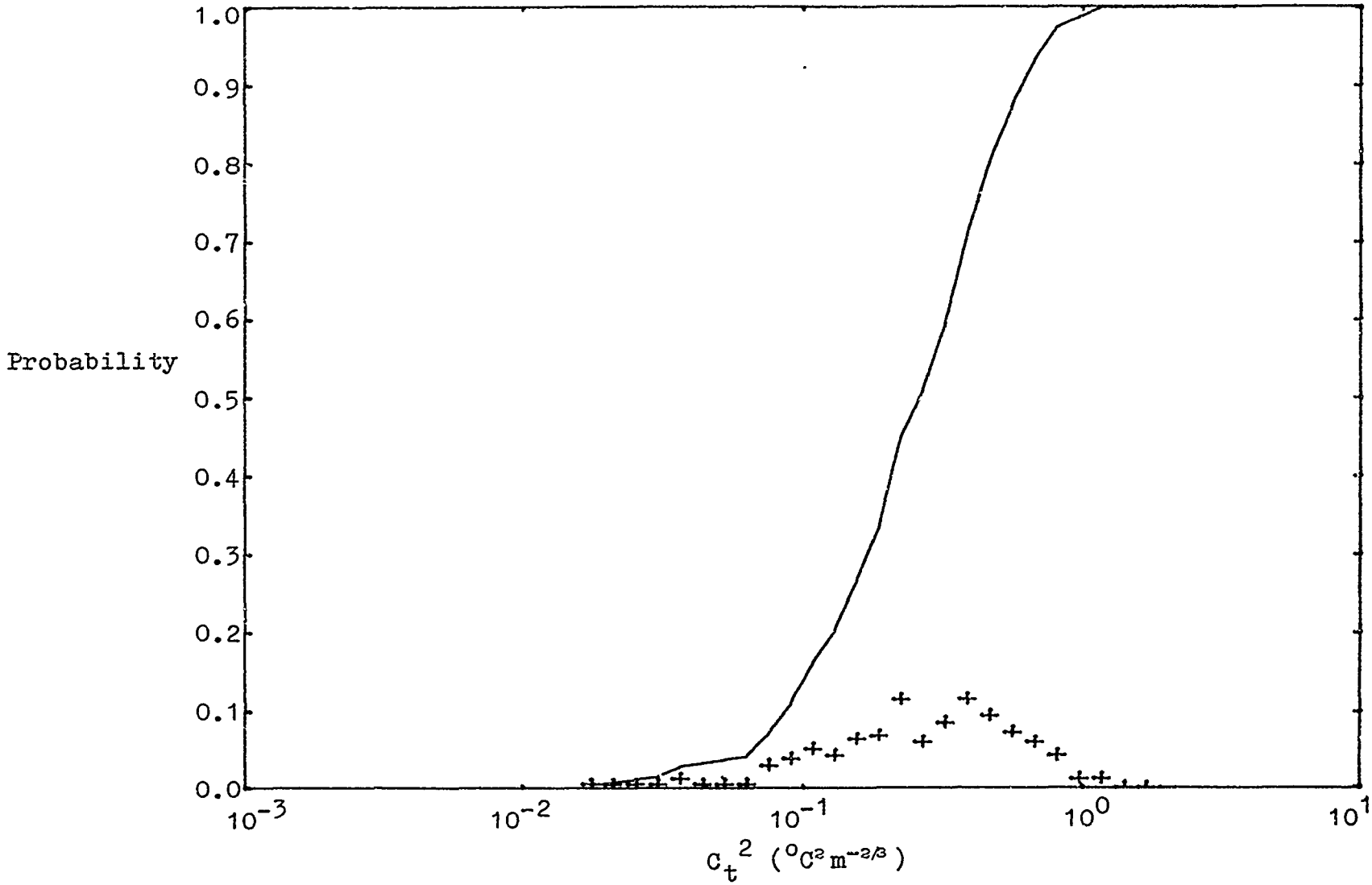

Figure A4. Discrete probability (+) and cumulative probability (solid line) of turbulence for 9-11 May 1975 (day values): 5-minute averages.

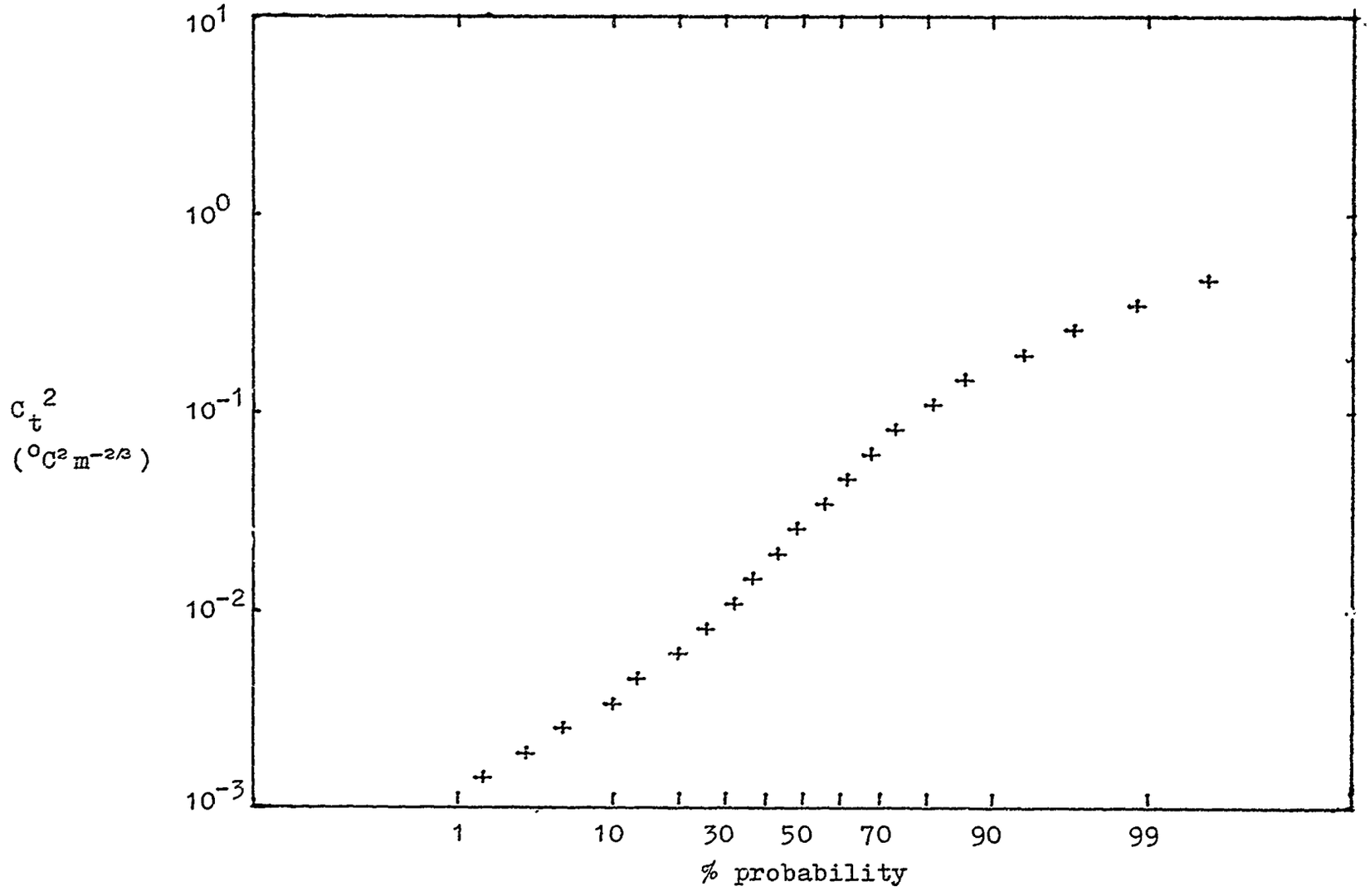

Figure A5. Cumulative probability function for 9-11 May 1975 (night values): 5-minute averages.

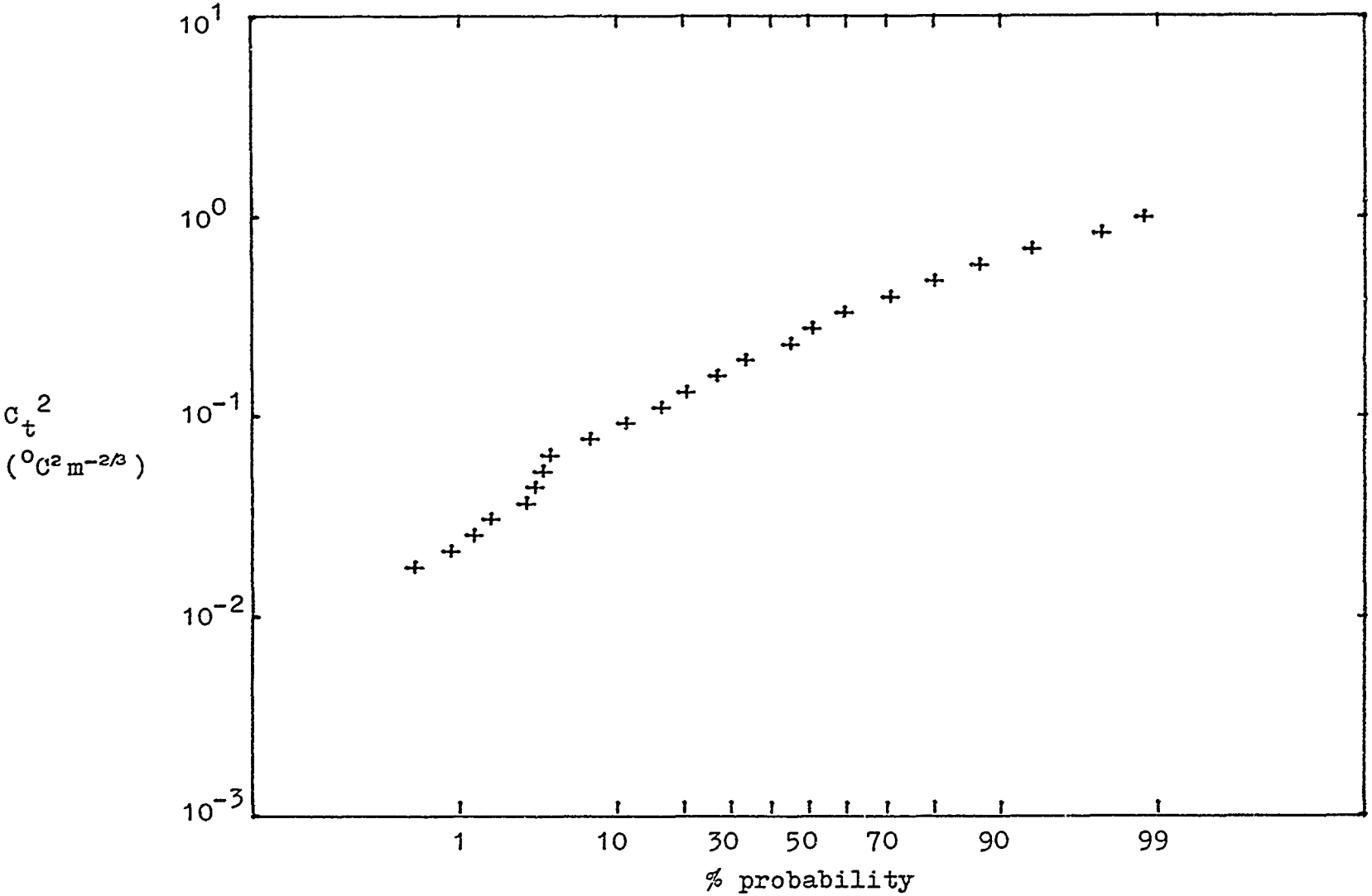

Figure A6. Cumulative probability function for 9-11 May 1975 (day values): 5-minute averages.

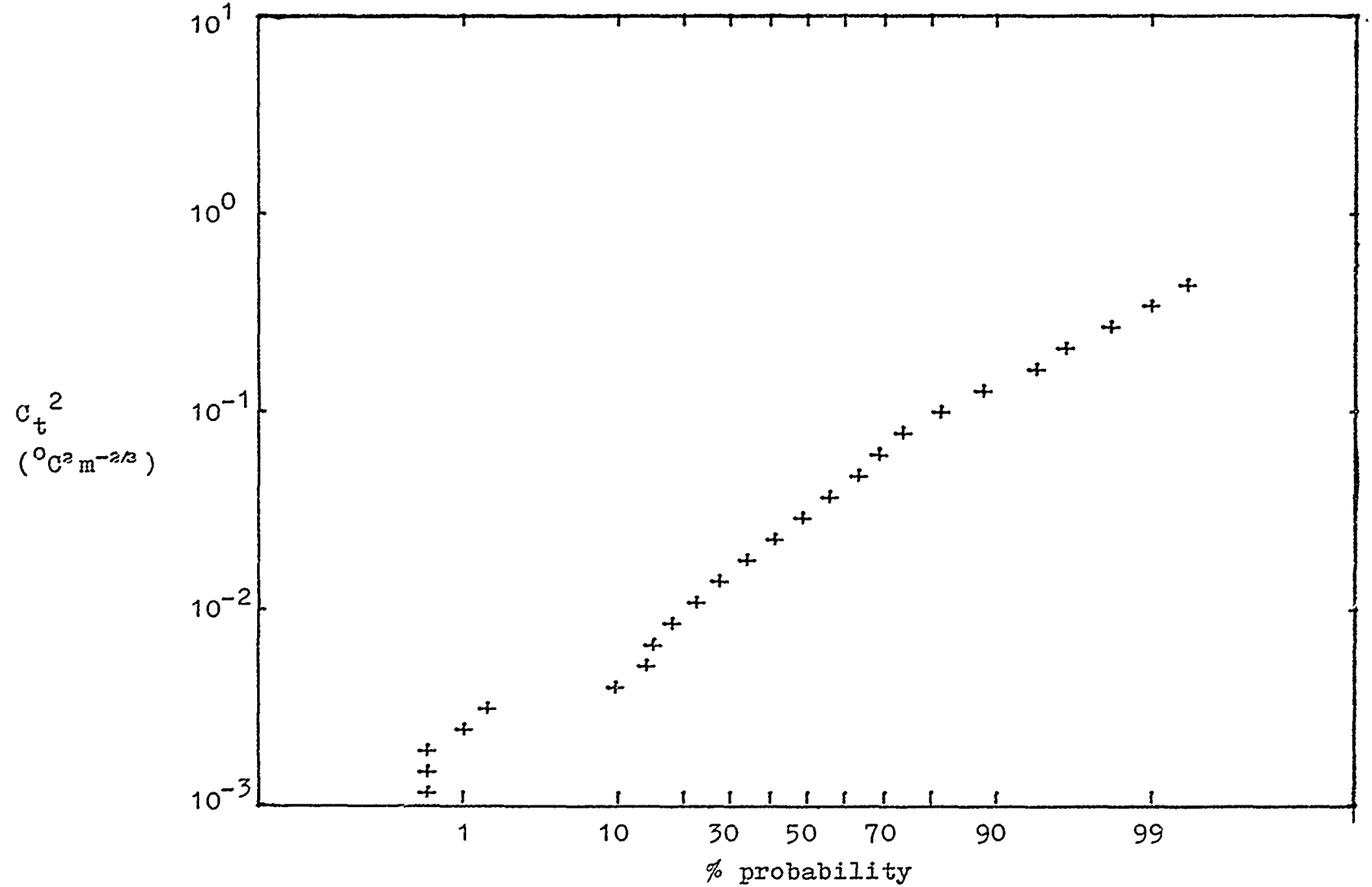

Figure A7. Cumulative probability function for May 1975, Type I turbulence (night values): 30-minute averages.

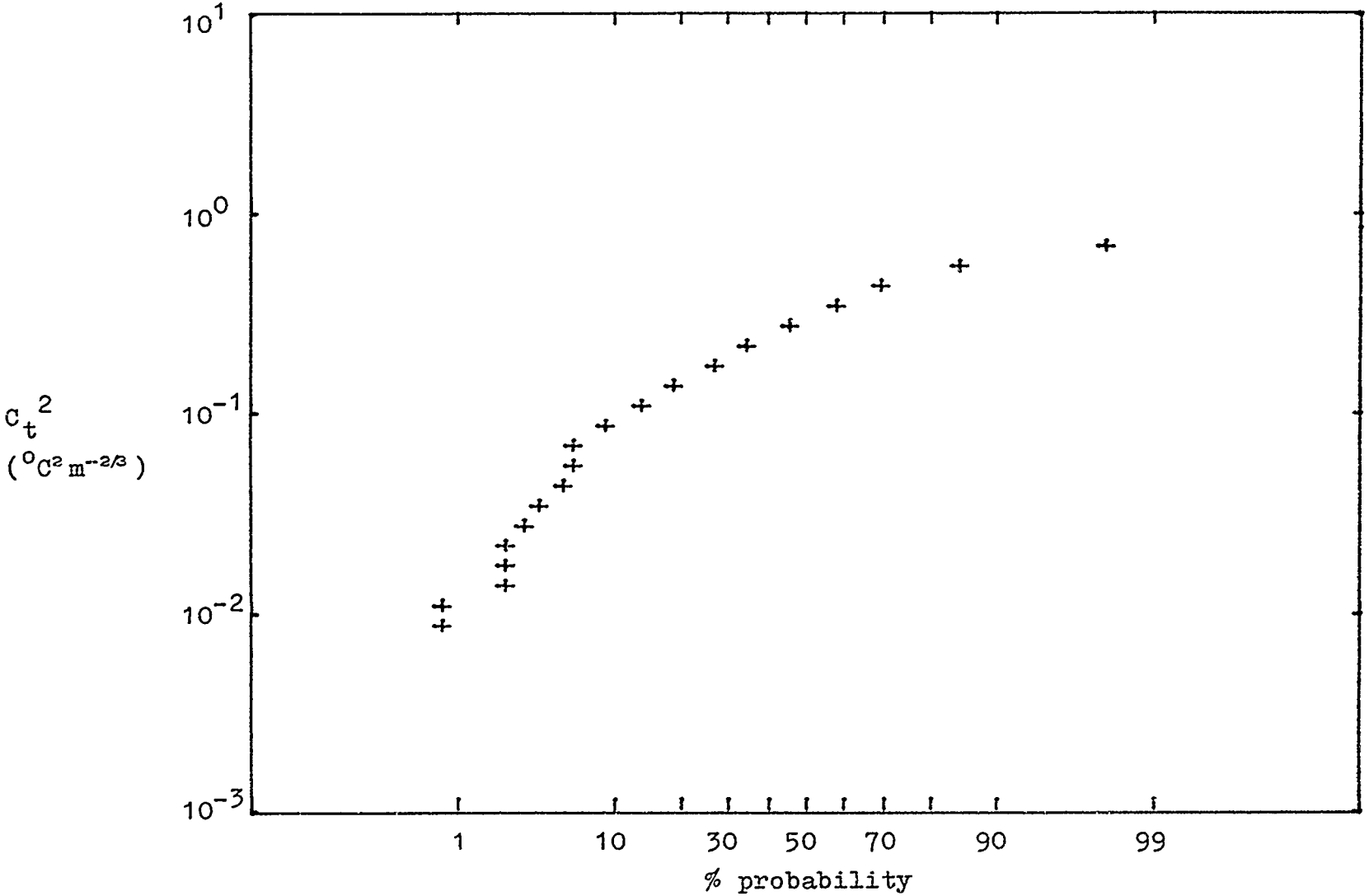

Figure A8. Cumulative probability function for May 1975, Type I turbulence (day values): 30-minute averages.

APPENDIX B - SENSOR NORMALIZATION ERRORS

The length of the thin platinum wire which is used as the temperature sensing element of microtemperature probes varies slightly from unit to unit. This causes the probes to have different gain factors, which results in nonuniform voltage-to-temperature conversions. The resistance of the platinum wire is measured and compared to a standard value for normalization. If the resistance measurements are in error for any reason, the probes will not be correctly normalized. It was feared that this could grossly affect the calculation of C_t^2. The following analysis explores the problem.

Since the probe voltage is AC coupled to ambient temperature changes (the time constant is approximately 100 sec),

$$< \text{voltage} > \approx 0 \tag{B1}$$

or, since the temperature T is directly proportional to voltage,

$$< T > = 0 \tag{B2}$$

Then

$$\sigma_1^2 = < (T_1)^2 > , \tag{B3}$$

$$(\sigma_2')^2 = < (T_2')^2 > , \tag{B4}$$

and

$$C_{12}' = < (T_1) (T_2') > \tag{B5}$$

where the primes indicate values affected by normalization errors. We can write

$$(T_2')^2 = (T_2)^2 (1+\epsilon) \tag{B6}$$

where ϵ accounts for possible differences between probe calibrations. C_t^2

is related to the temperature variances and covariances by

$$C_t^2 \propto \sigma_1^2 + (\sigma_2')^2 - 2C_{12}' \tag{B7}$$

From B4-B6 we find that

$$(\sigma_2')^2 = \sigma_2^2 (1+\varepsilon) \tag{B8}$$

and

$$C_{12}' = C_{12}(1+\varepsilon)^{1/2} \tag{B9}$$

Substituting back into B7, we have

$$C_t^2 \propto \sigma_1^2 + \sigma_2^2 (1+\varepsilon) - 2C_{12} (1+\varepsilon)^{1/2} \tag{B10}$$

If it is assumed that ε is "small", then

$$(1+\varepsilon)^{1/2} \approx 1+(\varepsilon/2) \tag{B11}$$

Note that for ε as large as 0.5, the approximation is less than 3% in error. Using (B11), (B10) becomes

$$C_t^2 \propto \sigma_1^2 + \sigma_2^2 (1+\varepsilon) - 2C_{12}(1+\tfrac{1}{2}\varepsilon)$$

$$=\sigma_1^2 + \sigma_2^2 - 2C_{12} + \varepsilon(\sigma_2^2 - C_{12}) \tag{B12}$$

The error has now been isolated to a single term. Suppose the desired accuracy is only 25%; then

$$\varepsilon(\sigma_2^2 - C_{12}) < (\sigma_1^2 + \sigma_2^2 - 2C_{12})/4$$

or

$$\varepsilon < \frac{\sigma_1^2 + \sigma_2^2 - 2C_{12}}{4(\sigma_2^2 - C_{12})} \tag{B13}$$

From turbulence theory, we expect $\sigma_1^2 \approx \sigma_2^2$ for sufficient averaging times. Equation (B13) then becomes

$$\varepsilon < \frac{\sigma_1^2 + \sigma_1^2 - 2C_{12}}{4(\sigma_1^2 - C_{12})}$$

$$= \frac{2(\sigma_1^2 - C_{12})}{4(\sigma_1^2 - C_{12})}$$

$$= 0.5 \qquad \text{(B14)}$$

Under the assumptions which have been made, errors in sensor calibration up to 50 percent will cause less than a 25 percent error in the calculation of C_t^2. Such a gross error in normalization is unlikely; a 10 percent error is more plausible. This would result in an error in C_t^2 of only 5 percent. Therefore, normalization errors should present no problem to data analysis.

APPENDIX C - PROBABILITY DISTRIBUTIONS

This appendix contains the plots of the probability distributions. The distributions were calculated for each turbulence type from the 30-minute C_t^2 values, divided into night, day, dusk and dawn. The cumulative probability functior (CPF) is plotted as a continuous line, while the discrete probability function (DPF) is plotted as a sequence of points which give the probability of a value occurring within the discrete interval around that point. Another common function, the probability density function, can be easily calculated from the discrete probability function by dividing the probabilities by the interval (width) that each point represents.

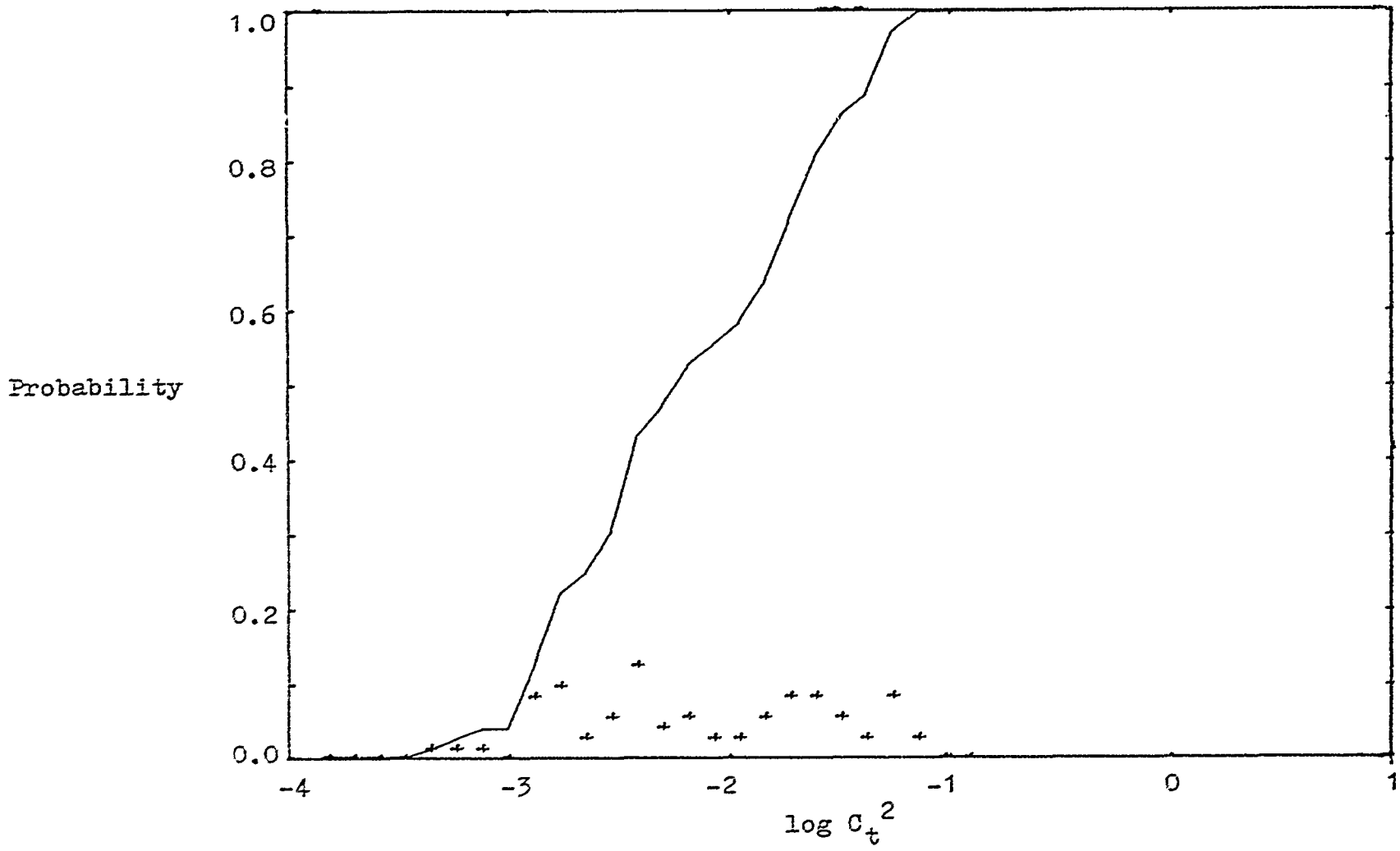

Figure C1. Discrete probability (+) and cumulative probability (solid line) for Type I turbulence: February 1975, night.

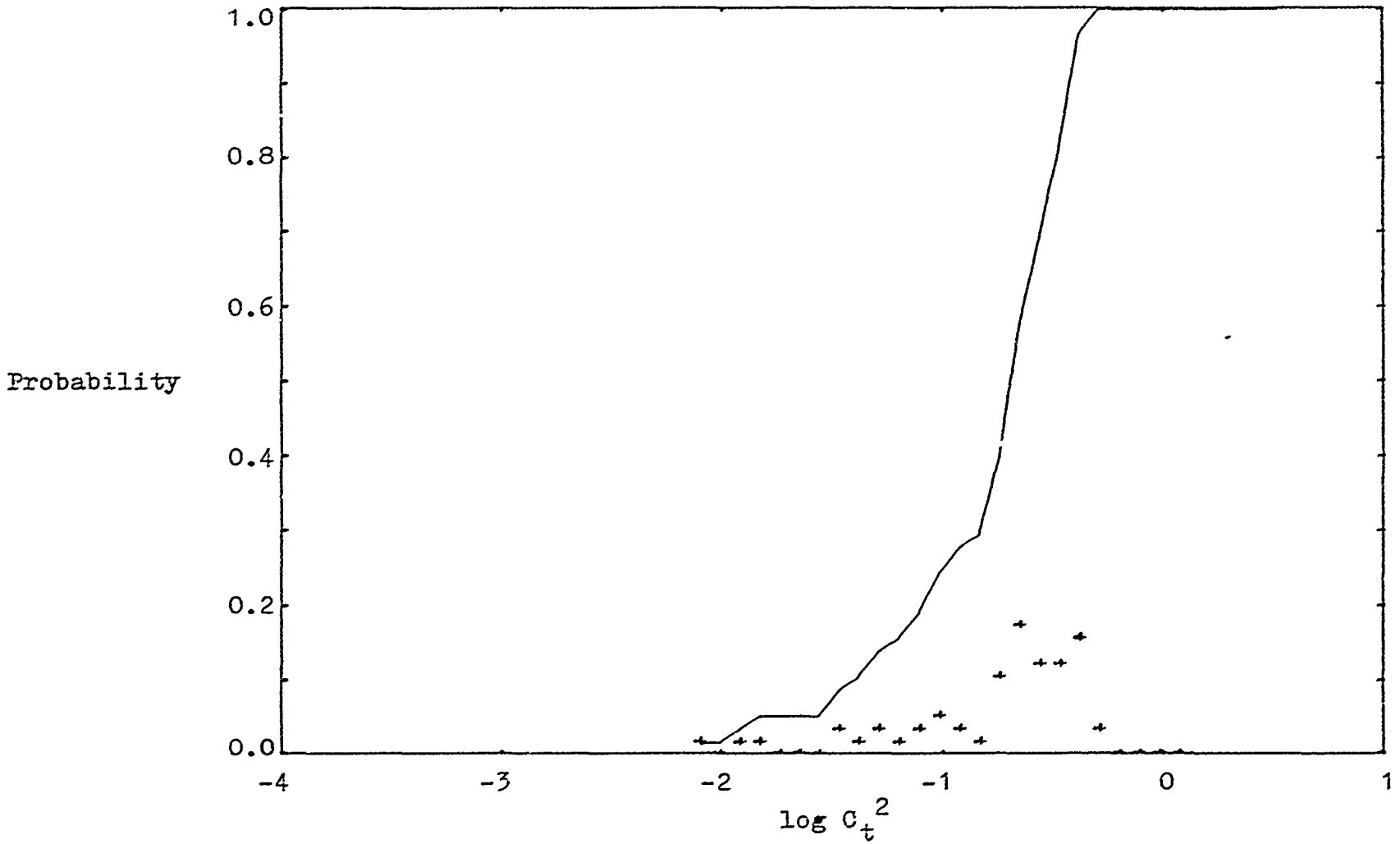

Figure C2. Discrete probability (+) and cumulative probability (solid line) for Type I turbulence: February 1975, day.

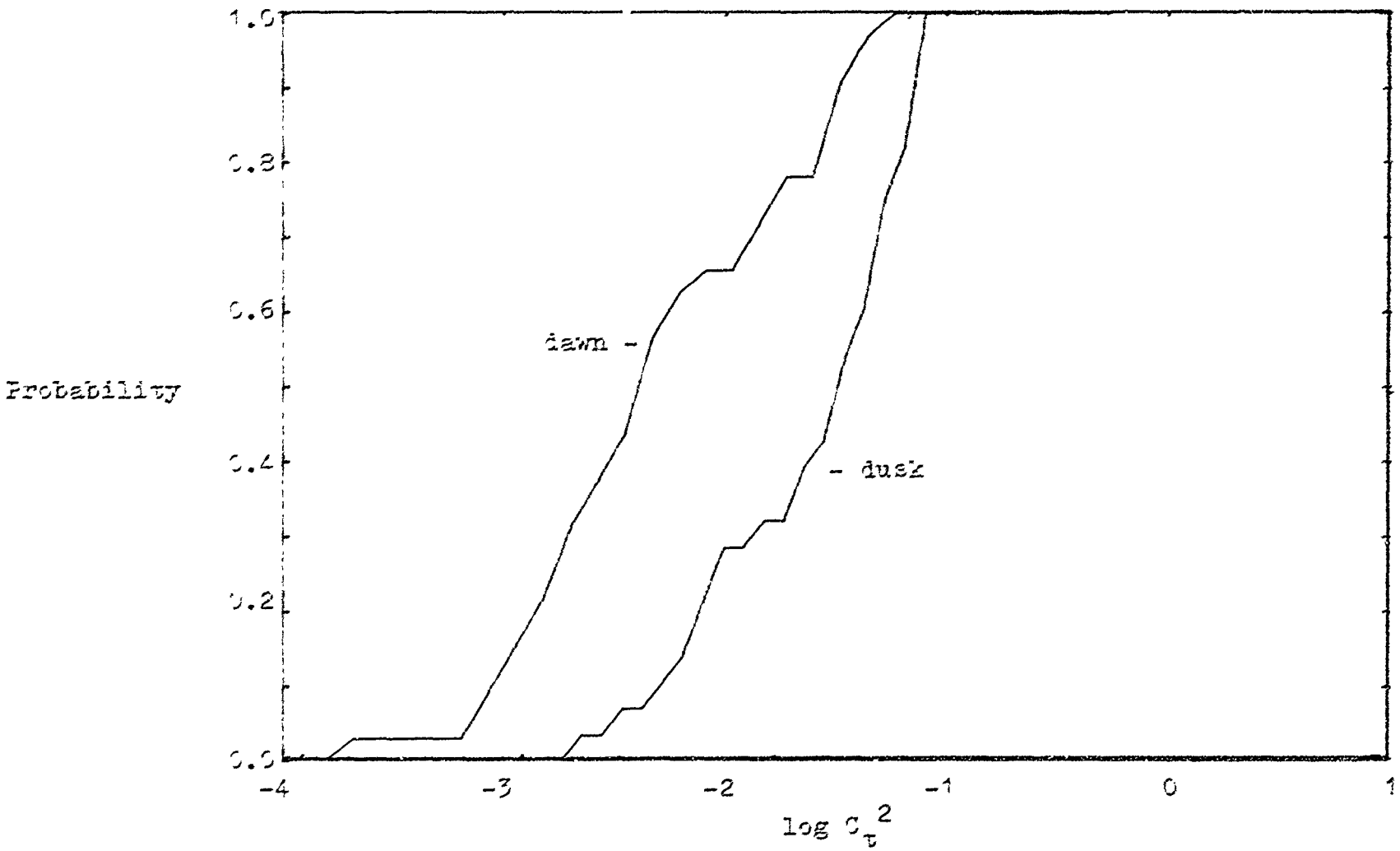

Figure C3. Cumulative probability functions for Type I turbulence: February 1975, dusk and dawn.

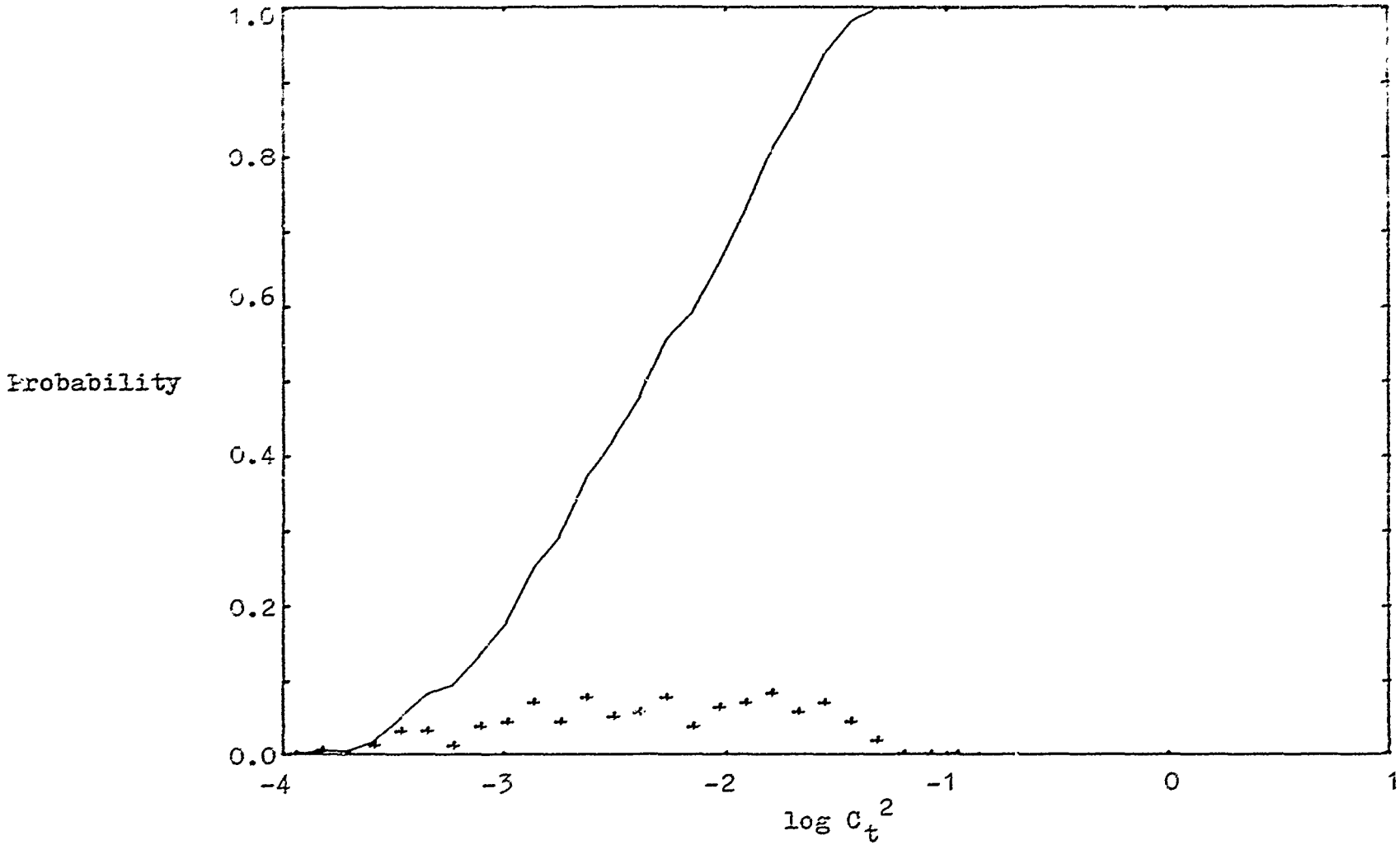

Figure C4. Discrete probability (+) and cumulative probability (solid line) for Type I turbulence: March 1975, night.

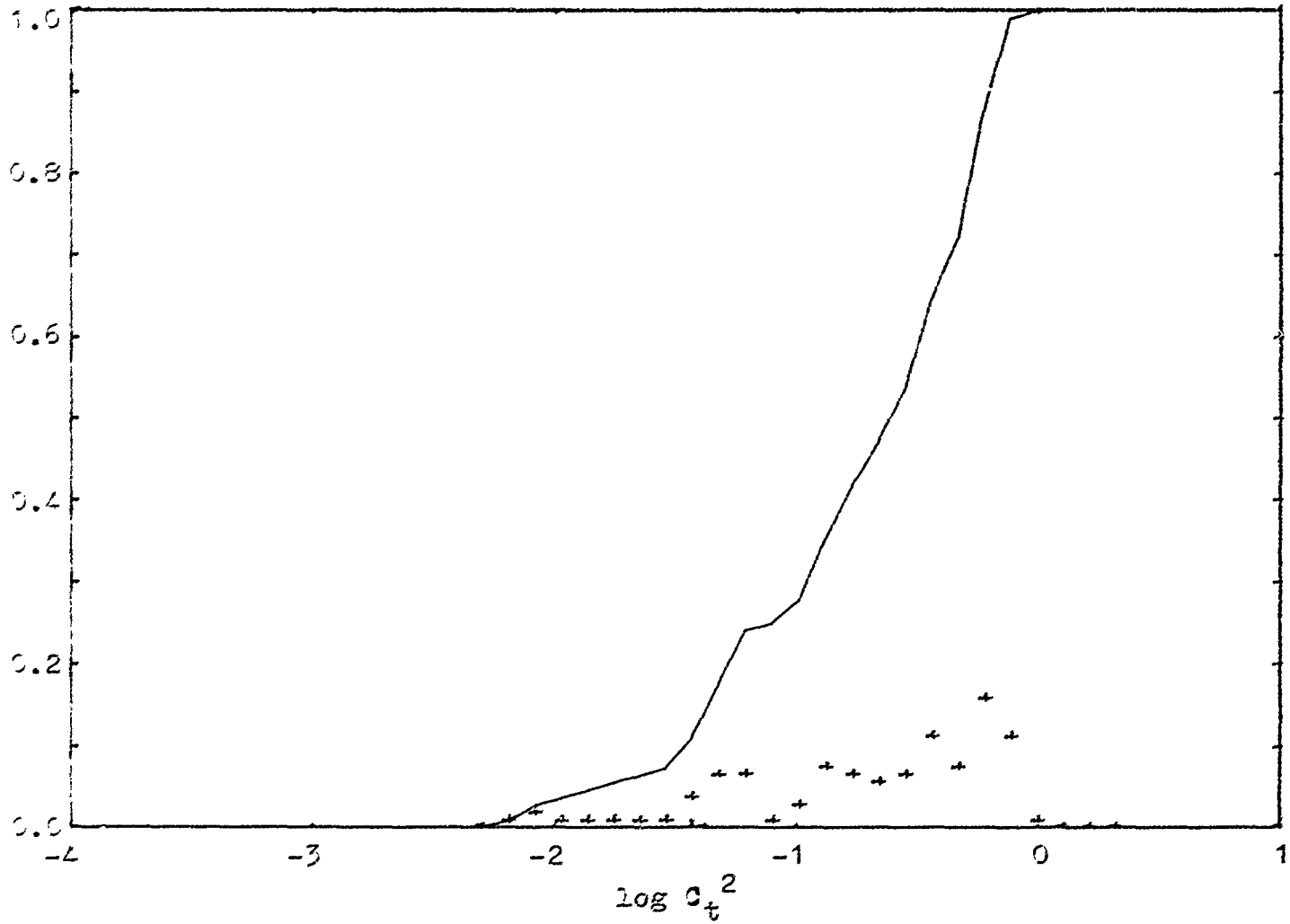

Figure 05. Discrete probability (+) and cumulative probability (solid line) for Type I turbulence: March 1975, day.

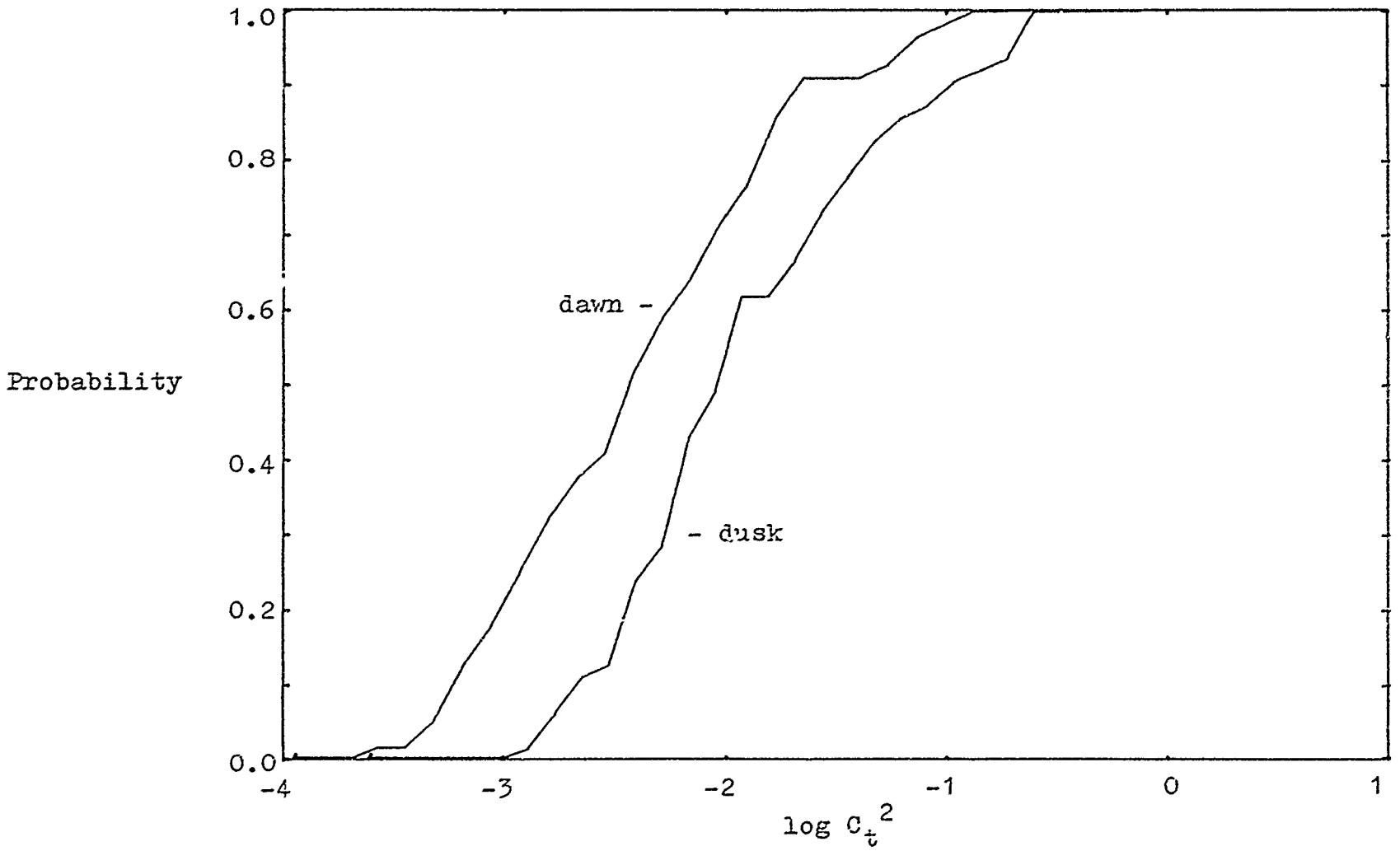

Figure C6. Cumulative probability functions for Type I turbulence: March 1975, dusk and dawn.

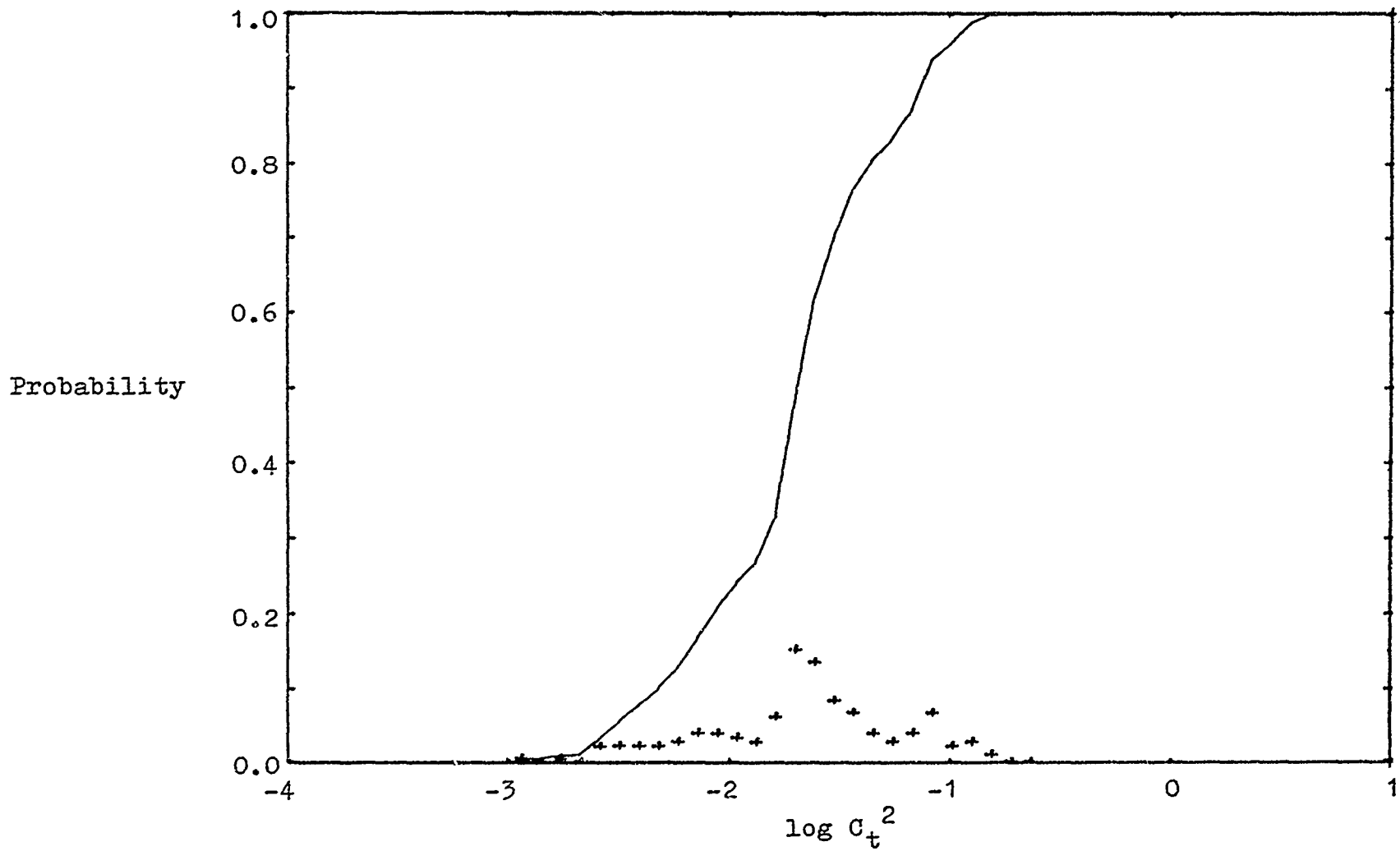

Figure C7. Discrete probability (+) and cumulative probability (solid line) for Type I turbulence: April 1975, night.

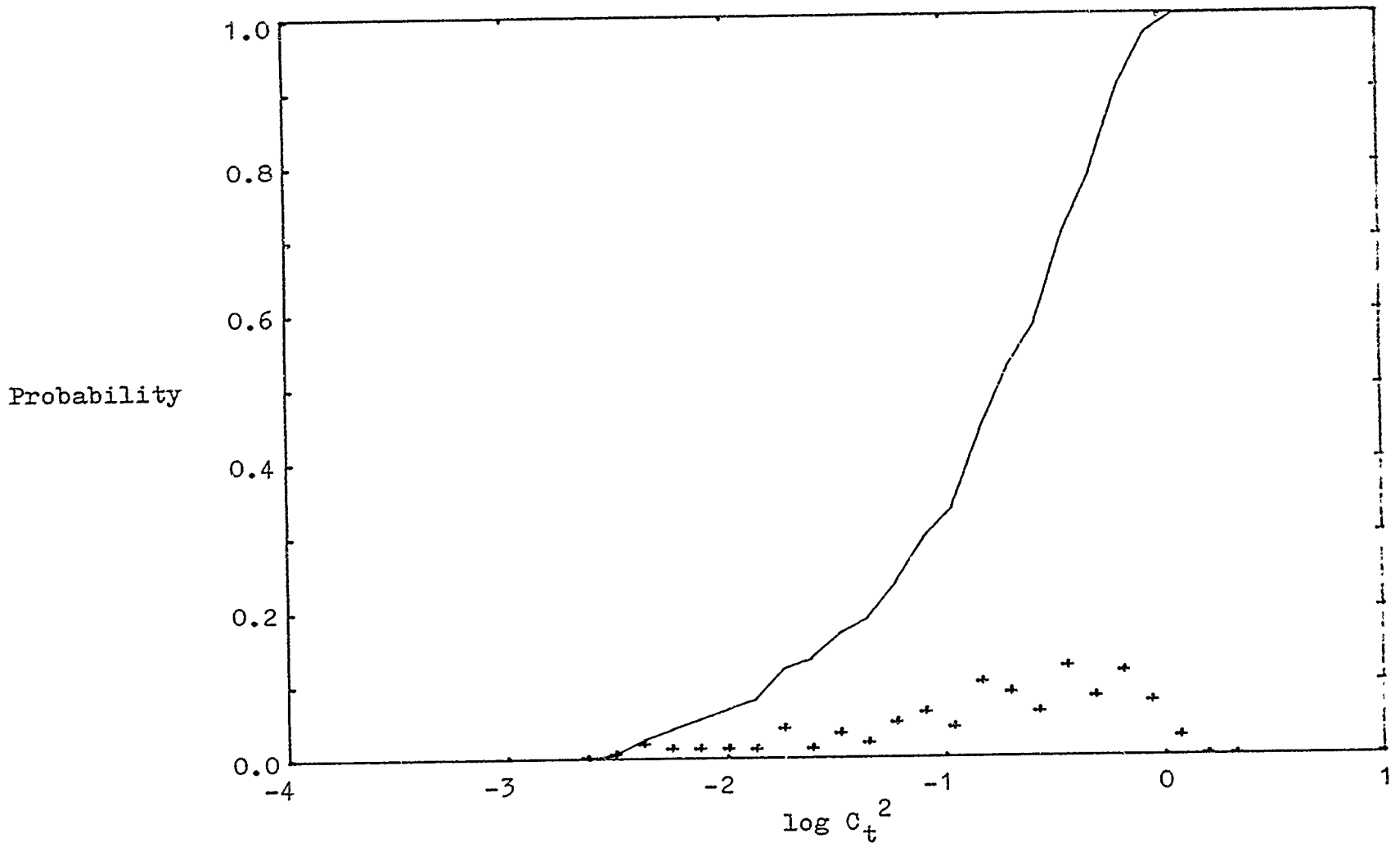

Figure C8. Discrete probability (+) and cumulative probability (solid line) for Type I turbulence: April 1975, day.

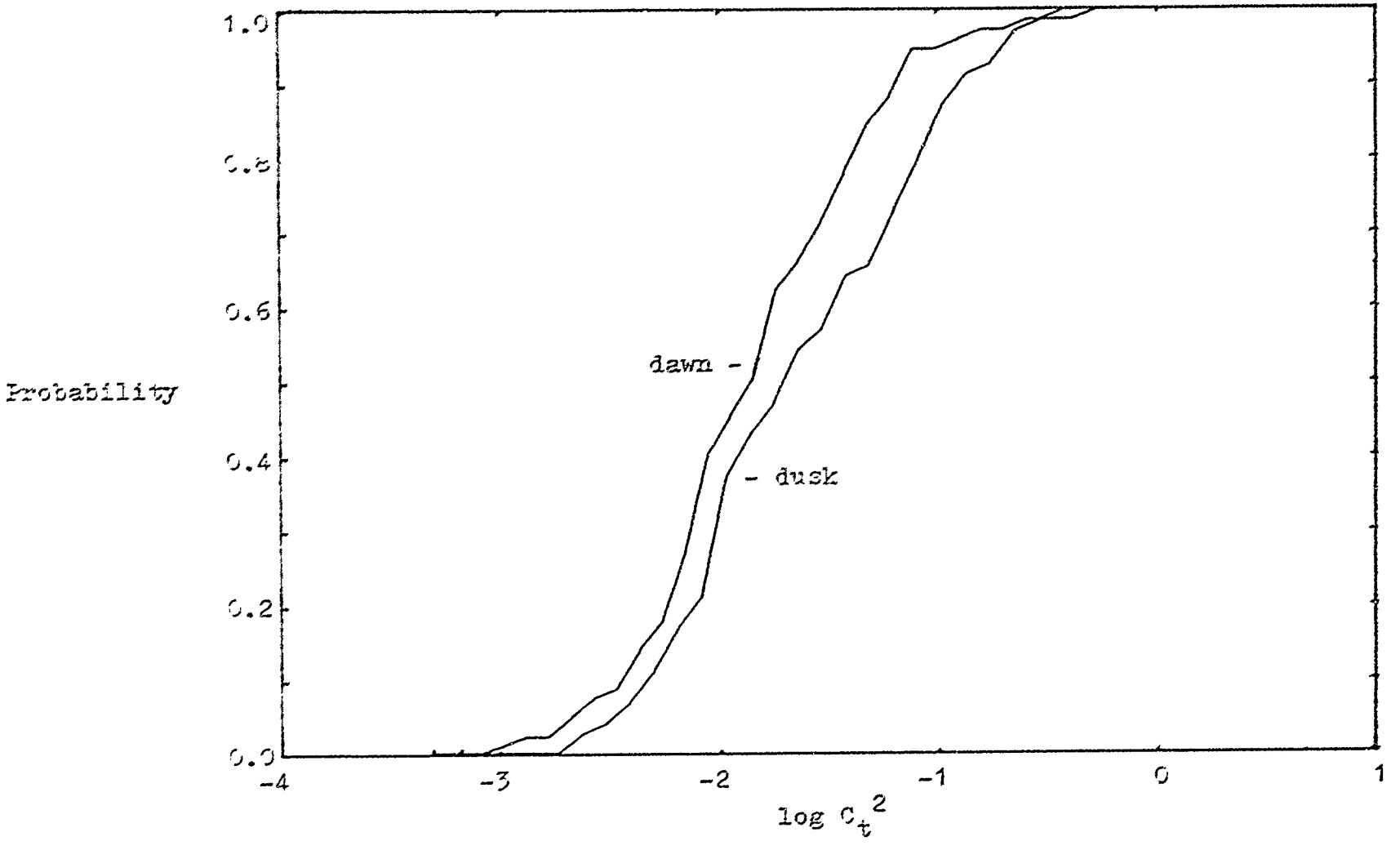

Figure 39. Cumulative probability functions for Type I turbulence: April 1975, dusk and dawn.

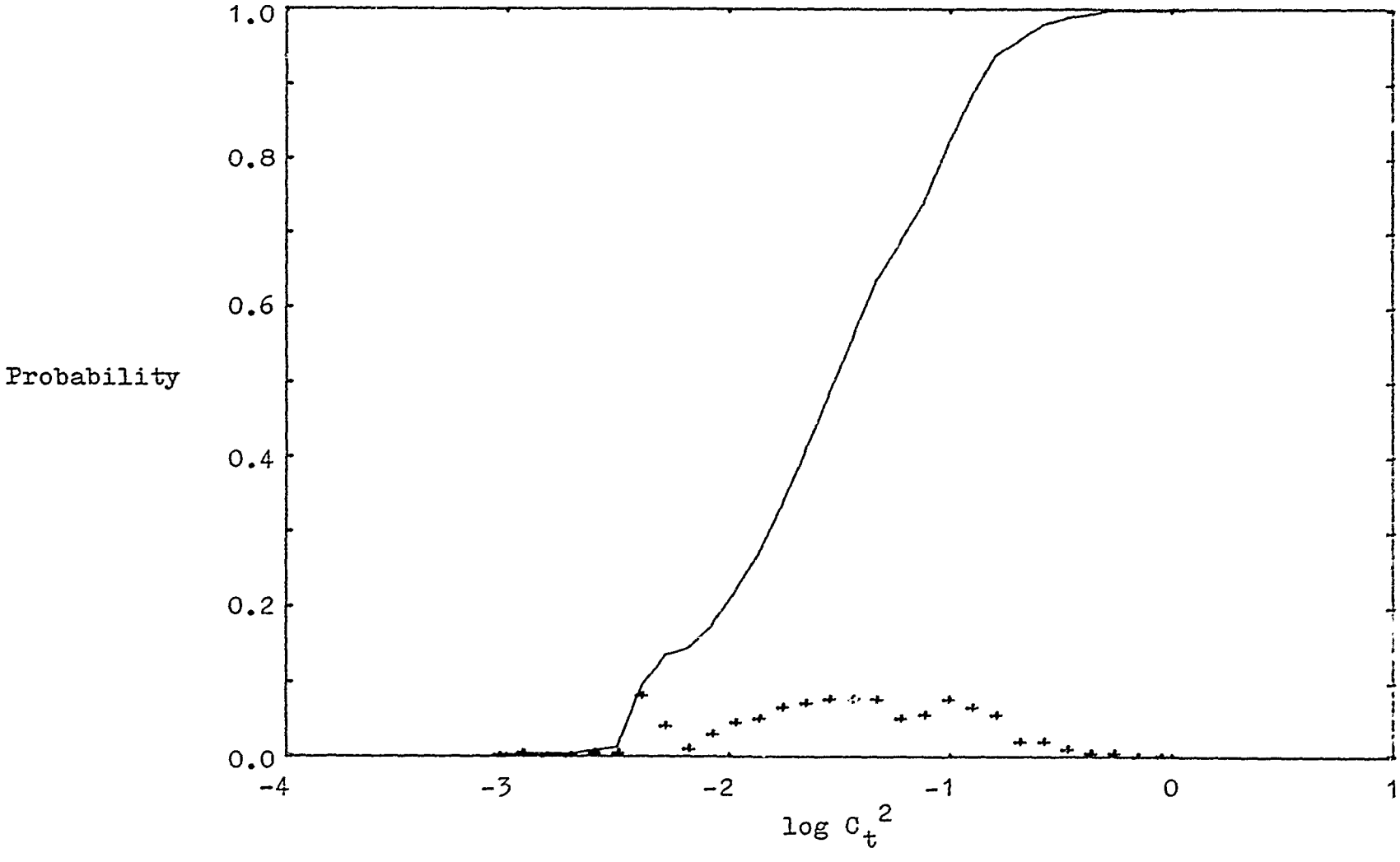

Figure C10. Discrete probability (+) and cumulative probability (solid line) for Type I turbulence: May 1975, night.

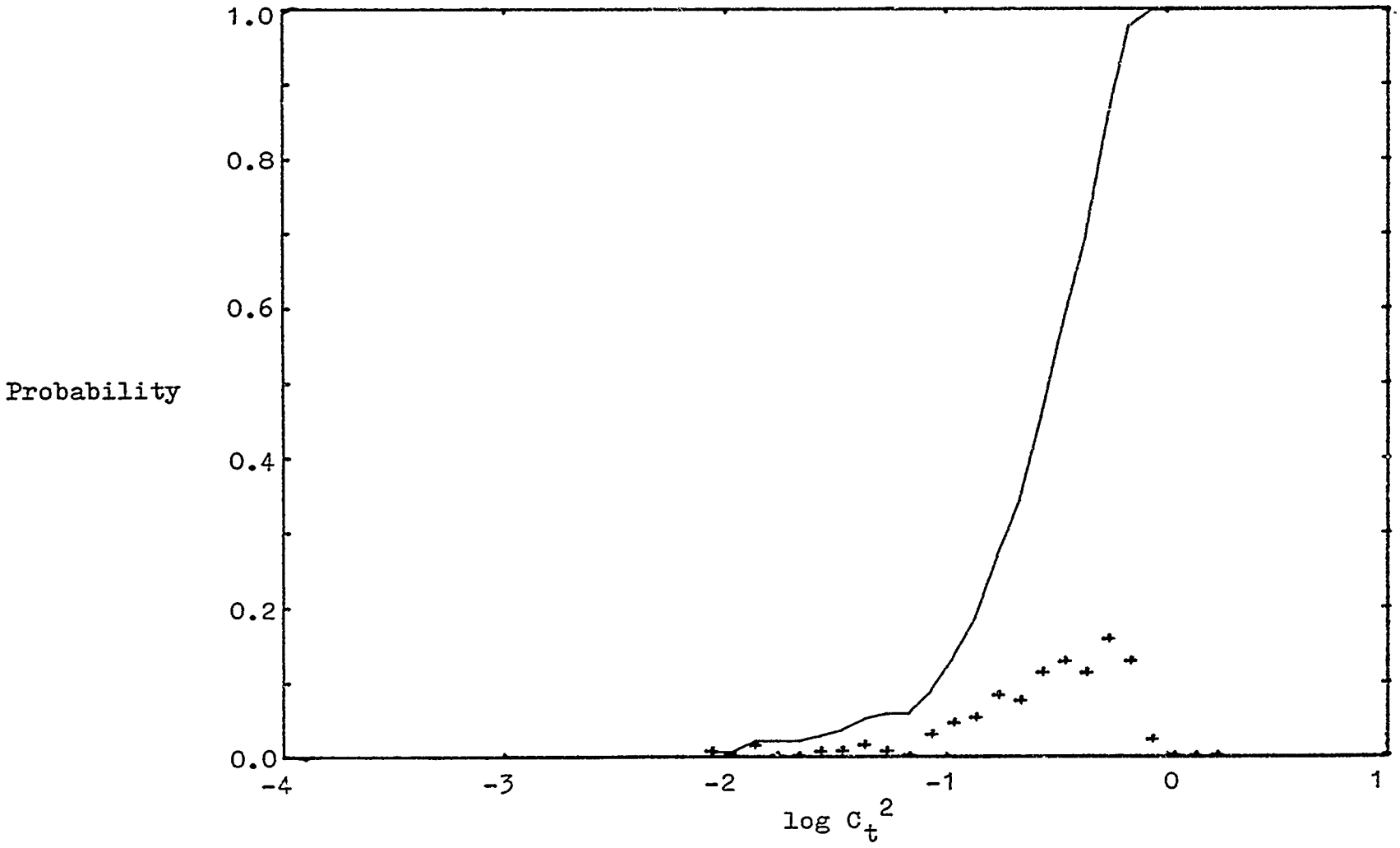

Figure C11. Discrete probability (+) and cumulative probability (solid line) for Type I turbulence: May 1975, day.

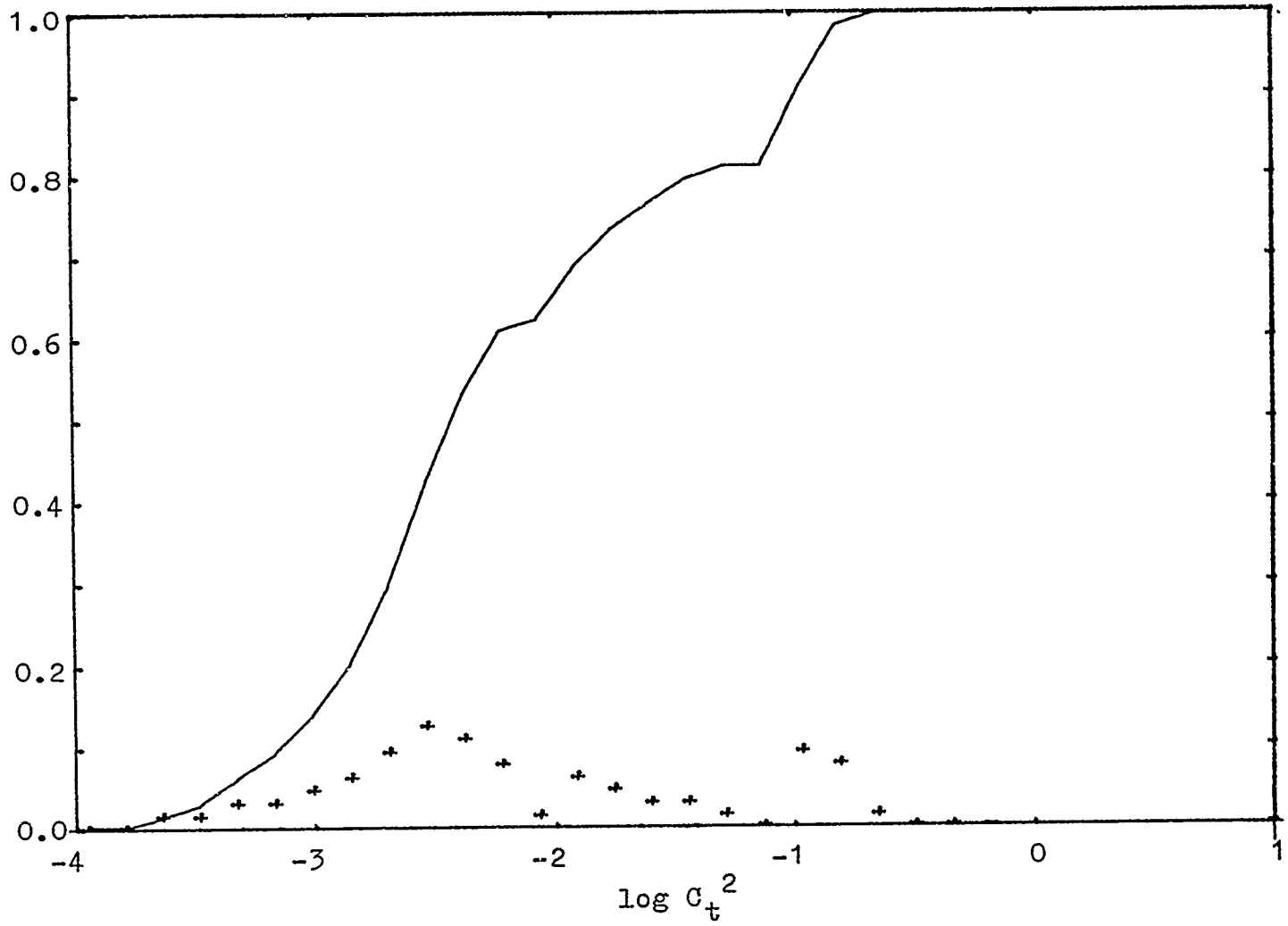

Figure C13. Discrete probability (+) and cumulative probability (solid line) for Type II turbulence: February 1975, night.

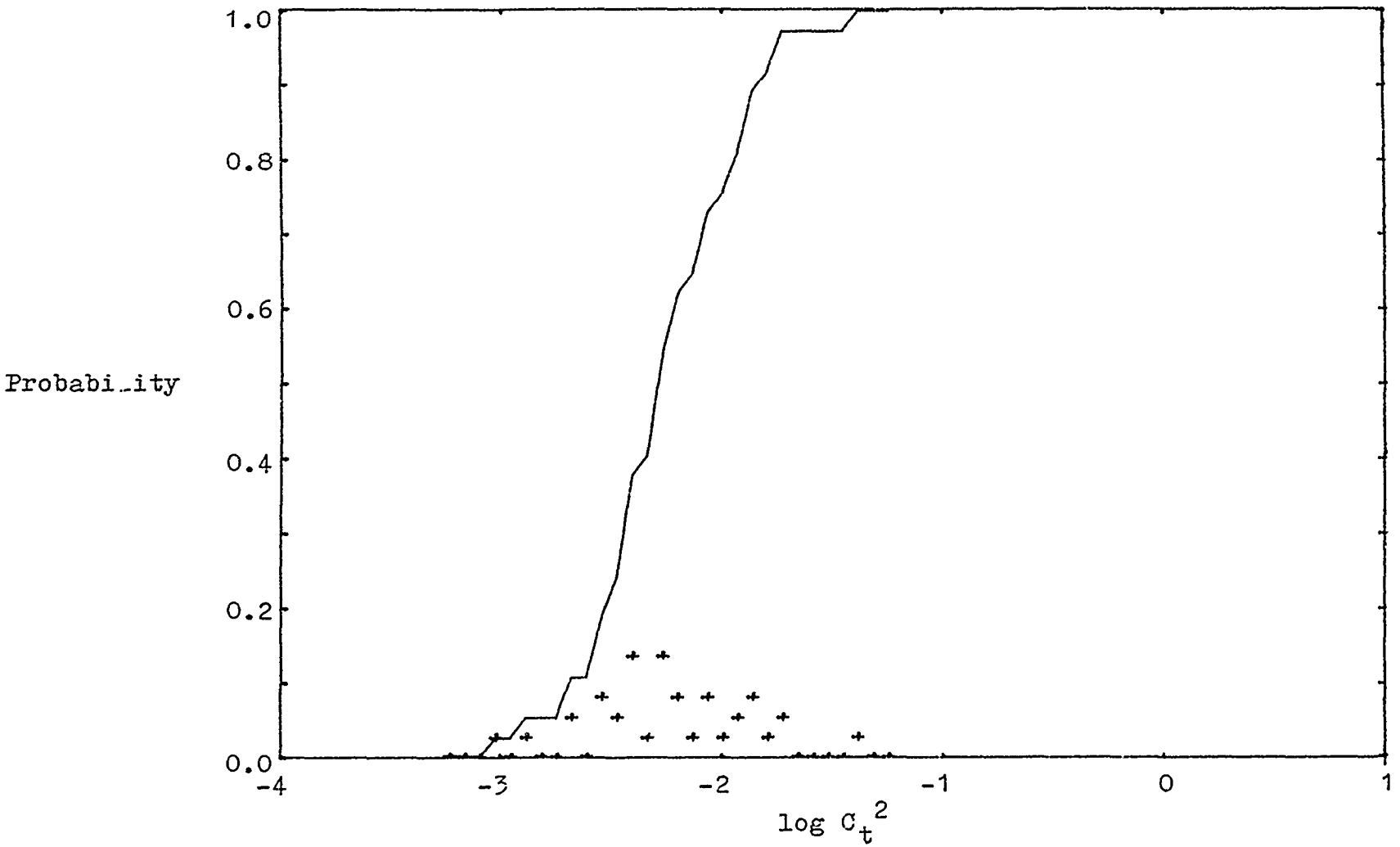

Figure C14. Discrete probability (+) and cumulative probability (solid line) for Type II turbulence: February 1975, day.

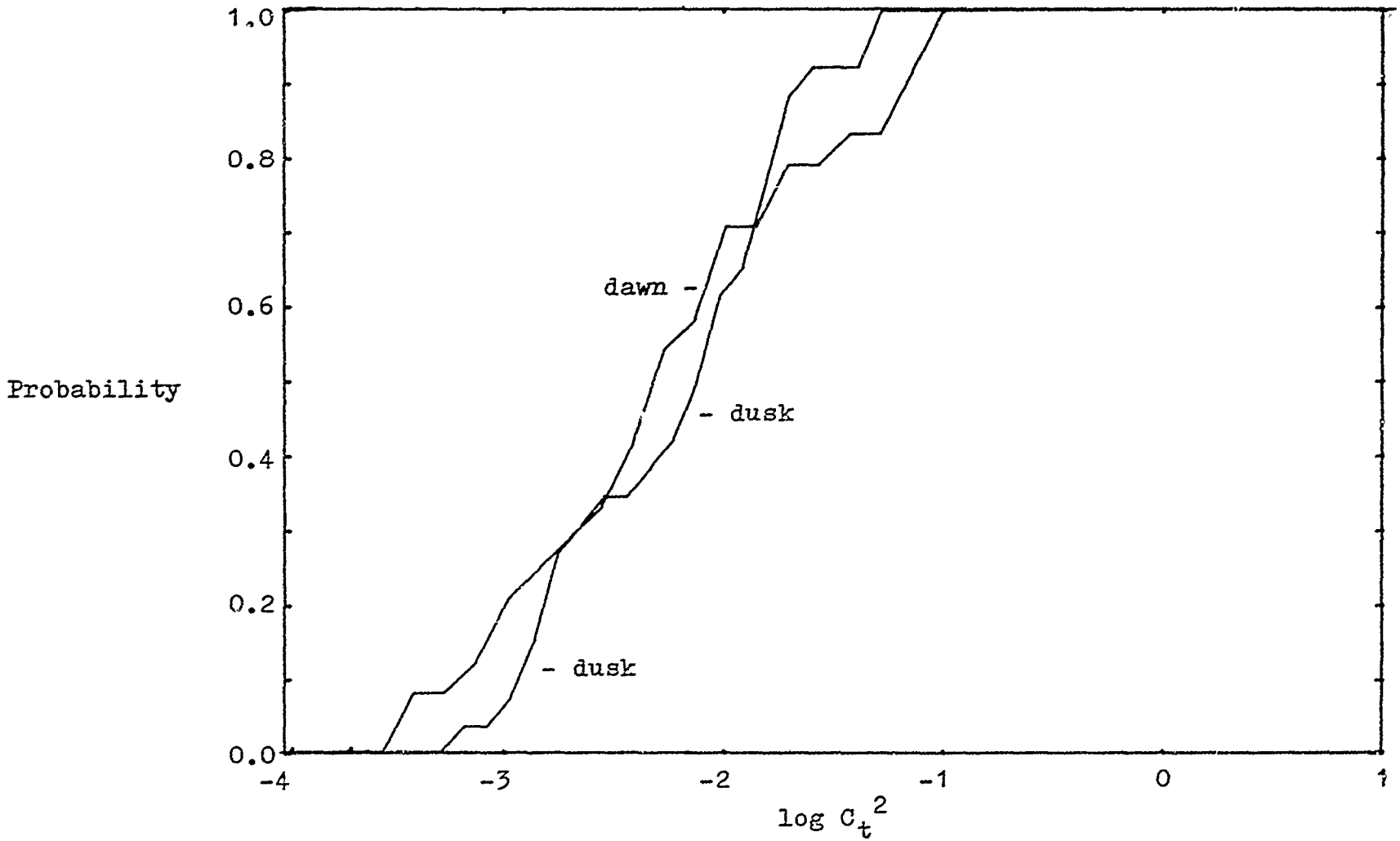

Figure C15. Cumulative probability functions for Type II turbulence: February 1975, dusk and dawn.

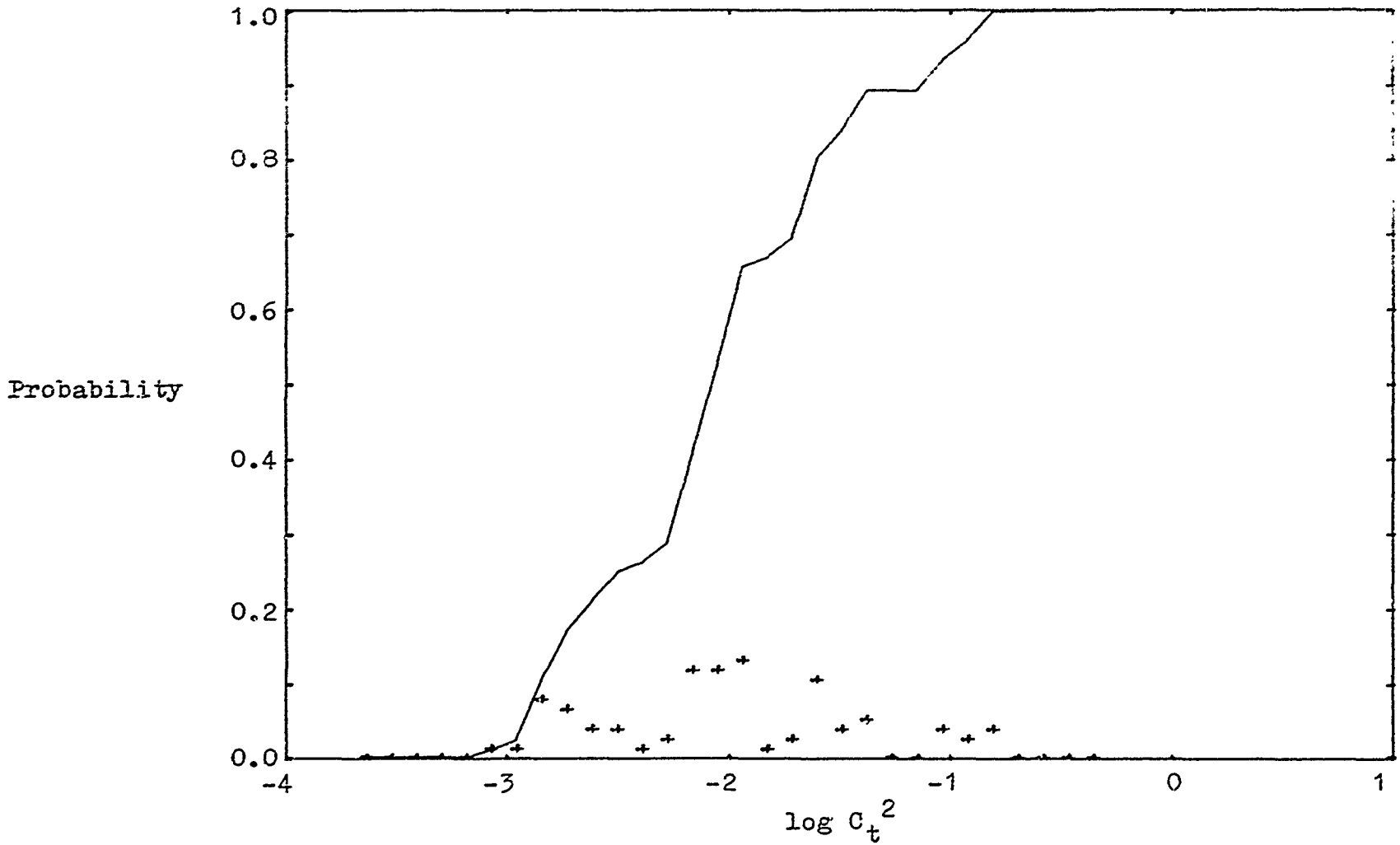

Figure C16. Discrete probability (+) and cumulative probability (solid line) for Type II turbulence: March 1975, night.

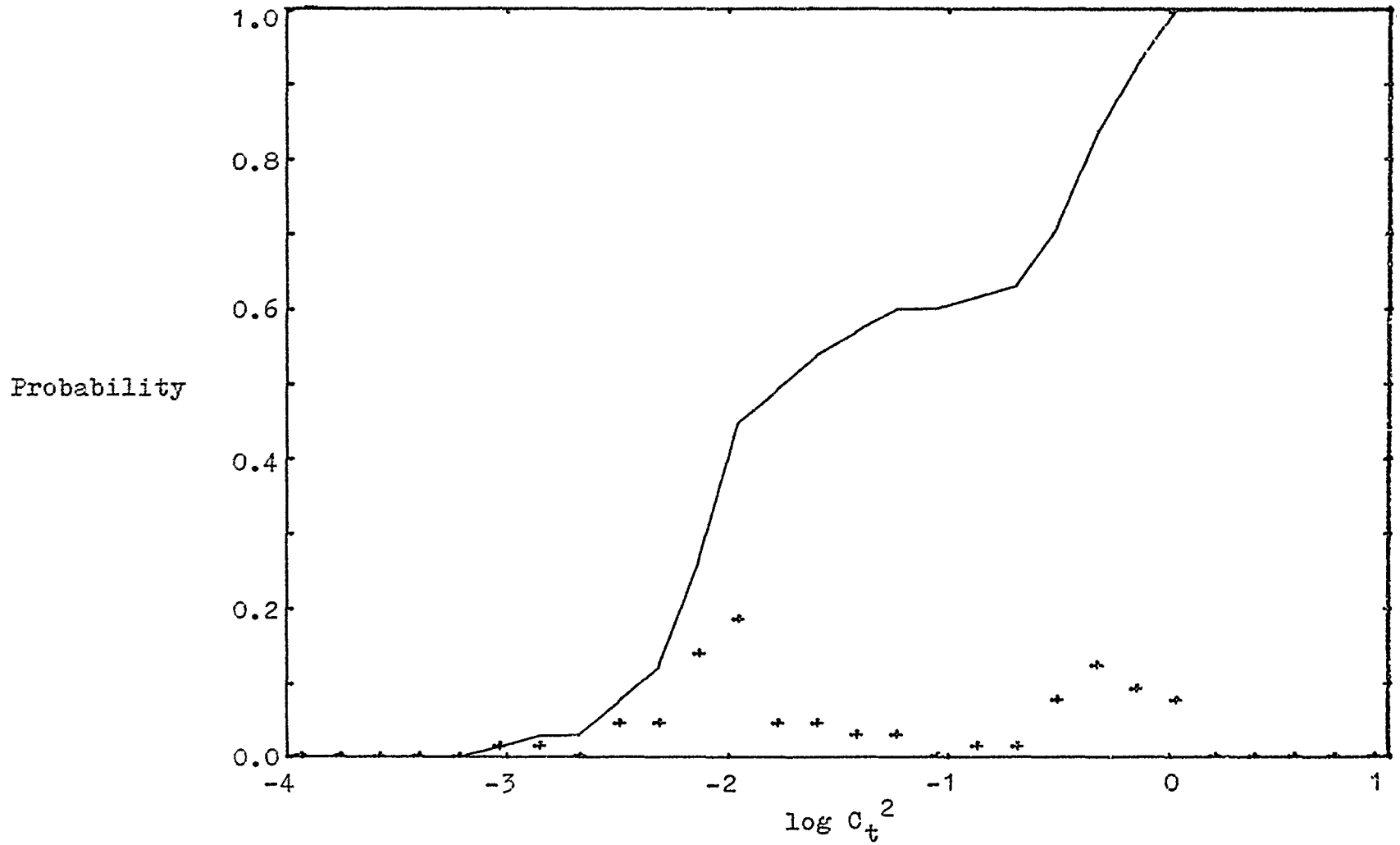

Figure C17. Discrete probability (+) and cumulative probability (solid line) for Type II turbulence: March 1975, day.

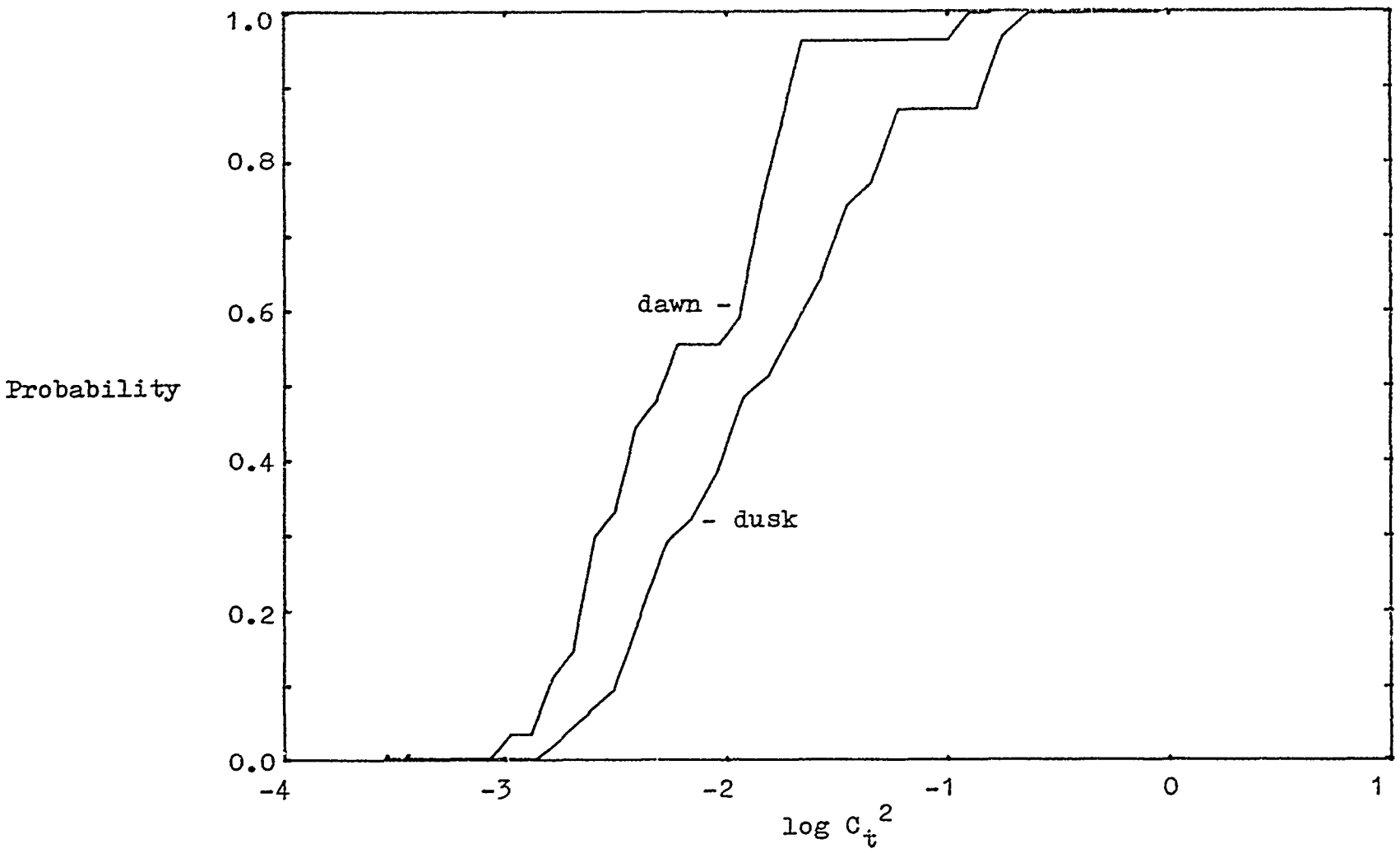

Figure C18. Cumulative probability functions for Type II turbulence: March 1975, dusk and dawn.

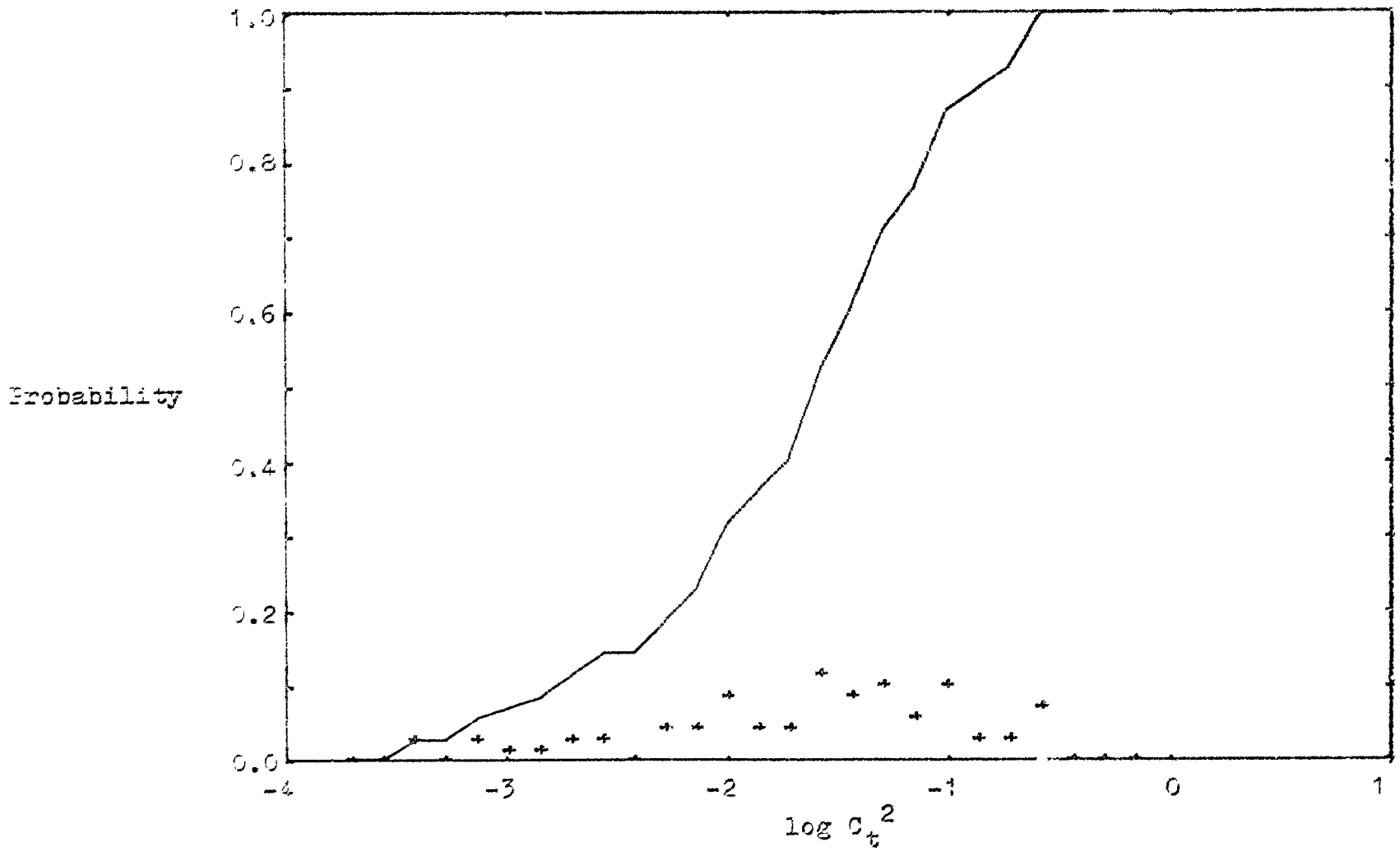

Figure C19. Discrete probability (+) and cumulative probability (solid line) for Type II turbulence: April 1975, night.

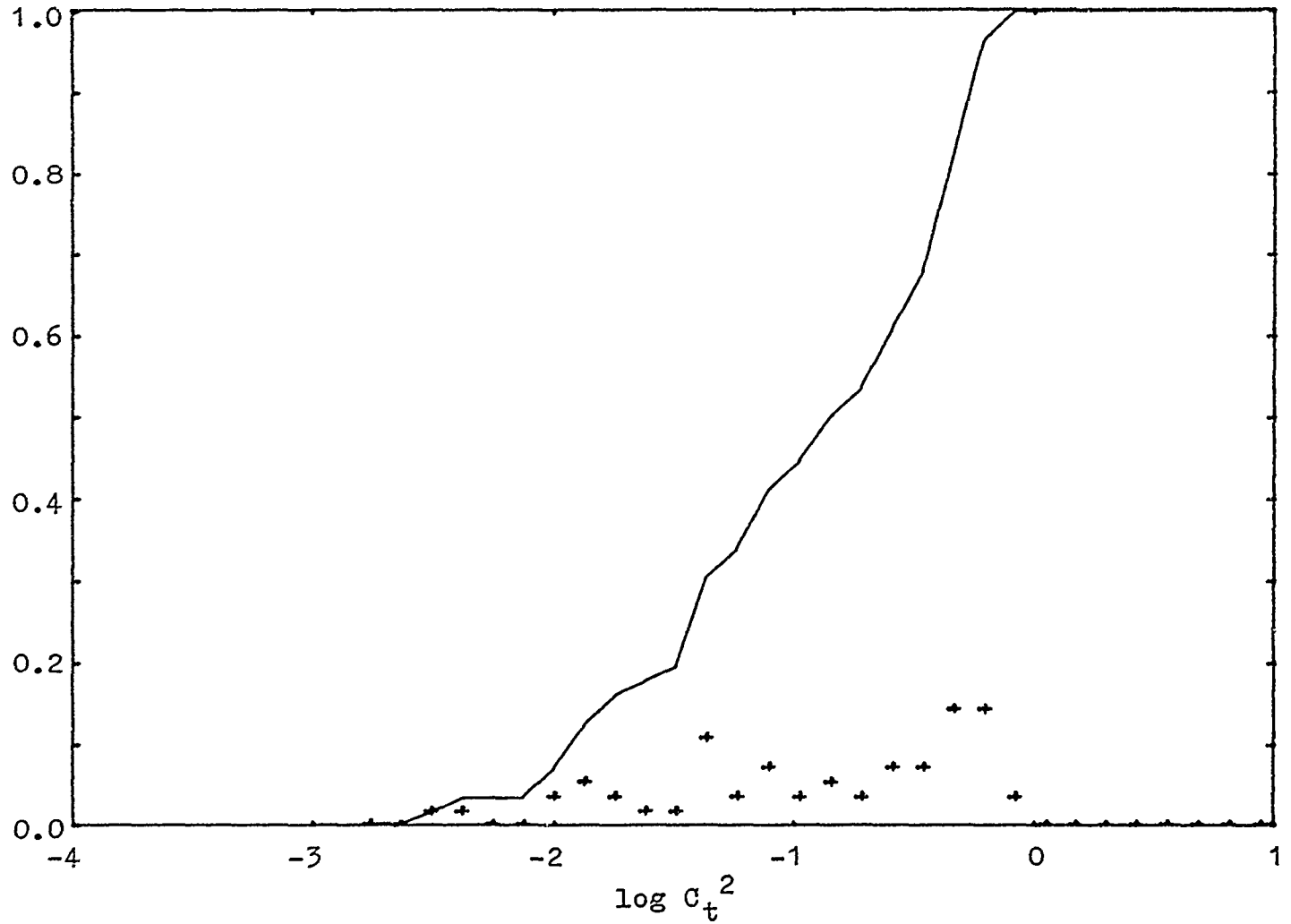

Figure C20. Discrete probability (+) and cumulative probability (solid line) for Type II turbulence: April 1975, day.

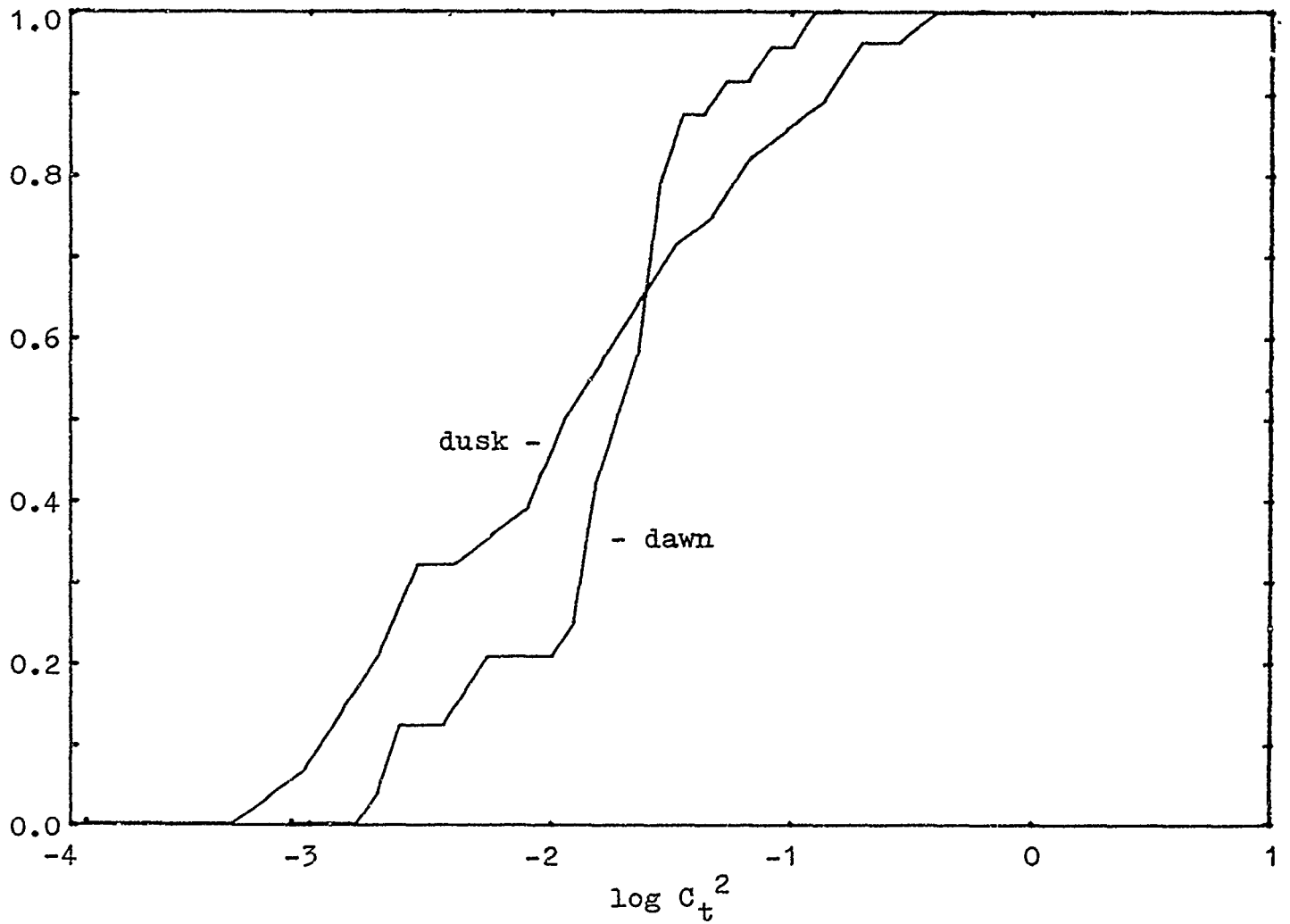

Figure C21. Cumulative probability functions for Type II turbulence: April 1975, dusk and dawn.

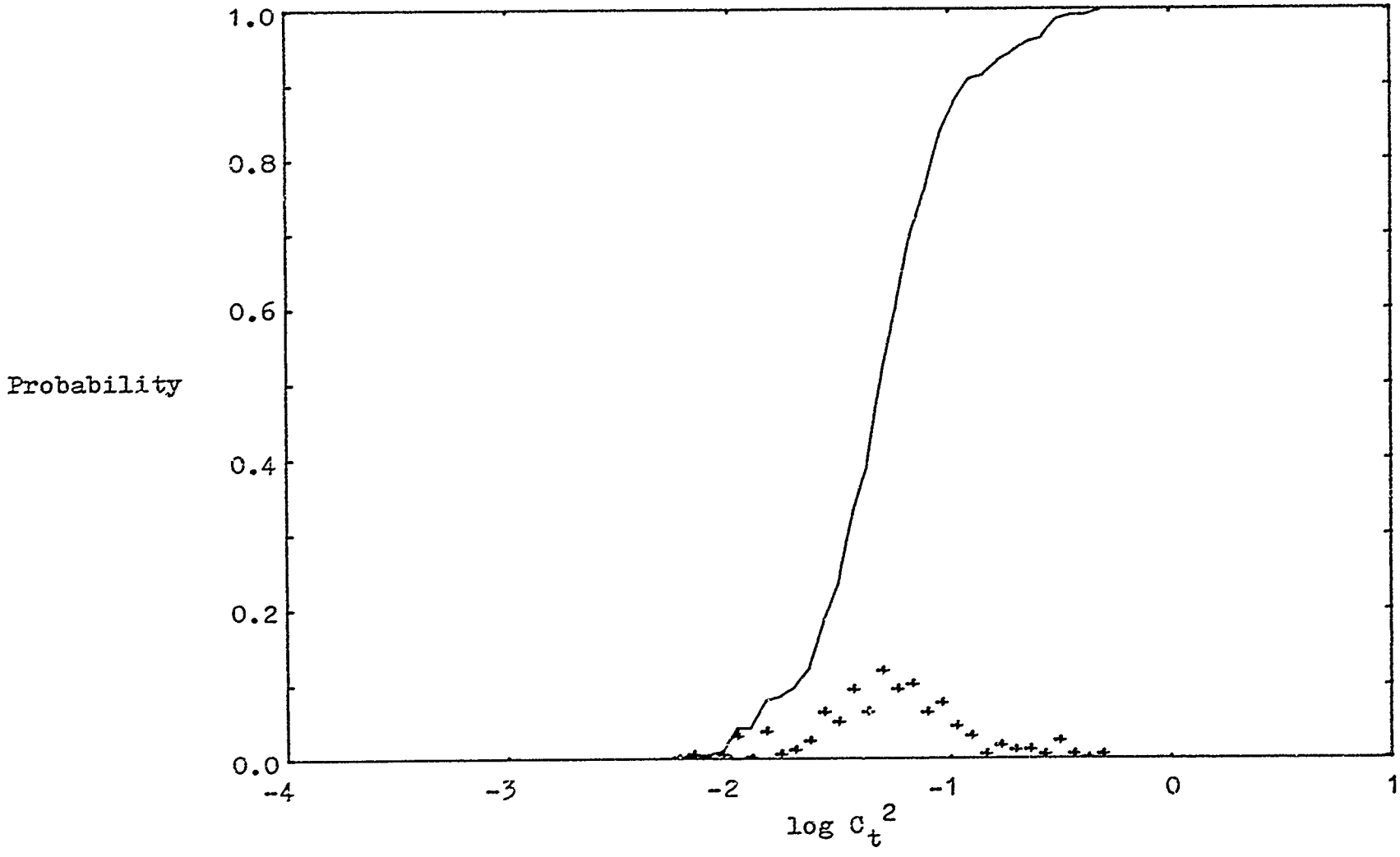

Figure C22. Discrete probability (+) and cumulative probability (solid line) for Type II turbulence: May 1975, night.

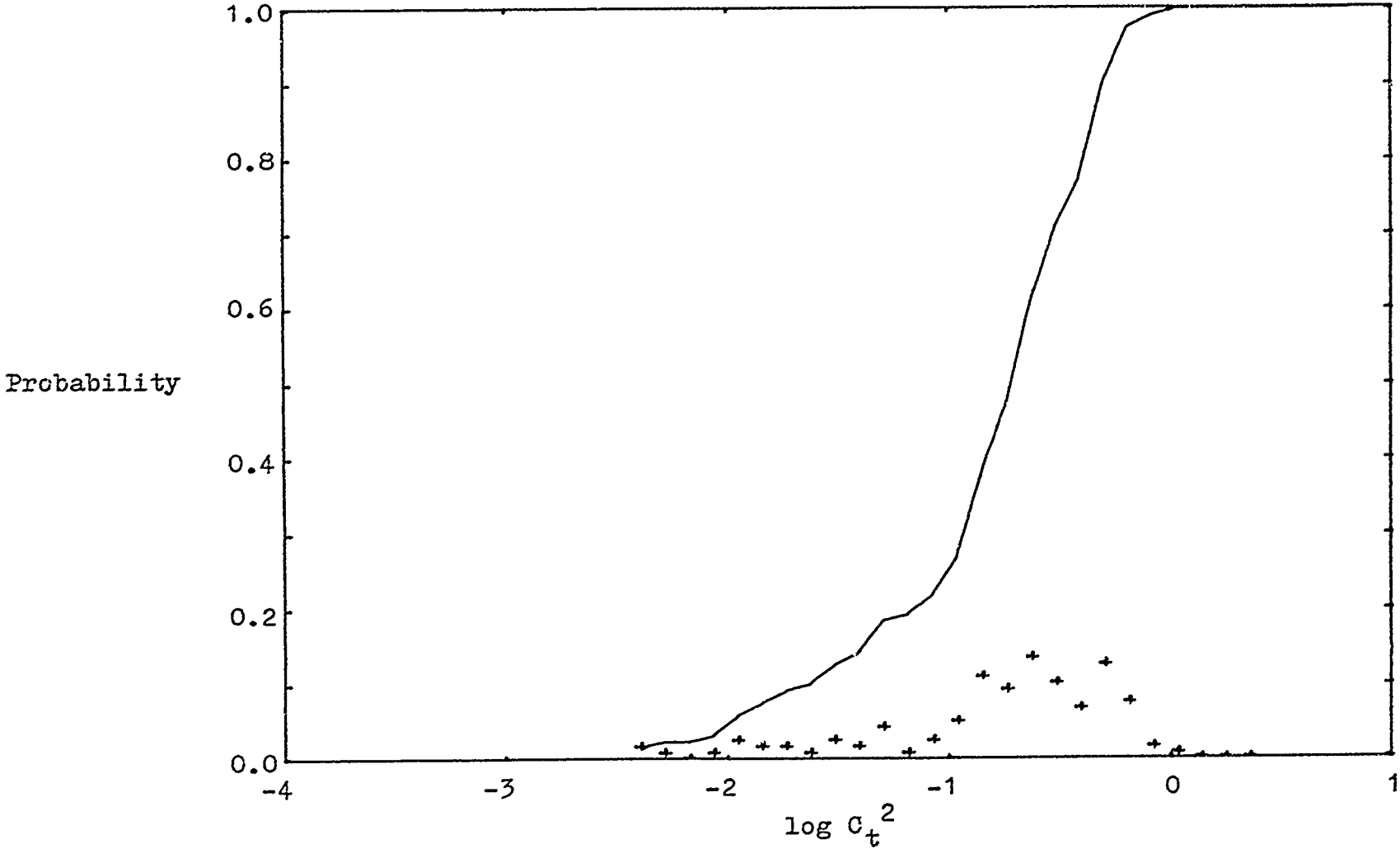

Figure C23. Discrete probability (+) and cumulative probability (solid line) for Type II turbulence: May 1975, day.

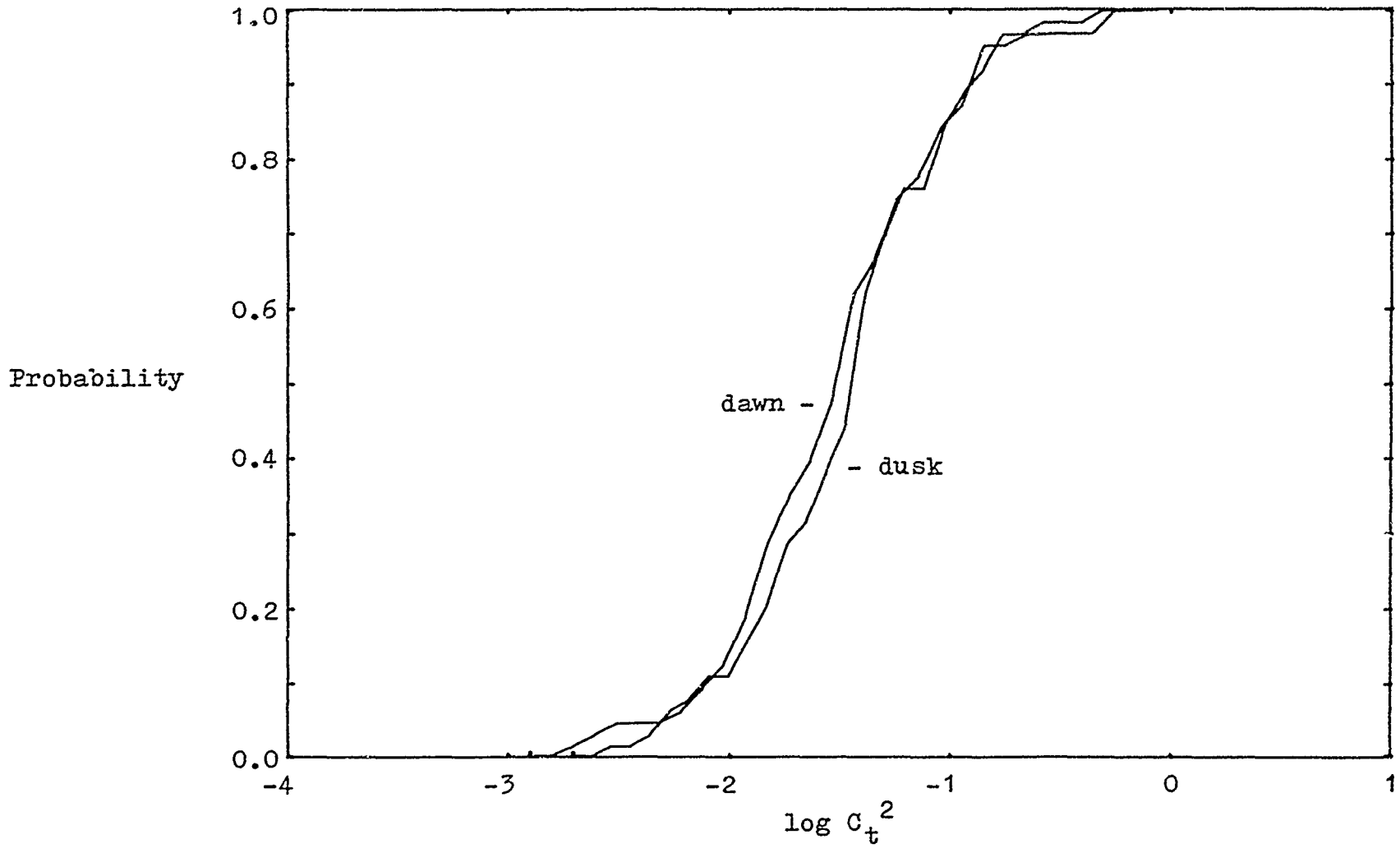

Figure C24. Cumulative probability functions for Type II turbulence: May 1975, dusk and dawn.

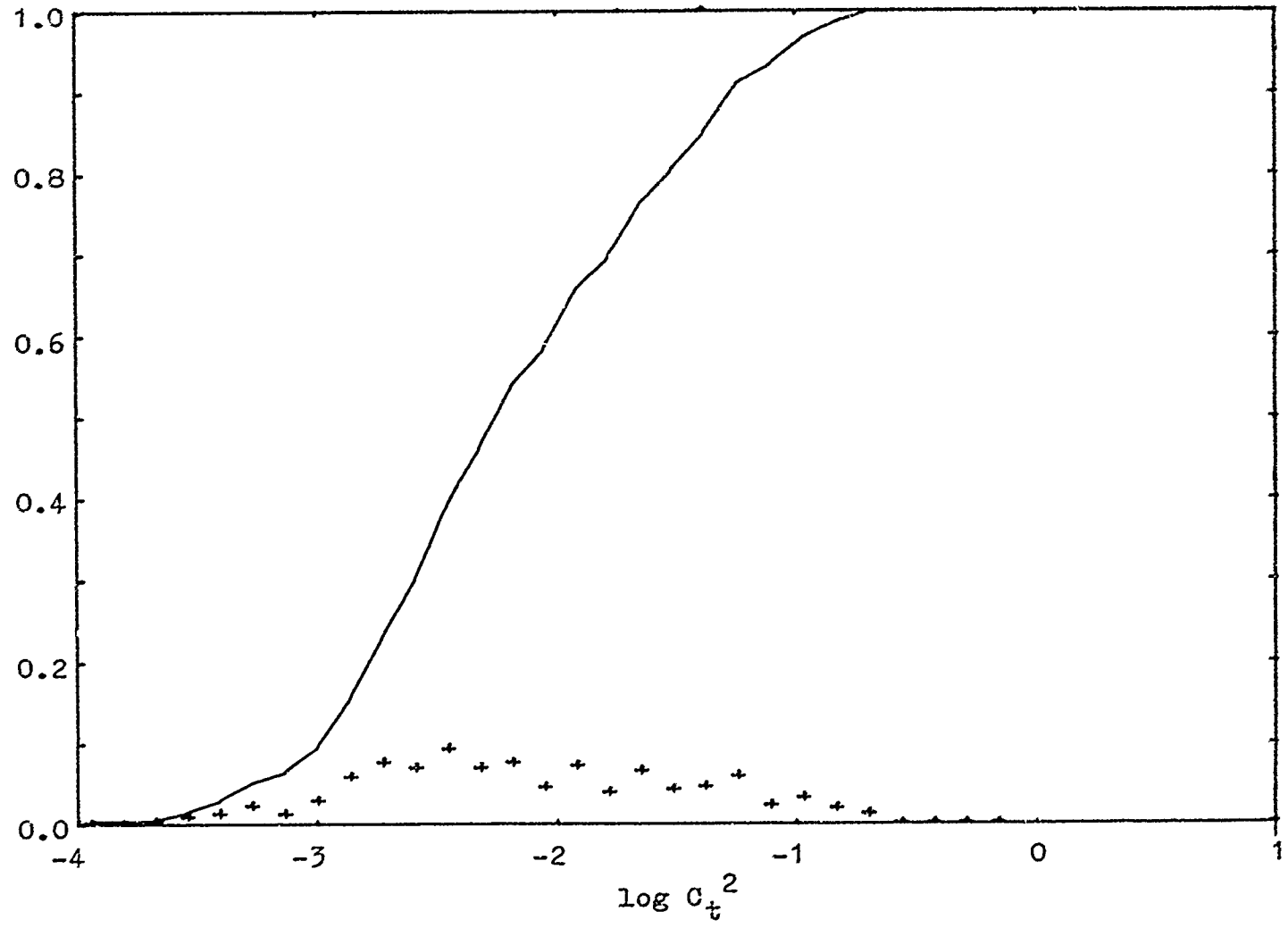

Figure C25. Discrete probability (+) and cumulative probability (solid line) for turbulence in "all weather": February 1975, night.

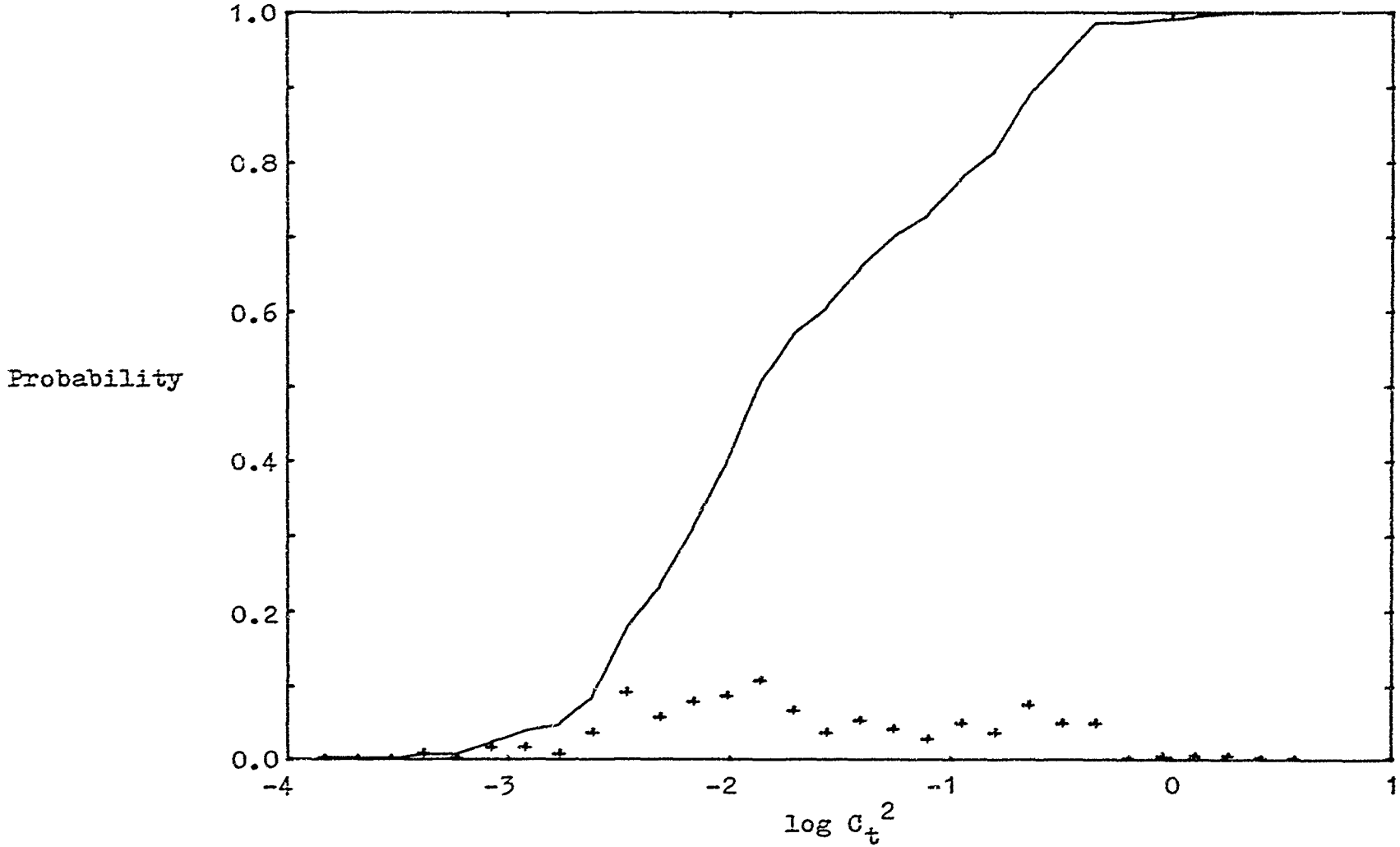

Figure C26. Discrete probability (+) and cumulative probability (solid line) for turbulence in "all weather": February 1975, day.

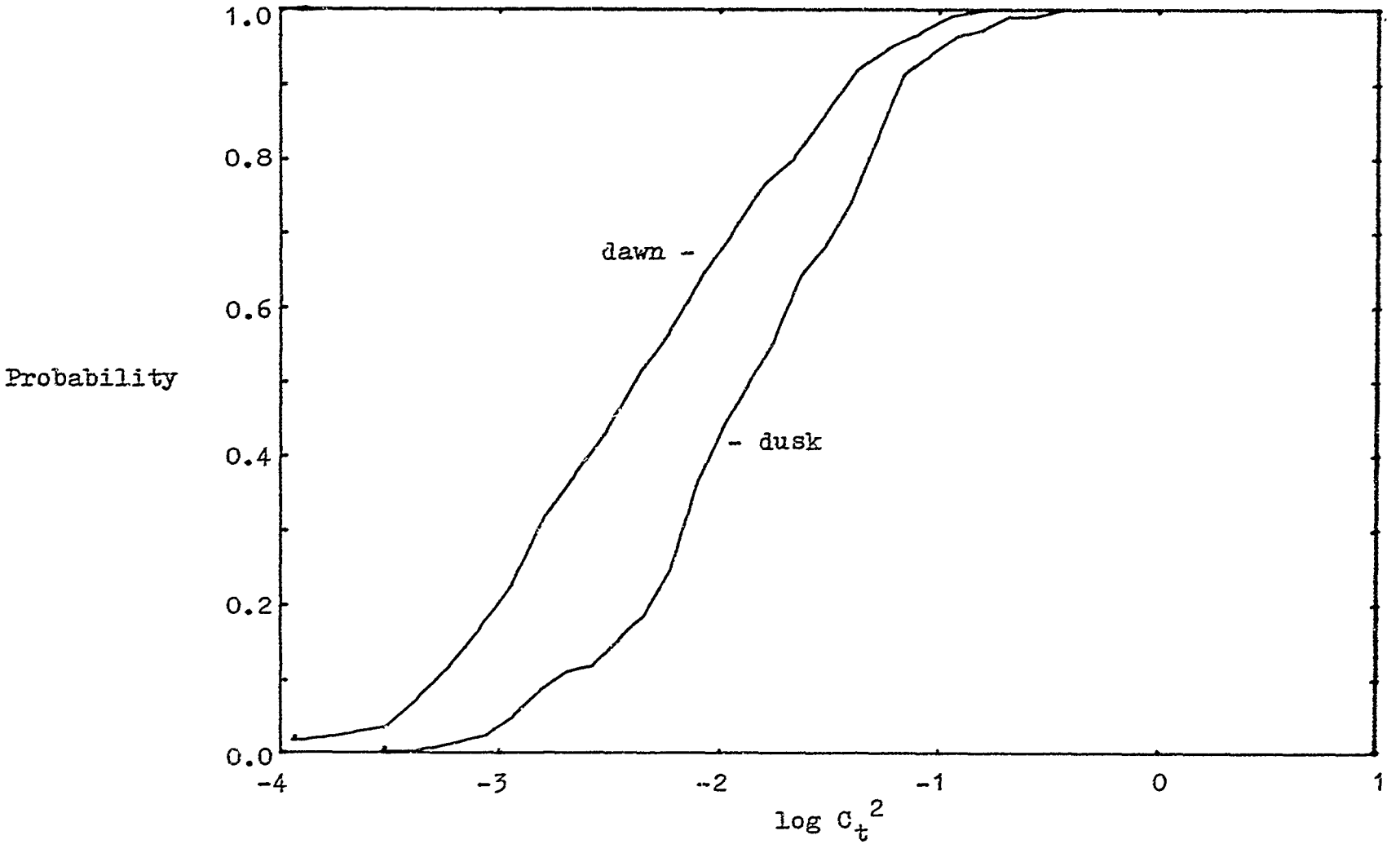

Figure 027. Cumulative probability functions for turbulence in "all weather": February 1975, dusk and dawn.

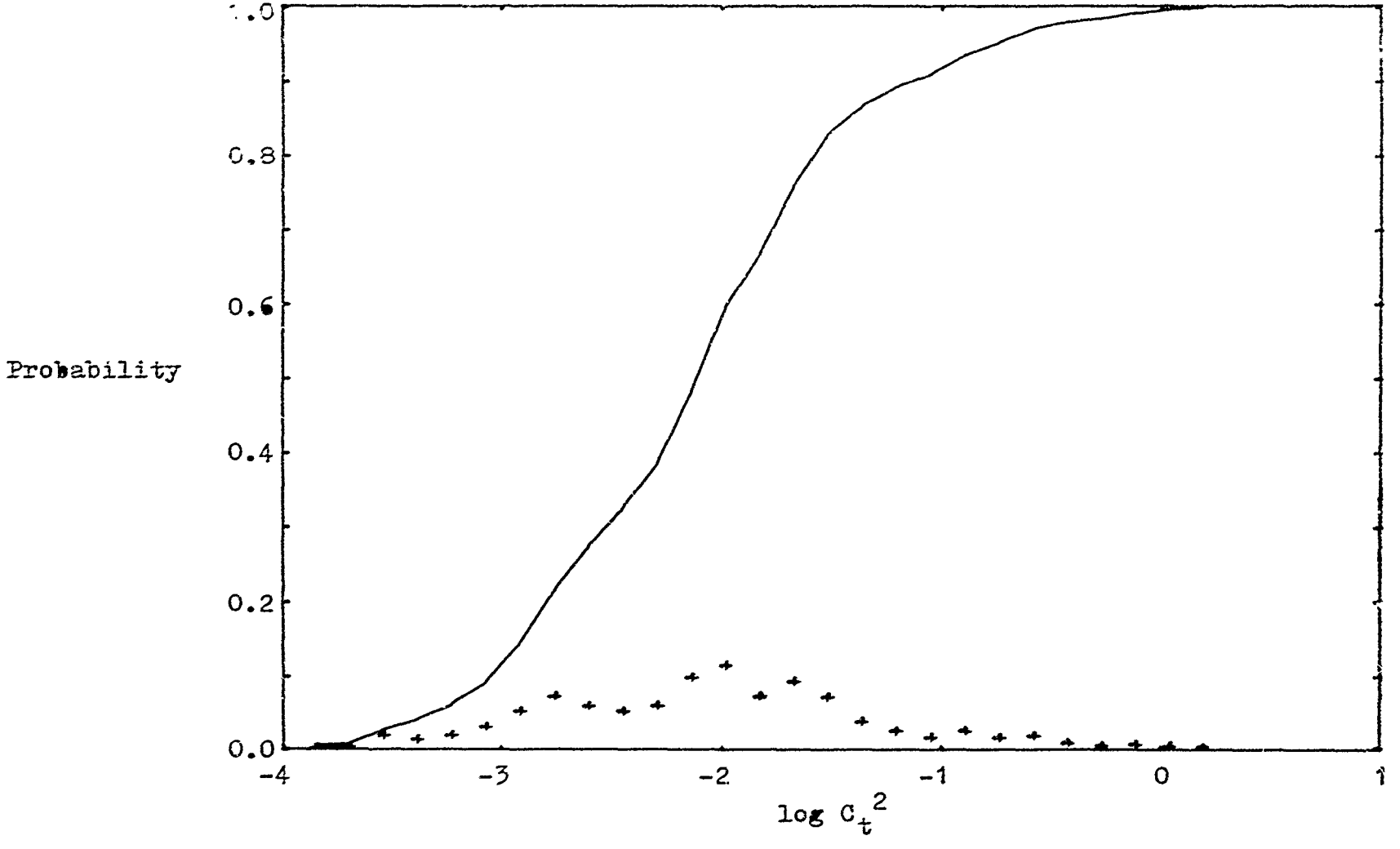

Figure C28. Discrete probability (+) and cumulative probability (solid line) for turbulence in "all weather": March 1975, night.

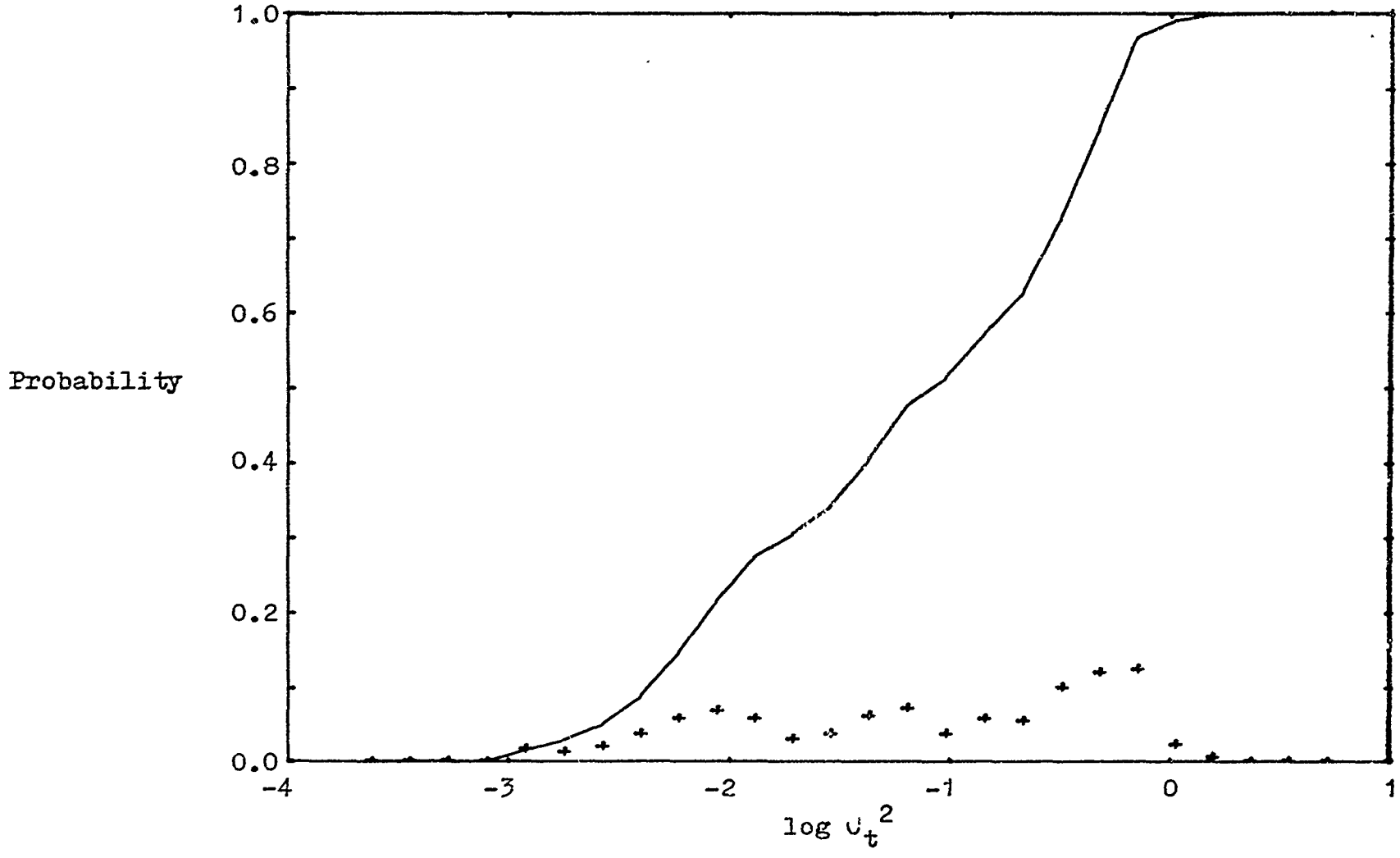

Figure C29. Discrete probability (+) and cumulative probability (solid line) for turbulence in "all weather": March 1975, day.

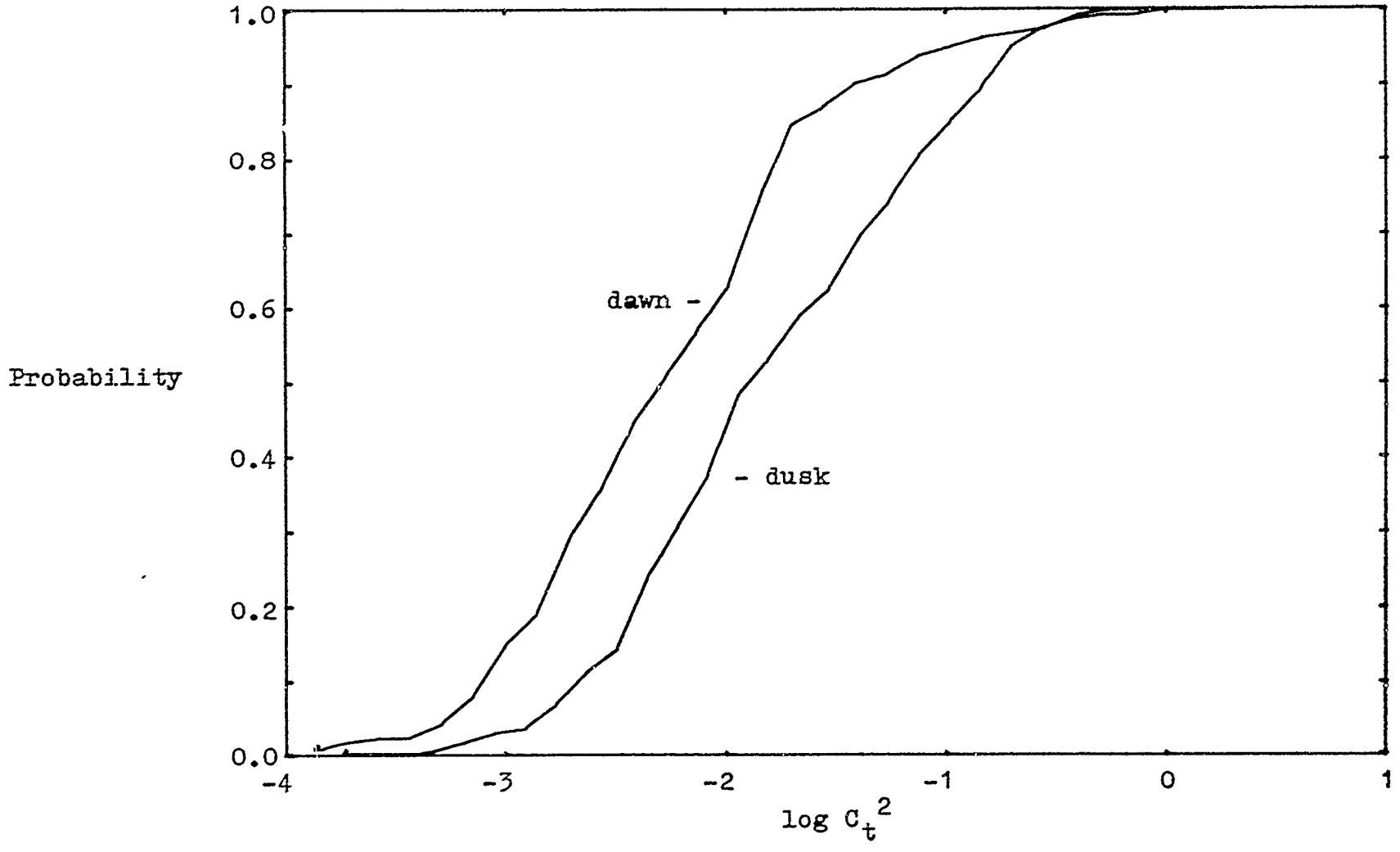

Figure C30. Cumulative probability functions for turbulence in "all weather": March 1975, dusk and dawn.

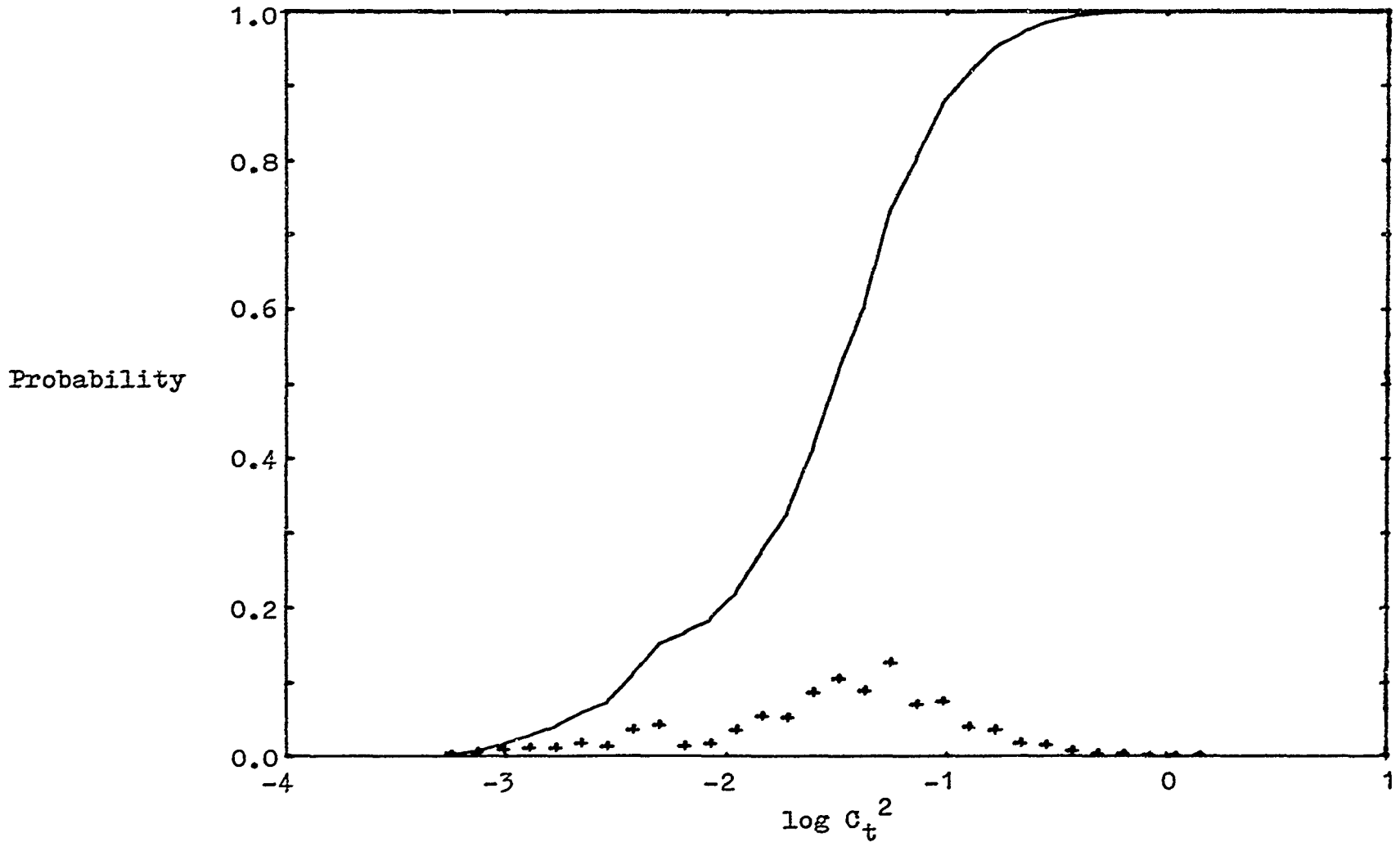

Figure C34. Discrete probability (+) and cumulative probability (solid line) for turbulence in "all weather": May 1975, night.

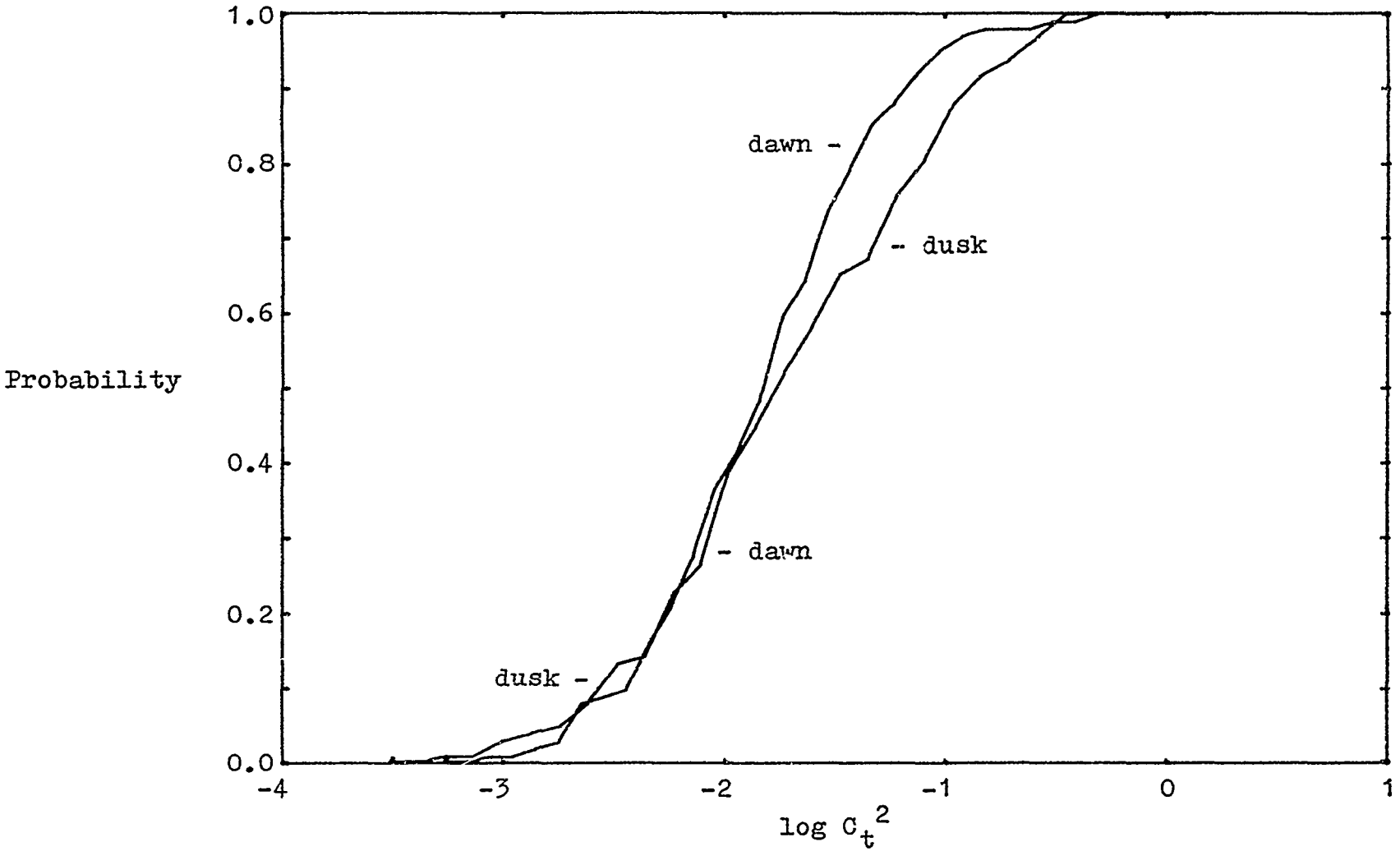

Figure C33. Cumulative probability functions for turbulence in "all weather": April 1975, dusk and dawn.

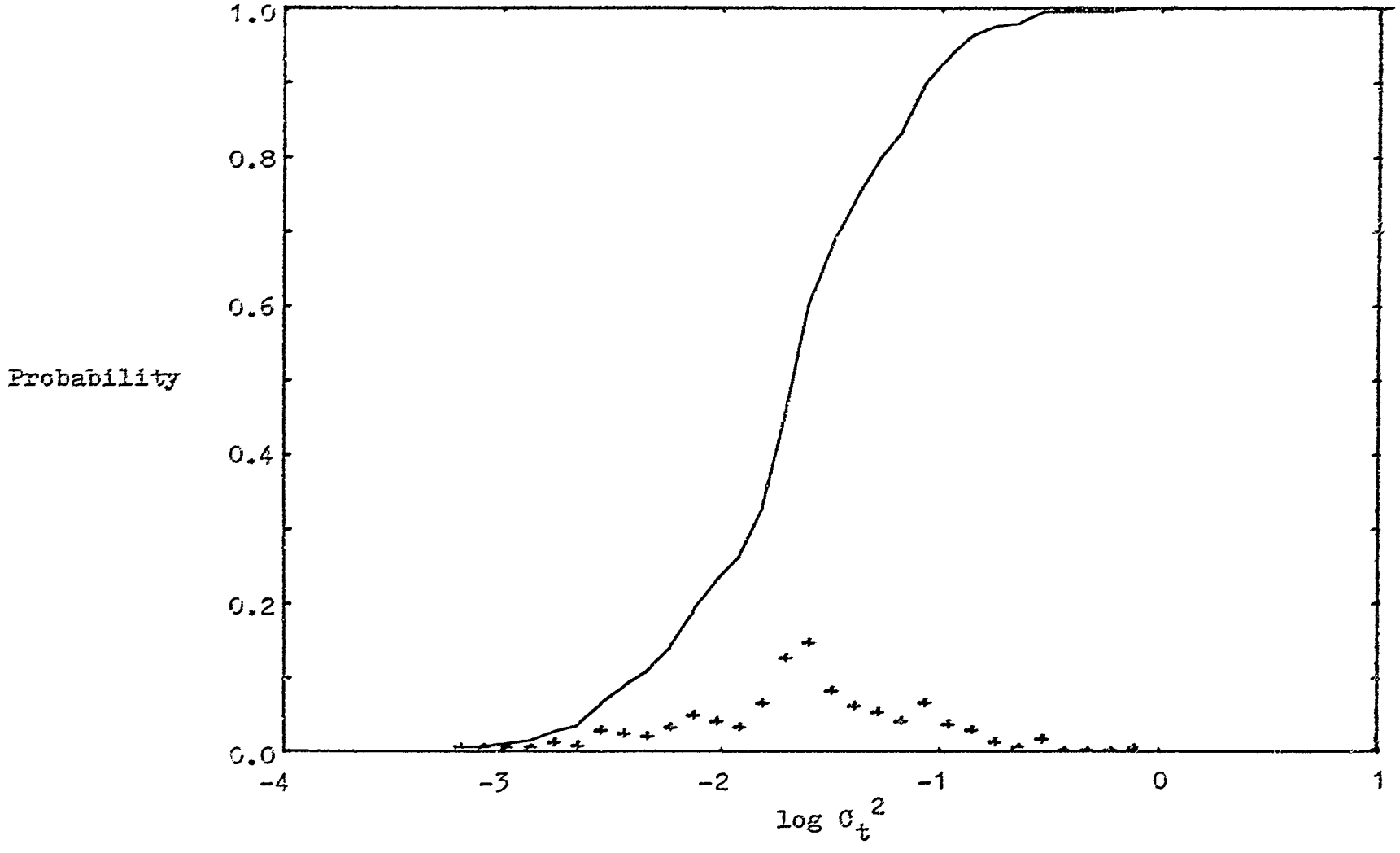

Figure C31. Discrete probability (+) and cumulative probability (solid line) for turbulence in "all weather": April 1975, night.

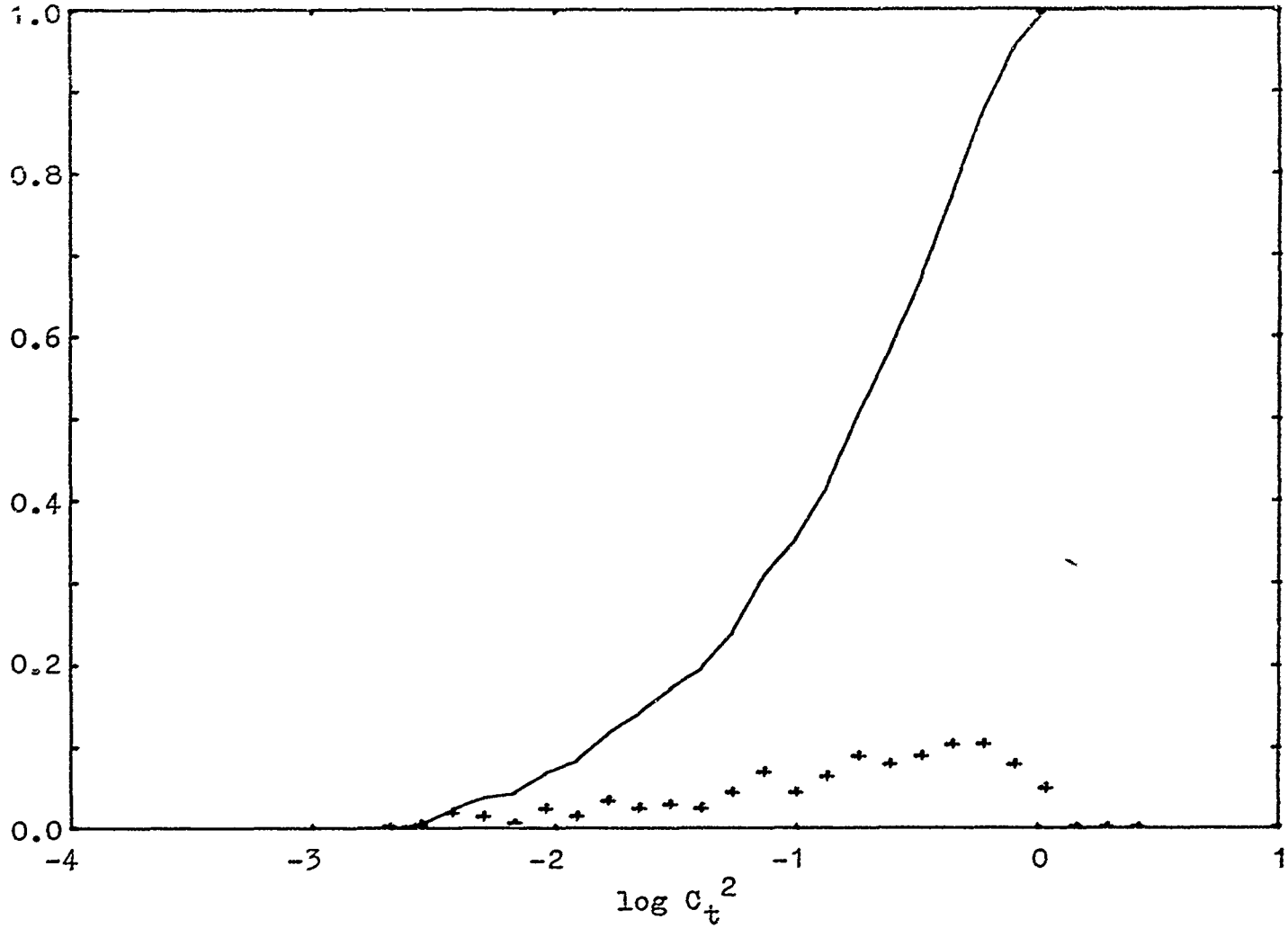

Figure C32. Discrete probability (+) and cumulative probability (solid line) for turbulence in "all weather": April 1975, day.

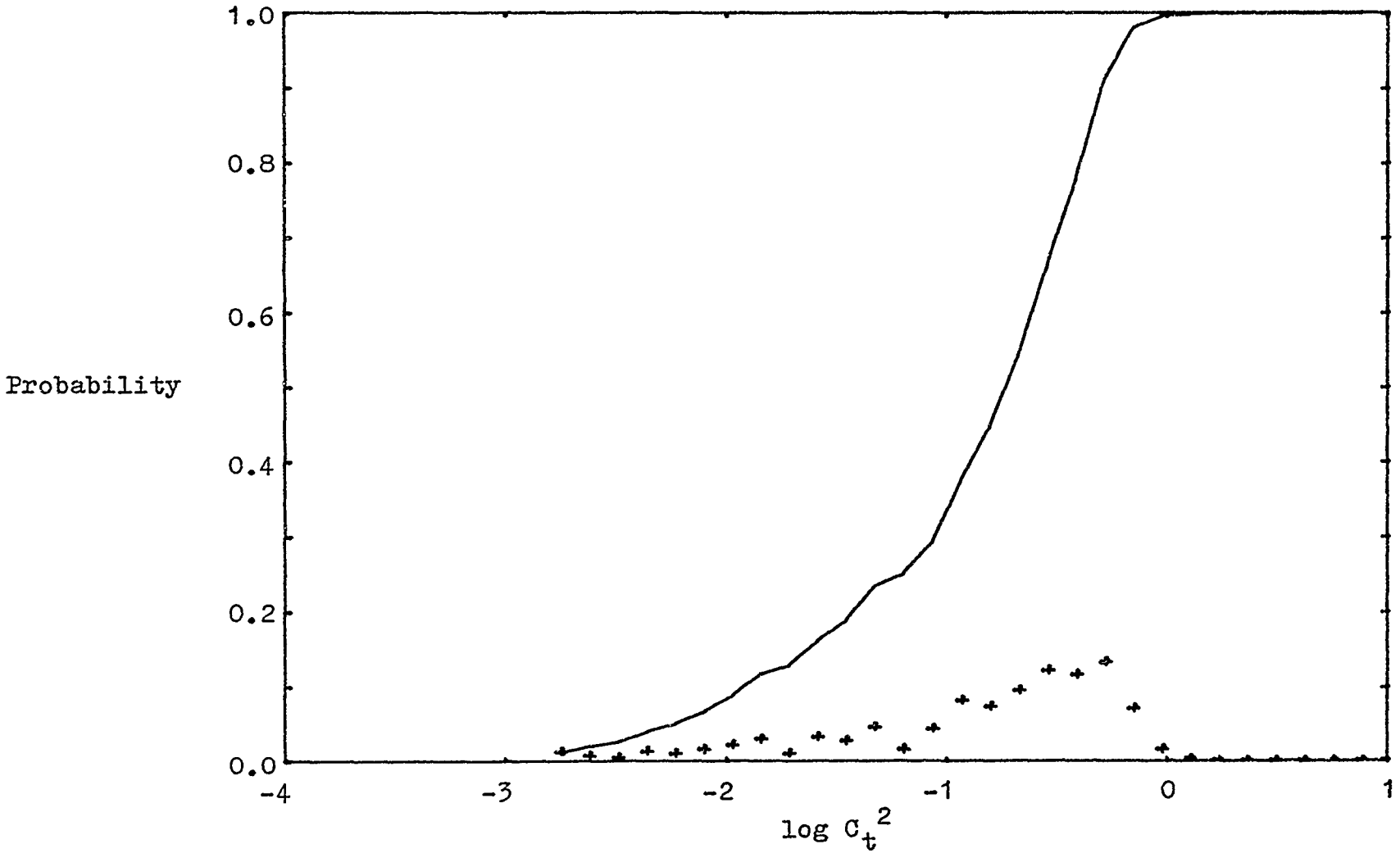

Figure C35. Discrete probability (+) and cumulative probability (solid line) for turbulence in "all weather": May 1975, day.

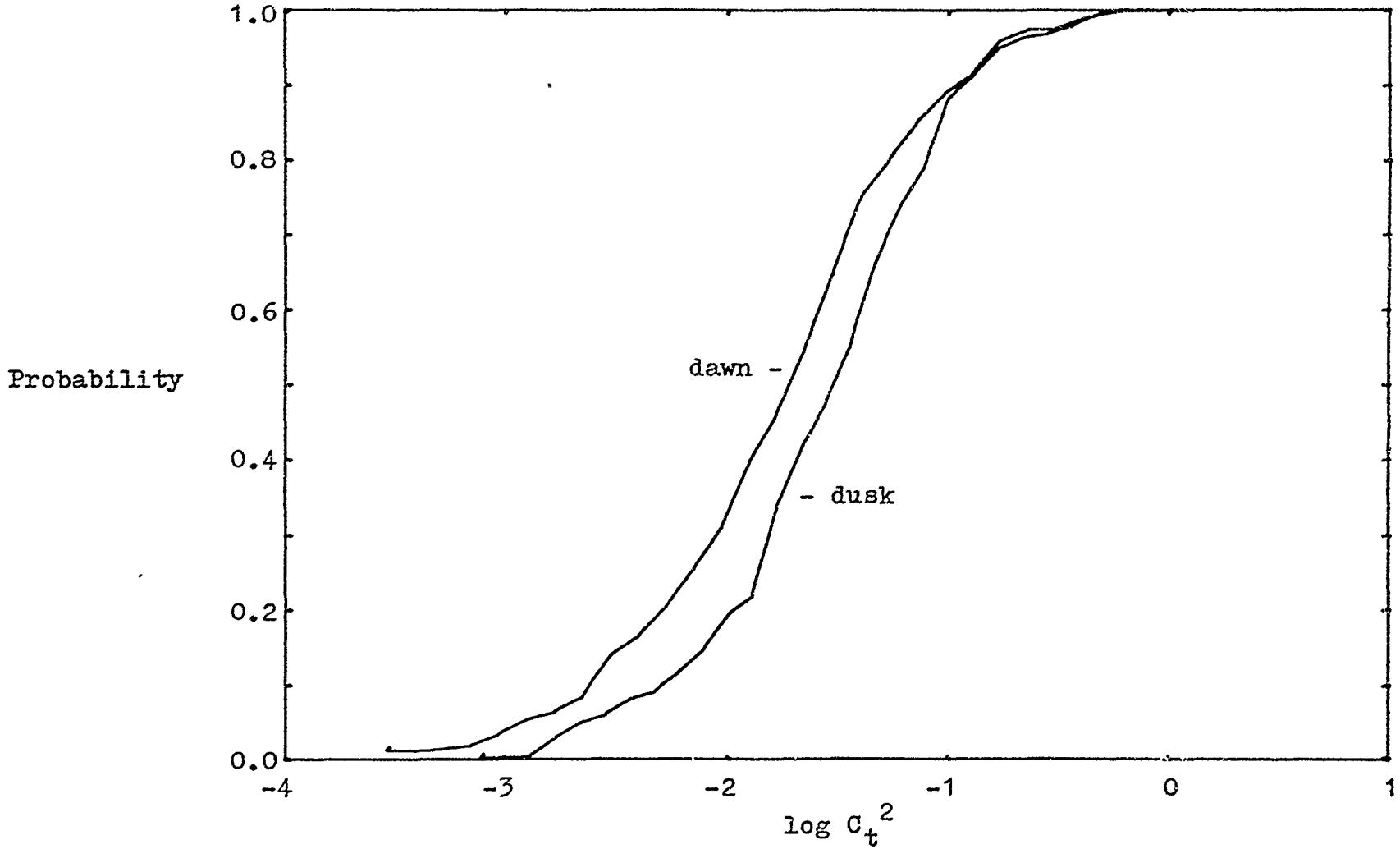

Figure C36. Cumulative probability functions for turbulence in "all weather": May 1975, dusk and dawn.

MISSION
of
Rome Air Development Center

RADC plans and conducts research, exploratory and advanced development programs in command, control, and communications (C^3) activities, and in the C^3 areas of information sciences and intelligence. The principal technical mission areas are communications, electromagnetic guidance and control, surveillance of ground and aerospace objects, intelligence data collection and handling, information system technology, ionospheric propagation, solid state sciences, microwave physics and electronic reliability, maintainability and compatibility.